AALBORG UNIVERSITET
ESBJERG

SEMI-SUBMERSIBLE TOPSIDE CONCEPTUAL DESIGN

TRANSITION PIECE

FERNANDO VIDAL PUCHE

SEPTEMBER 2014

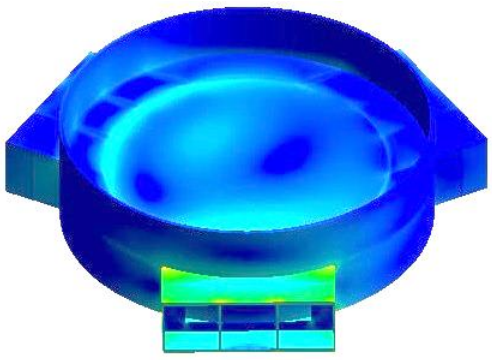

MSC THESIS IN STRUCTURAL AND CIVIL ENGINEERING

SEMI-SUBMERSIBLE TOPSIDE CONCEPTUAL DESIGN
TRANSITION PIECE

TITLE SHEET

Topic	Floating foundations, semi-submersible design. Transition piece fatigue life
Title	Semi-Submersible Topside Conceptual Design: Transition Piece
Period	03.02.2014 – 10.09.14
University	Aalborg University Esbjerg, Denmark
Department	Civil Engineering
Faculty	Structural and Civil Engineering
Semester	BM4-F14 MSc thesis
Supervisors	Ronnie Refstrup Pedersen, from Rambøll Offshore Wind and Aalborg University Esbjerg Christof Wehmeyer, from Rambøll Offshore Wind Esbjerg
Page count	88

MSc Structural and Civil Engineering candidate

Fernando Vidal Puche

Date

ABSTRACT

The subject of this project analyses the fatigue life of the transition piece in a semi-submersible conceptual design for offshore wind.

Various disciplines are involved in the completion of the master thesis. The assessment of the transition piece fatigue life, implies the use of different and suitable state-of-the-art software covering hydrodynamics and structural engineering.

Three distinctive parts compound this master thesis:

The first stage consist of validating of the CAE tools in use. The principal software looked into is ASAS, which is the offshore package in ANSYS [1]. Since it is the tool used to transfer the semi-submersible hydrodynamic loading. For validation purposes, ASAS and ROSAP results are compared by modelling the same jacket structure in both programs, due to the simplicity of setting up the models. The latter is a well-known software, Rambøll Offshore Structural Analysis Package, developed by Rambøll and widely used in offshore wind, and oil and gas.

Secondly, the hydrodynamic modelling of an offshore wind semi-submersible is completed in ANSYS AQWA, accordingly to a design scheme which has been developed by the author. The scope of this second part, is to define design basis for the hydrodynamic performance in modelling. The semi-submersible hydrodynamic design is a challenging task, given the location, mooring system and geometry of the different structural parts. The result is a valid hydrodynamic model, which is the base for the mechanical model.

Once validated, the hydrodynamic model is then evaluated from the mechanical point of view. The author presents a series of recommendations regarding topside, transition piece, and main columns mechanical design. The hydrodynamic loading computed in the second stage, is transferred to evaluate the fatigue life in the transition piece onto the mechanical model.

This third part includes: Semi-submersible mechanical design, and methodology for loading transfer between AQWA and ASAS. These procedures are developed by the author. The scope of load transfer is to allow the computation of stress-time series for an irregular sea-state.

Furthermore, different semi-submersible configurations are tested. These configurations reference to the addition of reinforcement bracing, with and without an tapered box girder or uniform box girder semi-submersible

Keywords: Floating; Foundation; Semi-submersible; ANSYS AQWA; NREL FAST; ASAS; Offshore Wind; FOWT; Fatigue life; Load transfer;

PREFACE

The present master thesis is submitted to the Department of Civil Engineering of Aalborg University Esbjerg, as fulfilment of the requirements for MSc Structural and Civil Engineering.

As floating foundations continue gaining a relevant importance in offshore wind. The subject of this master thesis regards the study of one the fundamental parts in the installation of offshore wind turbines, the transition piece and its fatigue life analysis. A semi-submersible is designed in this master thesis covering hydrodynamics and mechanical models. This document intends to provide a conceptual design of the transition piece, and present a workflow in a nutshell of relevant aspects in hydrodynamic and mechanical modelling.

This master thesis is principally directed to the university supervisors, and similarly to any other individuals and/or companies with an interest in offshore wind.

The author acknowledges the support and advice given by the following people during the elaboration of the master thesis:

Ronnie Refstrup Pedersen	Rambøll Offshore Wind, and Aalborg University. Esbjerg
Christof Wehmeyer	Rambøll Offshore Wind. Esbjerg
Andrew Zurkinden	FS Dynamics. Aalborg

CONTENTS

1. INTRODUCTION

During the last years, there has been a growing interest in offshore wind regarding floating foundations. The industry consideration for these foundations arise due to the search of more economical and feasible alternatives [2], compared to the classical bottom-fix offshore foundations. These events, follow a remarkable worldwide trend for the use of more developed and competitive technologies in the renewable energies sector.

The origins of floating platforms date back from the sixties [3]. Back when oil and gas prospections moved further towards deeper waters, fixed-bottom foundations, Figure 1, dominated the offshore marine structures. However, these long-term structures present limiting factors from the economical and feasible point of view in deep water conditions (>70 m).

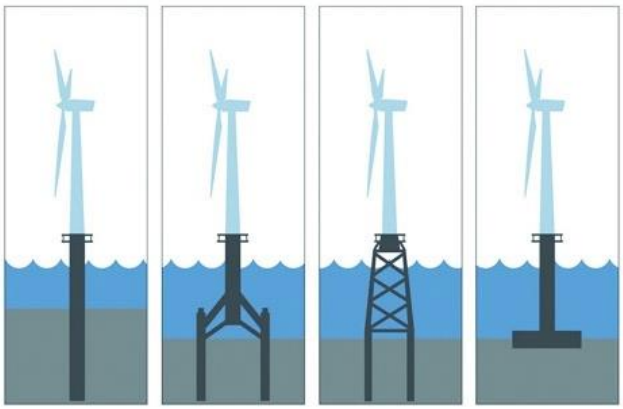

Figure 1 Bottom-fixed foundations - monopile, tripile, jacket, gravity

Through the use of floating foundations, new fields for exploitation were accessible. The earliest application in oil and gas was the semi-submersible concept. It consisted of a buoyant platform stabilised by four columns supporting the topside, and ballasted pontoons in 1961. It was the Blue Water Rig No.1, operated by Shell in the Gulf of Mexico.

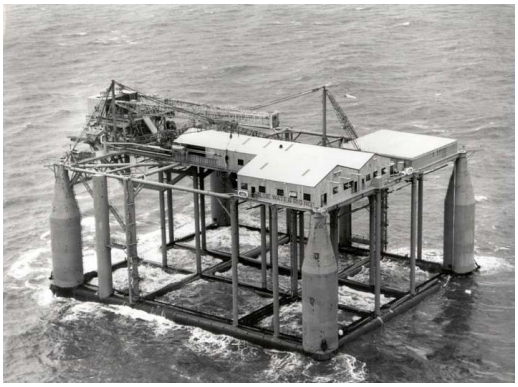

Figure 2 Blue Water Rig No.1 [4]

Back in the sixties, some of the main mechanisms and some design concepts making work a floating platform were not fully understood. These mechanisms refer to the importance of geometry and structural elements such as pontoons, which provide the stability and strength to the semi-submersible [3]. Nevertheless, there was a fast expansion and production of new afloat drilling rigs.
At the outset, the first standards, and technological assets such as mooring systems and raisers. In the course of thereafter decades, different generations of semi-submersible platforms were designed pushing the operational limits from 200 m up to 3000 m water depth [5].

Since the first offshore wind farm was in Denmark in 1991, the industry implemented existing state-of-the-art knowledge developed in the oil and gas. As a result, the floating foundation concepts born within the offshore industry, are the principal engineering applications to be transferred effectively into offshore wind.

Different floating foundation concepts have been operational since the 60's. The offshore wind industry aims to implement these in large scale as future foundations, presenting an alternative for bottom fixed foundations.

There are three main suitable concepts for offshore wind: spar, tension leg platform (TLP), and semi-submersible as shown in Figure 3

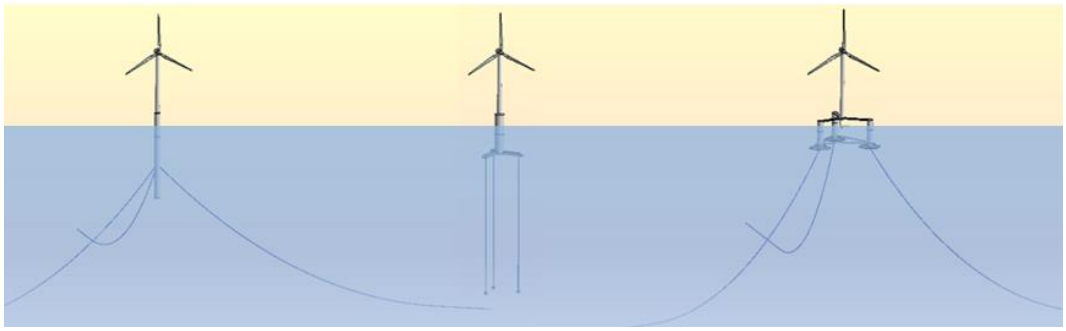

Figure 3 Spar – TLP – Semi-Submersible

Since engineering knowledge about floating foundations developed by the oil and gas sector remain mostly in secrecy. Nowadays, one of the main challenges in offshore wind is to widely develop know-how procedures and analysis tools, in order to produce economical floating foundation designs.

The main differences between floating wind offshore wind (FOWT), and offshore wind, regards the design basis of the foundations. Offshore wind relies on bottom-fixed foundations Figure 1, where the forces are calculated based on Morison equation, or relative Morison equation. On the other hand, FOWT presents a more complex problem due to the response amplitude of the a floating body, influence of the mooring system, and wave diffraction to obtain the forces and moments of the wave exciting forces on the structure.

Regarding offshore wind semi-submersibles, the first of its kind is deployed and located in Portugal. The prototype, WindFloat, mounts a Vestas V80 2MW wind turbine. Nowadays, the semi-submersible test prototypes can be found in Portugal, US and Japan, shown in Figure 4, Figure 5, and Figure 6 respectively.

Figure 4 WindFloat (2009), Aguçadoura

Figure 5 VolturnUS (2012), Maine

Figure 6 FORWARD (2013), Fukushima

1.1 TECHNICAL CHALLENGES

The initial approach taken to design an offshore wind semi-submersible is to determine the fundamentals that can be transferred from the designs in oil and gas, along with some of the prototypes in offshore wind. Some these concepts are: ballasting, pontoons/heave plates, and mooring lines (catenary lines in this case).

Figure 7 shows a general front, side, and top view where the different structural parts of a semi-submersible are noted.

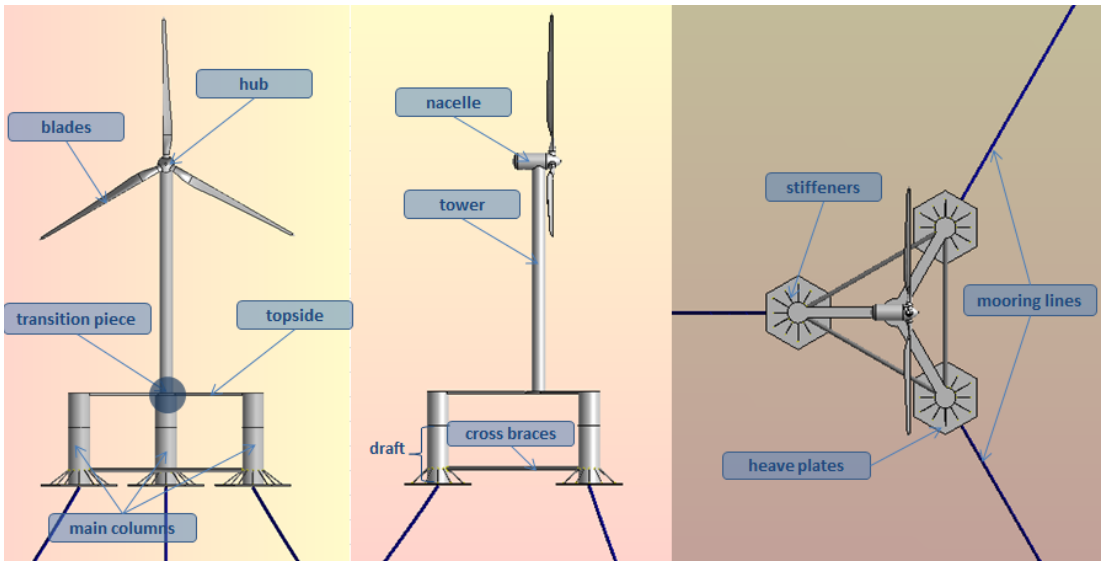

Figure 7 Semi-submersible structural parts

The first technical challenge is the geometry of the semi-submersible. The dimensions determine big part of the hydrodynamic performance. This could range from buoyancy (hydrostatic stability), and natural frequencies to response amplitude operators (RAOs). The latter are an important indicator of a floating platform behaviour in the sea.

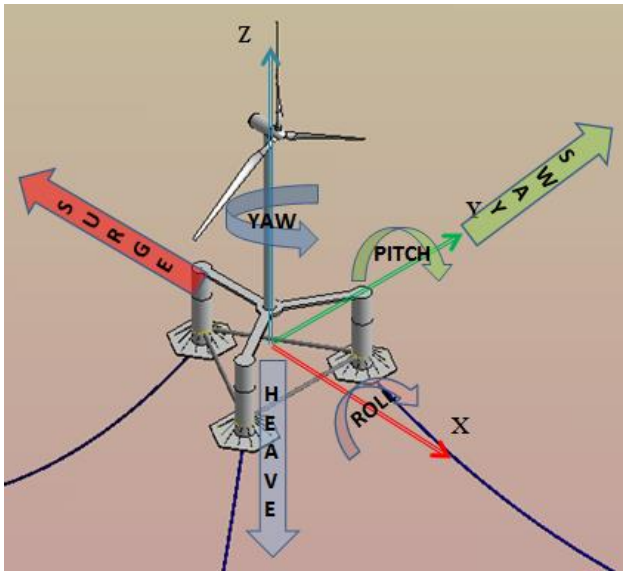

Figure 8 Floating body, 6 rigid body DOF

In Figure 8 the 6 rigid body DOF in a floating body are shown. Three correspond to displacements ± in the X-surge, Y-sway and Z-heave. The last three are rotational motions ± around each one of the axis: roll, pitch and yaw respectively.

The natural frequencies to determine correspond to each DOF, and in consequence the RAOs describe the response of the semi-submersible when the foundation is subjected to regular unit amplitude waves.

In structural engineering, any design must include a natural frequency analysis of the structure. Likewise, when offshore foundations are installed on a given location in the open sea, the structural design is adapted to avoid that large dynamic amplification effects due to structural eigenfrequencies within the environmental loading frequency spectrum. To such extent, the floating structure is mainly subjected to wave loading. This environmental loading is normally defined as a combination of irregular sea-states, with difference probability of occurrence for an specific site.

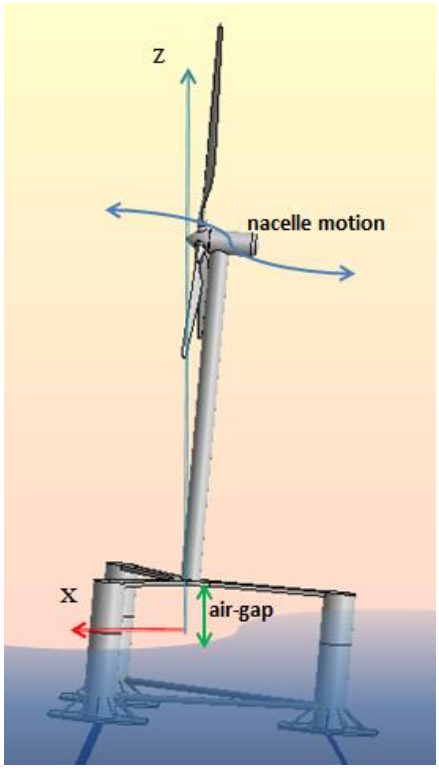

Figure 9 Pitch motion around Y-axis illustation of the nacelle influence and air-gap

Another fundamental in a semi-submersible concerns the so-called pontoons, or alternatively heave plates. These elements are installed at the submerged bottom part of the main columns. In both structural options, the function of installing such aims to lessen heave and pitch motions. It is important to point out, that pitch is specially critical in floating offshore wind turbines (FOWT) as it compromises the structural integrity due to the dynamics induced by the wind turbine.

Heave motion is significant as well. Large displacements along the Z-axis risk a lack of air-gap. As a result, the topside and tower will be subject to wave loading, which is a case to avoid and prevent in early design stages.

In this master thesis, heave plates are the structural element implemented. The characteristics of this structural part is cover in 4.2.5.

In this first point, the goal is to determine the platform dimensions and tune the structure eigenfrequencies out of the wave loading spectrum. Regarding the natural frequencies; structural steel mass, heave plates, ballast levels and mooring lines have an essential contribution in the outcome results for the design. Thereby, these parameters are adjusted for an optimal hydrodynamic performance with reference to the procedure developed in [6].

Afterwards, different mechanical models need to be prepared. This includes the details in the transition piece, as well as internals in the semi-submersible topside.

1.1.1 LOCATION

The chosen location for the semi-submersible is the Moray Firth, in the North Sea.

Figure 10 Moray Firth, Scotland [8]

The water depth, 40.2 m LAT, comprehends another challenging factor in the design. Whereas, the floating platform applications are mainly deep water oriented. To remark one difficult, as mentioned in [7] one of the design basis in semi-submersibles, is a moderated draft of the platform. This means that a significant length of the main columns are submerged.
The reduced depth of the location, the draft of the main columns limits the suspended catenary length. This submerged part of the mooring line, constitutes a restoring mechanism against motions by means of weight. To balance this drawback, the catenary section requires special attention and further detail is shown in section 4.1.3.

1.1.2 CAE TOOLS

The main software used in the elaboration of this master thesis is listed below and explained in the following subsections:

- ANSYS AQWA
- ASAS
- NREL FAST

1.1.2.1 ANSYS AQWA

The semi-submersible designed in this thesis is a three-dimensional floating body. Due to its nature and dimensions, the different structural parts presented in Figure 7 are modelled by employing suitable elements used in hydrodynamics attending the characteristics of each one. To determine which elements are modelled as panels or Morison elements, the structural parts are evaluated on regards of the Keulegan-Carpenter number (KC number), in section 4.2.2.

Thus, the hydrodynamic model is composed by pressure panels and Morison elements. This model is simpler than the mechanical, as it does not include internals or a detailed section of the transition piece. AQWA solves the linearized diffraction/radiation problem to compute the pressures and motions on the wetted surfaces in the frequency-domain. In addition, Morison equation calculates the forces on members such as cross braces (tubes) and heave plates (disc).

1.1.2.2 ASAS

This tool is the structural offshore module in ANSYS. The analysis of the hydrodynamics in AQWA does not allow itself a direct transfer for an structural assessment. In order to transfer the hydrodynamic loading the programs AQWA and ASAS are linked to produce a load mapping of the structure.

The result of hydrodynamic load mapping, permits to output the subsequent stress levels on the structure which are to be used in the fatigue life analysis.

Both, load transfer and fatigue require the developing of a procedure in the thesis. Besides, different standards in offshore such as DNV-OS-J103 and DNV-RP-C203 are used to assess the floating foundation.

For benchmarking reasons, and to gain understanding in ASAS, results from ROSAP are compared with the former. Both programs are compared modelling the same structure and boundary conditions. For this case, a jacket structure defined in section 3, with fixed joints is the subject of study.

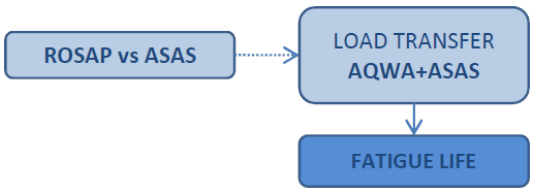

Figure 11 Software validation workflow

1.1.3 FAST AND ASAS

FAST is a aeroelastic code which has evolved with capabilities from land-based wind turbines to offshore foundations. The utility of FAST in this document, regards the analysis of the reference NREL 5MW offshore wind turbine, and output of the sectional forces due to environmental loading. The results produced are plugged into the mechanical model to complement the hydrodynamic loading, and evaluate the fatigue life.

1.1.4 HEAVE PLATES

The hydrodynamic performance of the offshore wind semi-submersible depends on roll, pitch and heave motions. The installation of heave plates provides with stability to the platform, lessening these RAOs [6]. The geometry of the heave plates, has a notable influence regarding drag and added mass coefficients [9] [6]. In the hydrodynamic modelling, the author develops a procedure to implement heave plates and dimensioning regarding a relation with the main column diameter.

1.1.5 SUMMARY

To conclude, some of the most remarkable technical difficulties are:

- Use of ASAS to establish an accurate model in comparison with ROSAP
- Design of the semi-submersible in Moray Firth
- Mooring lines adjustment for reduced water depth
- Heave plates implementation accordingly to platform geometry
- Load transfer and processing from hydrodynamic to mechanical model
- Sensitivity study of the topside proposed configurations
- Develop methodology for the fatigue life analysis of the transition piece

2. SCOPE OF THE WORKS

In order to assess the fatigue life of the semi-submersible TP, this project considers an structured workflow from hydrodynamic design to the mechanical model. An overview of the master thesis contents is shown below in Figure 12

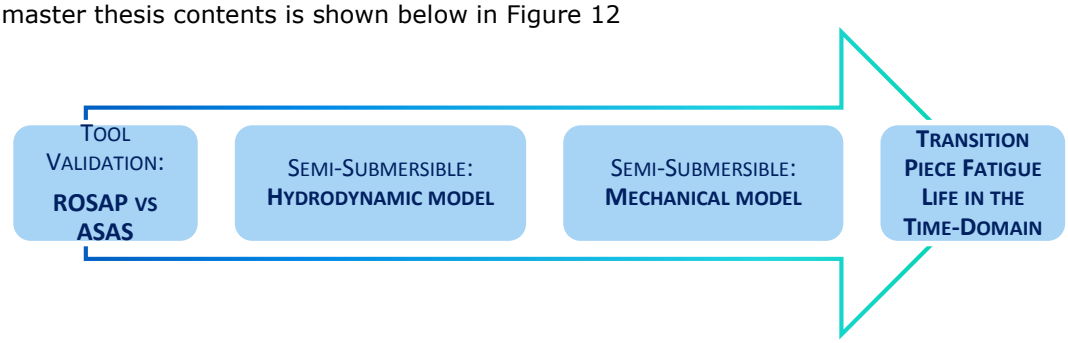

Figure 12 Project overview

2.1 TOOL VALIDATION

As a previous step, one of the key tools used in the project, ASAS, is validated for a jacket structure, Figure 13 and Figure 14. The comparison established is ROSAP vs ASAS, and the check points are:

- Nodal displacements
- Reactions in the supports
- Member sectional forces
- Natural Frequency Analysis (NFA)

The criteria for validation is that the results to compare must not differ over a 10% forces and reactions in a static load case. To complete the assessment, a wave loading stream function wave (no. order 25) are analysed. Independently, NFA is run in both programs to compare eigenfrequencies and mode shapes. Despite the criteria aforementioned, it is important to mention that larger differences are expected in wave loading. There is a built-in main difference between ROSAP and ASAS. The former makes use of Morison equation, and the latter relative Morison equation. In other words, relative Morison equation includes the motions of the structure in terms of velocity and acceleration due to wave loading.

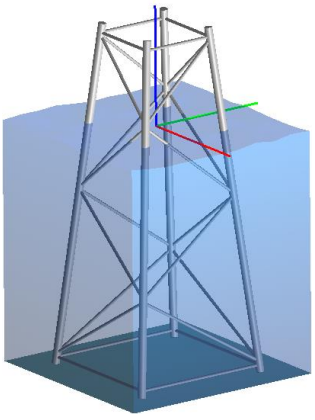

Figure 13 Jacket in ROSAP

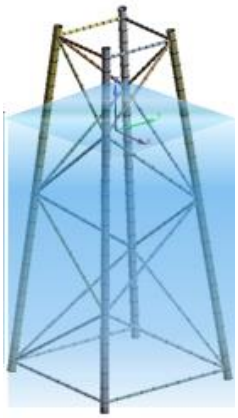

Figure 14 Jacket in ASAS

2.2 SEMI-SUBMERSIBLE: HYDRODYNAMIC MODEL

The hydrodynamic model is carried out in ANSYS AQWA. The author develops and presents a validation workflow for the design. The semi-submersible design is adapted to the conditions in Moray Firth. This includes a review on the geometry, heave plates, mooring lines and ballast levels. The new model is evaluated accordingly to the flowchart shown in Figure 15.

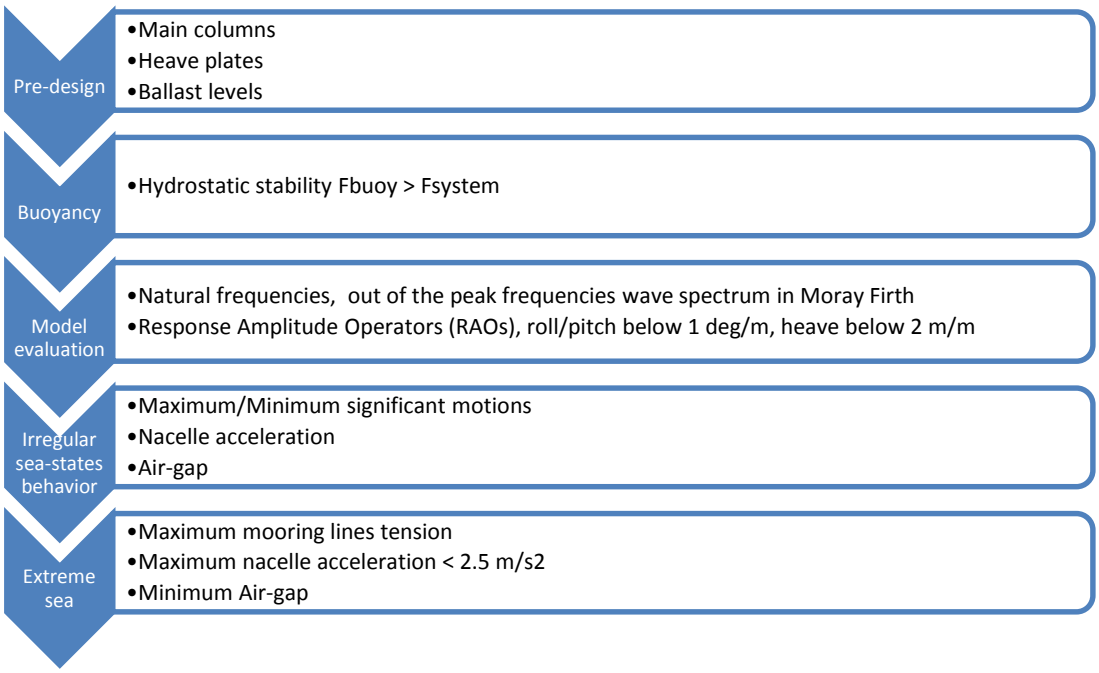

Figure 15 Semi-submersible hydrodynamic modelling flowchart [6]

2.3 SEMI-SUBMERSIBLE: MECHANICAL MODEL

A second part, comprehends the mechanical model and wave loading transfer.
The design of the geometry is not straight forward. Additional structural parts need to be included on the hull designed for the hydrodynamic model to complete the mechanical model. This is referred to the modelling of internals, Figure 16, which reinforce the hull structure used in the hydrodynamic model to withstand wave and wind loading. The objective of designing the internals, aims to strengthen the structure to resist the stress induced by environmental loading.

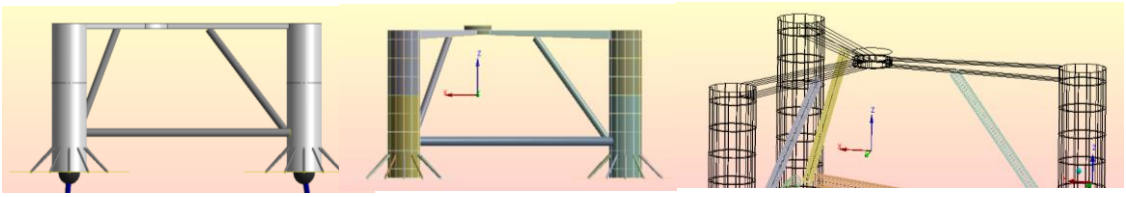

Figure 16 From left to right: Hydrodynamic model (hull), Mechanical model (shell) and wireframe view

Due to the topside span, it is assumed that additional cross braces will be necessary to reinforce the semi-submersible. The mechanical model is firstly evaluated in four different configurations, which are illustrated in Figure 17 and Figure 18.

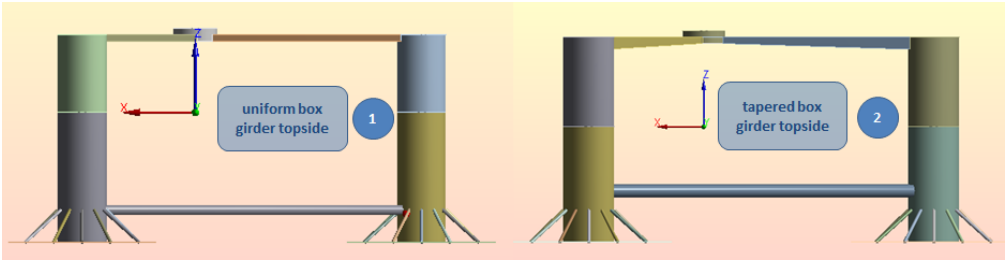

Figure 17 Uniform and tapered box girder topside

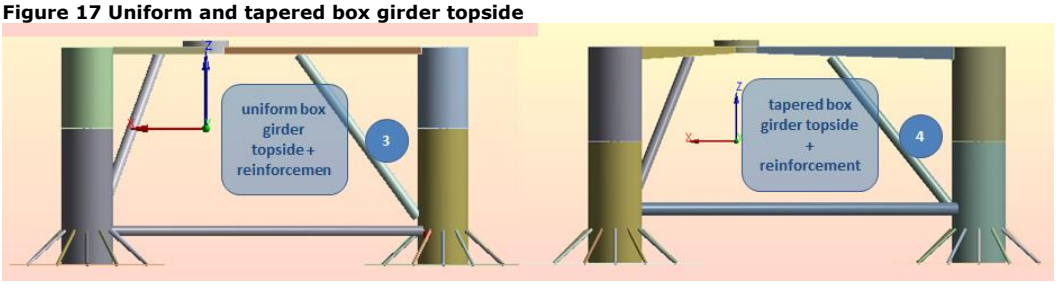

Figure 18 Uniform and tapered box girder topside with added reinforcement cross bracing

This initial analysis, only applies Earth's gravity. As a consequence, those models which yield the higher stress level on the TP are discarded. With this step, one model is selected to design the internals.

After selecting the model, the design basis which follows is a suggested approach. The procedure is based on assessing the structural elements individually. These are main columns, and most importantly topside and transition piece. For simplicity, the heave plates are considered infinitely stiff. Due to the extent and computational resources of the MSc thesis, the fatigue life assessment of the mechanical model is confined to the sea-state (Hs=3.25 ; Tp=8.56 ; wind speed=11.5 m/s), which regarding wind speed is the most similar to the rated wind speed of the NREL 5MW wind turbine.

The methodology developed, consist of an evaluation of the structural stress level in defined points of interest of the transition piece. Briefly described, the procedure starts with a quasi-static analysis, by stepping the wave passing through the structure centre of mass. An example is illustrated below in Figure 19 and Figure 20.

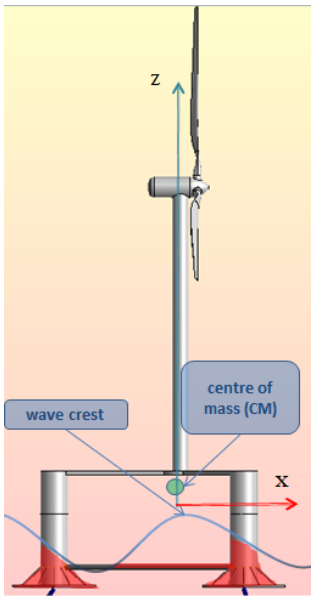

Figure 19 Wave crest passing through the CM

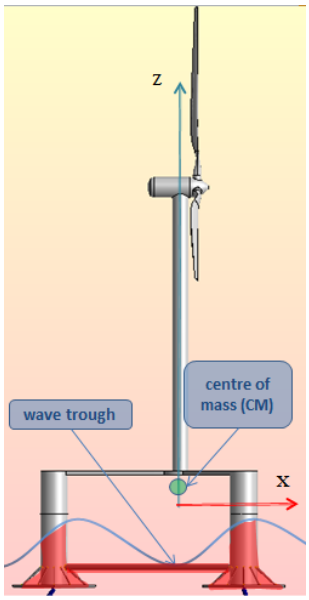

Figure 20 Wave trough passing through the CM

The example illustrates two different steps. The red-shaded areas are included to show more clearly the difference in wave loading as the wave passes through the CM.

The stress output is extracted for each of the steps in the TP points of interest. With the data collected, it follows to produce stress transfer functions of the each structural detail. The author computes these functions in Matlab to predict a time-series of the stress level in irregular sea. The irregular sea-state is obtained by generating a wave surface elevation from JONSWAP Spectrum to time-domain. As a result, stress time-series are then based on the individual wave components of JONSWAP.

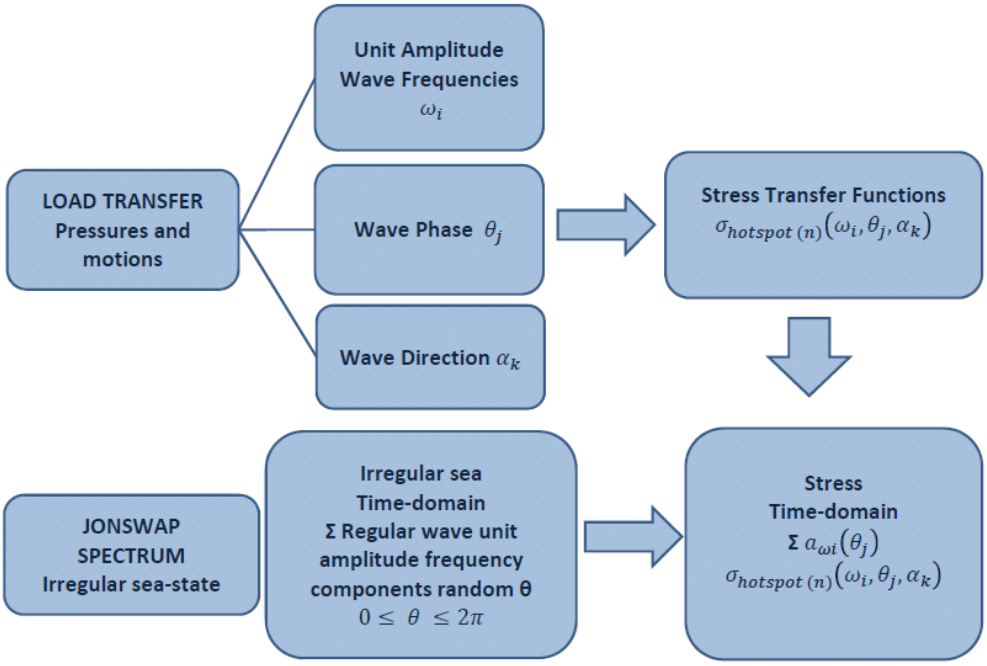

Figure 21 Load transfer scheme

This flowchart is developed by the author in chapter 6.

Under this section, it is also aimed to compute in FAST the aerodynamic loading in the wind turbine, for input in the mechanical model.

2.4 TRANSITION PIECE FATIGUE LIFE IN THE TIME-DOMAIN

Thirdly, a deterministic fatigue life analysis is conducted for the transition piece. The data used in this chapter regards the use of the stress transfer functions, to obtain the stress time-series for the omni-directional irregular sea-state considered in the points of interest of the TP.

The points of interest are identified in the mechanical model, and the transfer functions produce the stress-time series in the TP, Figure 22. Afterwards, Rainflow counting, Figure 23, is applied on the stress time-series to identify and count the repetitions of different stress amplitude blocks.

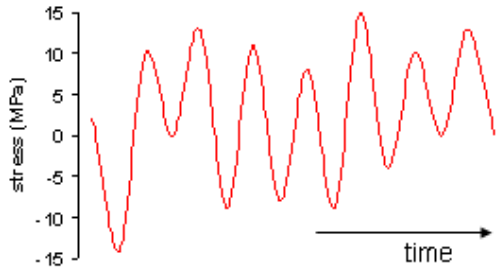

Figure 22 Spectrum loading example [10]

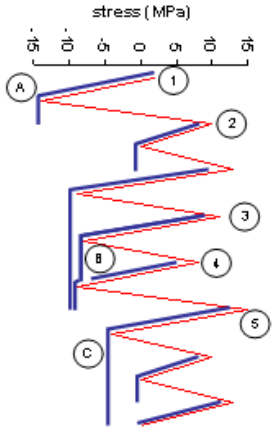

Figure 23 Rainflow counting example [10]

The transition piece structural detail is studied and evaluated according to DNV-RP-C203. Due to this, the stress transfer functions account directly for the effective hotspot stress, which is used together with the S-N Curves. The hotspot method [11] from FE analysis is used to compute the stress time-series, and accordingly the S-N Curve, D is used to calculate the fatigue life.

Palmgreen-Miner's rule is used to calculate the accumulated damage in the transition piece points of interest. The accumulated damage is obtained for all the points of interest. The environmental direction probability is taken in account by the wind rose in Moray Firth and combined with the accumulated damage to estimate resulting fatigue life.

3. ROSAP vs ASAS

In this chapter, an study and comparison of ROSAP and ASAS is covered. To validate ASAS results, the program is compared to ROSAP. The setup of ocean environment and loading is replicated in both programs. This first part helps to gain the necessary knowledge about modelling in ASAS, and setup the ocean environment needed for the semi-submersible in chapter 6.

The checklist in 2.1, includes a simplified method to justify the accuracy of the results. It is considered, that the checkpoints defined are sufficient to proceed and validate the use of ASAS in further sections. The validation of the tool, includes NFA 3.2, static load case 3.3, and a wave load case 3.4.

The dimensions of the jacket, environmental and boundary conditions are defined in sections 3.1.1, and 3.1.2 respectively.

For agreement between software, the nomenclature assigned in ROSAP is followed in the ASAS model.

3.1 JACKET MODELLING

The following list compiles the series of assumptions and/or simplifications taken into account:

- Fixed joints between legs and cross braces
- The joint node lies on the centreline of the leg
- Fixed supports at mud-line level
- Only jacket structure is analysed, no wind turbine included
- Flooded members up to LAT+sea level
- No sea-current

The input in both ROSAP and ASAS is done maintaining the same naming for the nodes and tubular members.

3.1.1 JACKET DIMENSIONS

The jacket structure has a square base, which goes from the mud-line up to the interface level. The layout is composed by two types of structural elements, legs and cross braces. Both members are tubular sections with specified dimensions in Table 1.

A 3-D view of the model in ASAS can be seen in Figure 24 and Figure 25, which include the dimensions and the z-coordinate for the different levels where the joints are located.

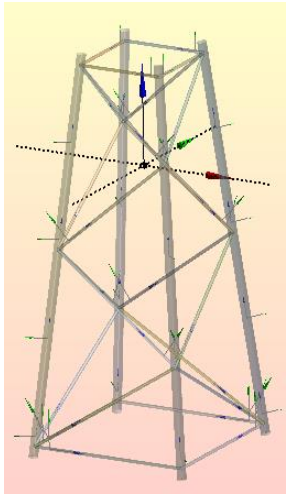

Figure 24 Jacket 3-D view

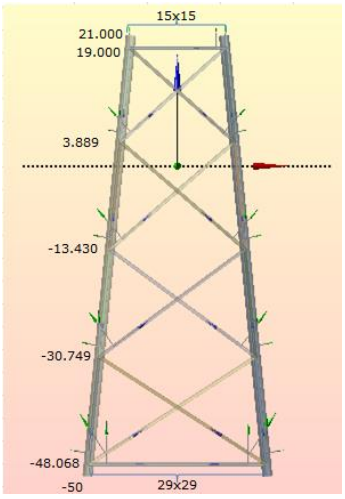

Figure 25 Joints z-level wrt LAT. Mud-line and interface level dimensions in m

Member	Ro (m)	Ri (m)
Leg	0.825	0.800
Brace	0.305	0.280

Table 1 Jacket member geometry

3.1.2 Environmental loading and boundary conditions

The environmental setup for the jacket accounts for a water depth in the location set to 50 meters. The load cases defined in 3, include by default buoyancy and the self-weight of the structure. The jacket structure is fully clamped in the supports, and no soil interaction is considered.

The static load case input, is done in still water conditions. Therefore, there is no water motion and the only loading consist of four node loads on the interface level.

In the wave load case, stream function (no. order 25) is run with a wave height of 19 meters and a wave period of 12.82 seconds. This extreme wave, could be considered as the 50-year wave for the marine structure.

3.2 Natural Frequency Analysis

NFA is a good reference when comparing finite element models between programs. Providing no gross errors in modelling are introduced, the resulting eigenfrequencies and eigenmodes should match between ROSAP and ASAS.

To carry out the NFA, a modal analysis is set up in ROSAP and ASAS. The boundary conditions on both programs are ocean environment with LAT 50 m, and fully clamped supports at the mud-line level.

The results from the modal analysis are shown below for comparison in Table 2, as well as the mode shapes of the jacket structure in Figure 26.

MODE SHAPE	ROSAP (Hz)	ASAS (Hz)	Difference (%)
1	1.9581	1.9408	-0.9
2	2.0048	1.9936	-0.6
3	2.0184	2.0169	-0.1
4	2.1753	2.1775	0.1
5	2.4450	2.4164	-1.2
6	2.4563	2.4564	0.0

Table 2 Jacket eigenfrequencies

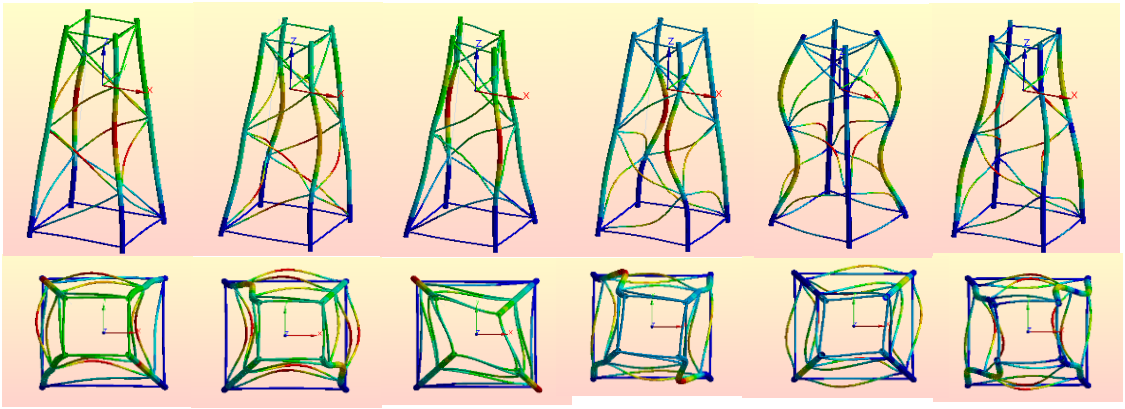

Figure 26 Jacket mode shapes 1-6, perspective and top-view

The NFA shows good agreement the finite element models in both programs. Thereby, geometry, boundary conditions and input it is considered as validated to continue with further analysis of the jacket.

3.2.1 FREE-DECAY

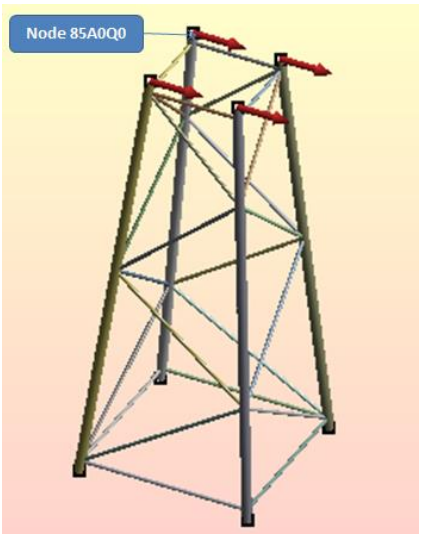

Figure 27 Free-decay setup

A free-decay test is setup in both programs to compare the 1st natural frequency with the result obtained in the modal analysis. The intention is to activate the first eigenmode by running a transient analysis with initial force on the interface level nodes as shown in Figure 27. The initial force of 250 kN applied at four interface level is constant at the beginning of the simulation and then released. The jacket enters in a free-decay and the time-series of the control nodes at the interface levels is analyzed in Matlab by an FFT script to identify the eigenfrequency of interest. The setup is shown in below.

The time-series in Figure 28 shows the free-decay in the control node. The FFT, Figure 29 and Figure 30, shows a good match between the 1st eigenfrequency obtained in the modal analyses from ROSAP and ASAS, and the free-decay test, Figure 28.

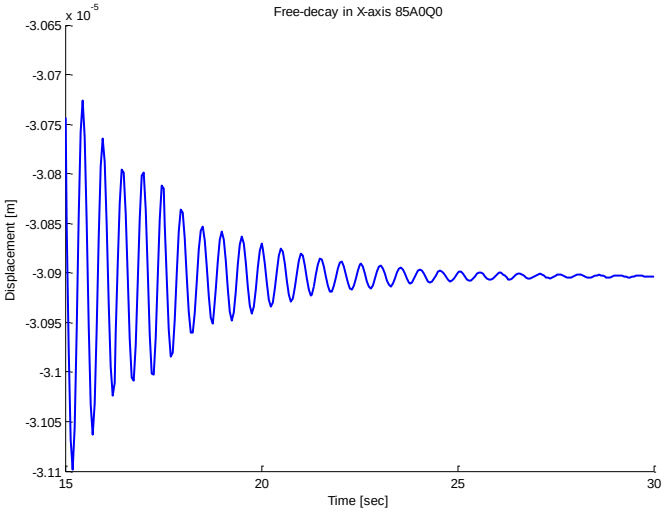

Figure 28 ASAS Free-decay test node 85A0Q0

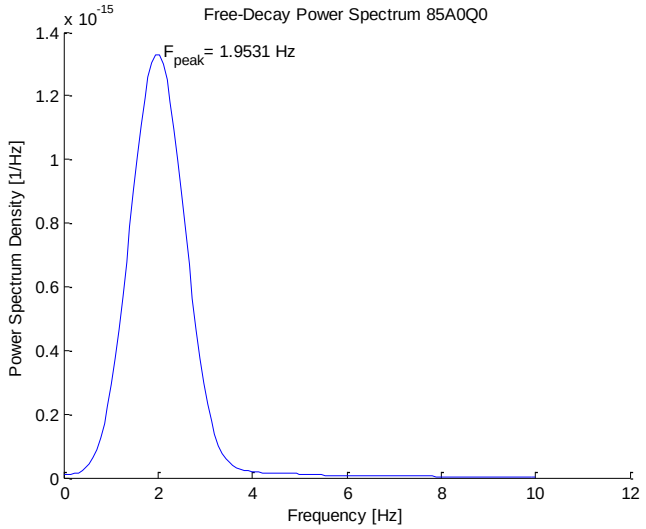

Figure 29 ASAS Power Spectrum node 85A0Q0

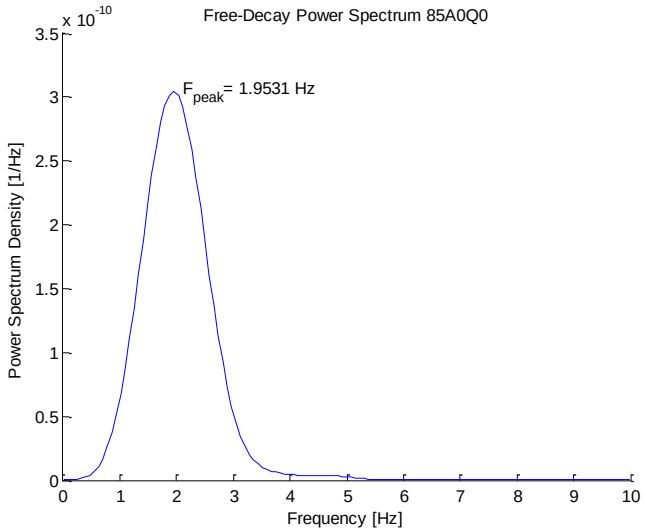

Figure 30 ROSAP Power Spectrum node 85A0Q

3.3 STATIC LOADING CASE

The static load case is introduced to further validate the model before subjecting it to wave loading. The node loads of 500 kN are applied symmetrically on the interface nodes. The water depth remains set to 50 m, and no water motion is included. The setup for this analysis is shown below in Figure 31 and Figure 32.

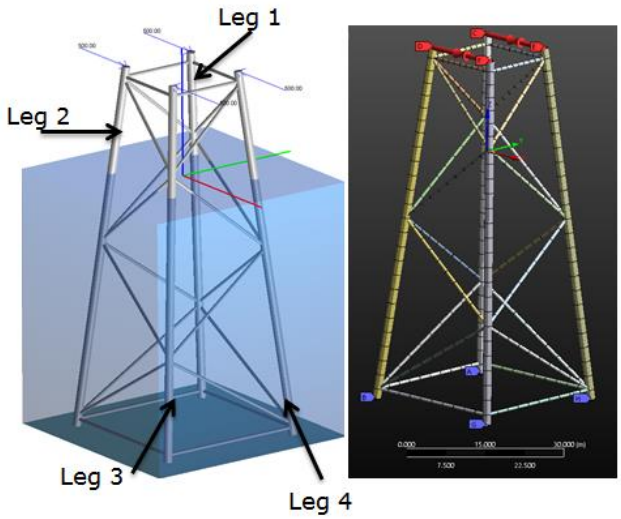

Figure 31 ROSAP and ASAS static load case

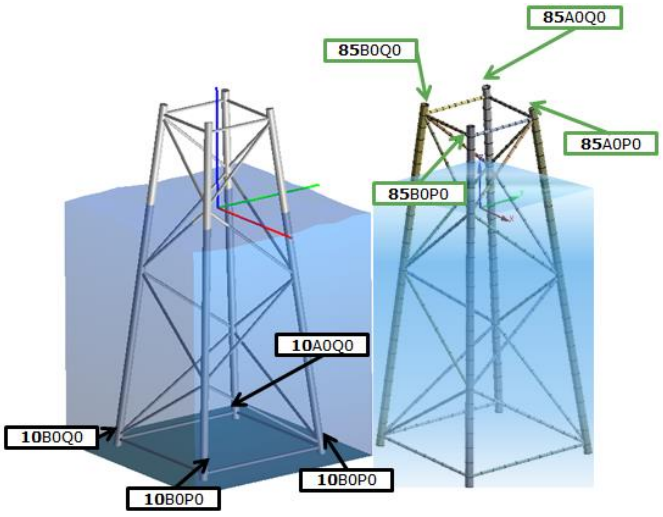

Figure 32 Nodes at support and interface level

3.3.1 NODAL DISPLACEMENTS

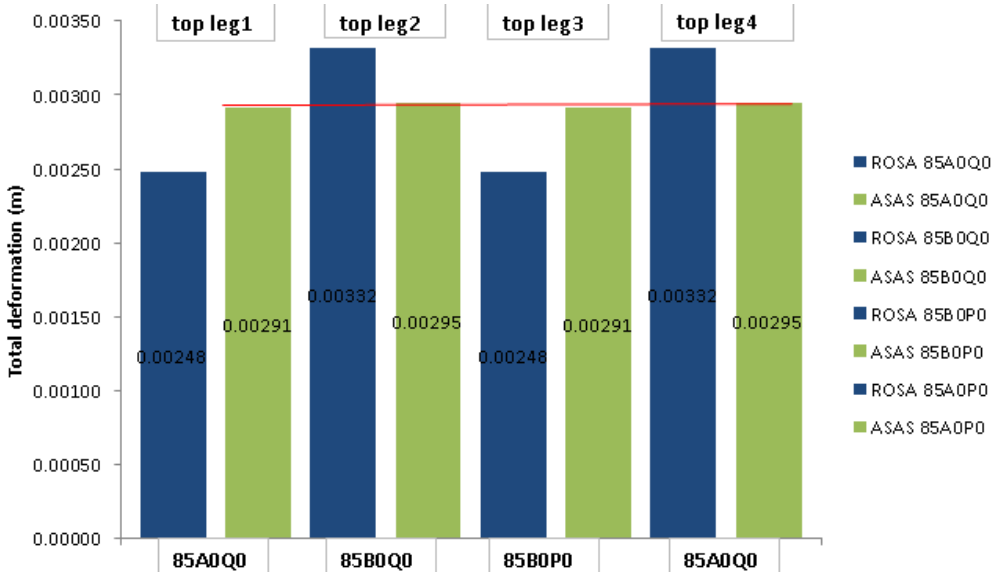

Figure 33 Nodal displacements along x-axis for interface level nodes

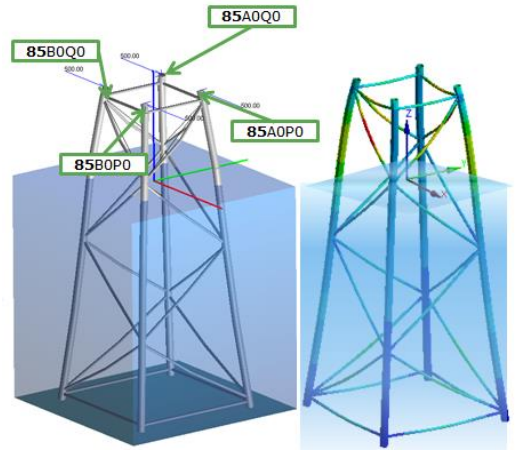

Figure 34 Deformation scaled x200

The results present more homogenous displacements at interface level, for the symmetrical static load case in ASAS.

The red horizontal line in Figure 33 remarks a mean value of the total deformation in ASAS of 0.00290 m. Despite the differences in the nodal displacements in ROSAP, the average total deformation is 0.00293. The resulting percentage difference is a 0.96%.

3.3.2 REACTIONS IN THE SUPPORTS

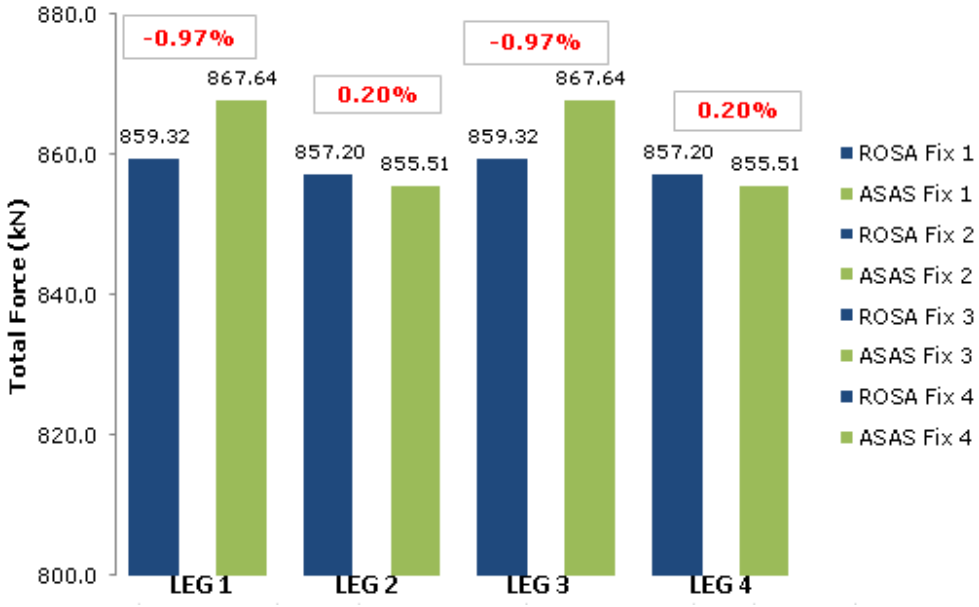

Figure 35 Total reaction force (kN) in the fixed supports

ASAS fixed support			ROSAP fixed support		
10A0Q0	**result**	**units**	**10A0Q0**	**result**	**units**
Fx	50.34	kN	Fx	-39.81	kN
Fy	-44.97	kN	Fy	36.27	kN
Fz	865.01	kN	Fz	-857.63	kN
Total	**867.64**	**kN**	**Total**	**859.32**	**kN**
10A0P0	**result**	**units**	**10A0P0**	**result**	**units**
Fx	-48.35	kN	Fx	39.27	kN
Fy	-43.98	kN	Fy	36.60	kN
Fz	853.01	kN	Fz	-855.52	kN
Total	**855.51**	**kN**	**Total**	**857.20**	**kN**
10B0Q0	**result**	**units**	**10B0Q0**	**result**	**units**
Fx	48.35	kN	Fx	-39.27	kN
Fy	43.98	kN	Fy	-36.60	kN
Fz	853.01	kN	Fz	-855.52	kN
Total	**855.51**	**kN**	**Total**	**857.20**	**kN**
10B0P0	**result**	**units**	**10B0P0**	**result**	**units**
Fx	-50.34	kN	Fx	39.81	kN
Fy	44.97	kN	Fy	-36.27	kN
Fz	865.01	kN	Fz	-857.63	kN
Total	**867.64**	**kN**	**Total**	**859.32**	**kN**
TOTAL ASAS	**3446.30**	**kN**	**TOTAL ROSAP**	**3433.04**	**kN**

Table 3 Component and total reaction in the supports, static loading

On contrast with the comparison of nodal displacements in 3.3.1, ROSAP shows more higher reactions at the supports than ASAS.

Overall, the total reaction in the supports compared between both models only represents a difference of 0.38%, with ASAS slightly above ROSAP total reaction, Table 3.

3.3.3 MEMBER AXIAL FORCES

To complete the static loading case, the axial forces on one of the faces of the jacket are compared. The members are identified in Figure 36, and the axial force along the member length is plotted for each comparing ROSAP and ASAS.

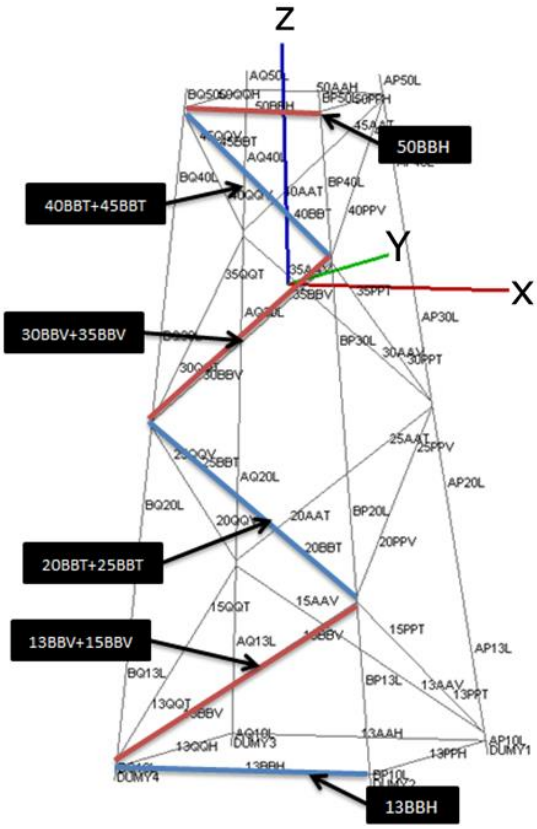

Figure 36 Jacket members checked. ROSAP model

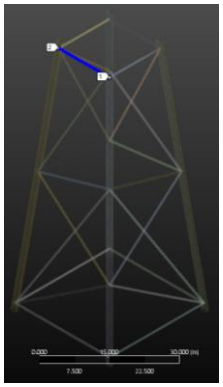

Figure 37 ASAS, member 50BBH

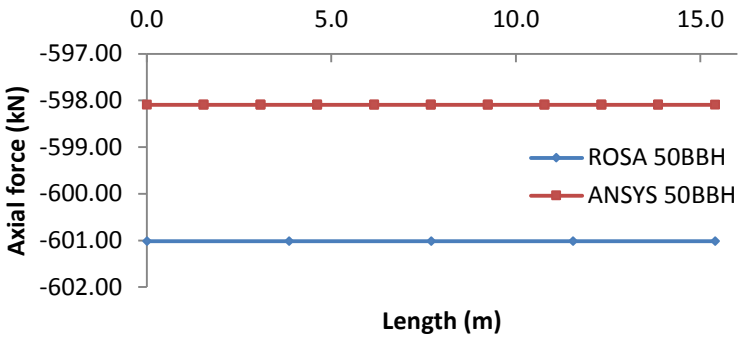

Difference 0.49% of ASAS above ROSAP

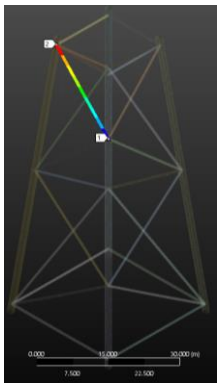

Figure 38 ASAS, member 40BBT+45BBT

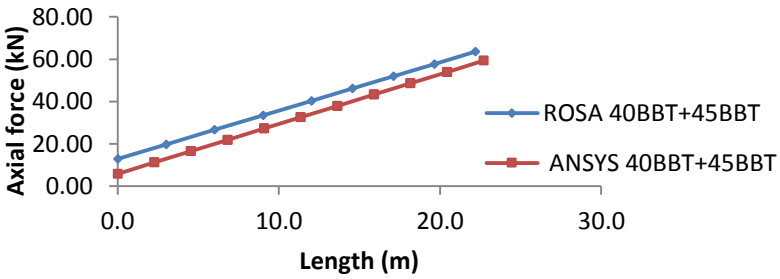

ROSAP is loaded a 6.69% over ASAS in the most loaded member length. Length 0.0 m indicates the lowest point w.r.t. z-axis for inclined members.

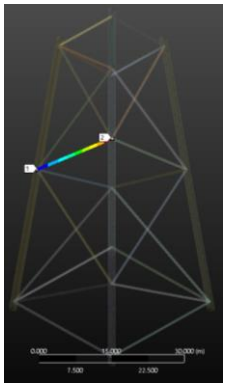

Figure 39 ASAS, member 30BBV+35BBV

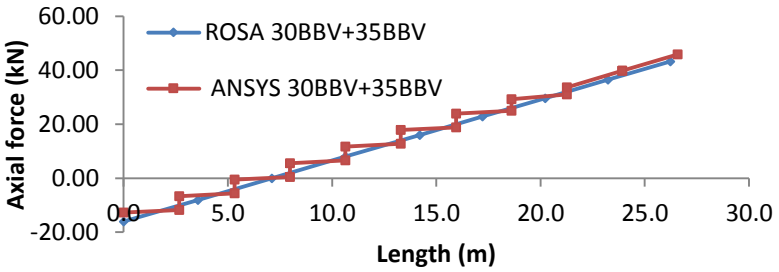

ASAS is a 6.15% above ROSAP in the most loaded member length.

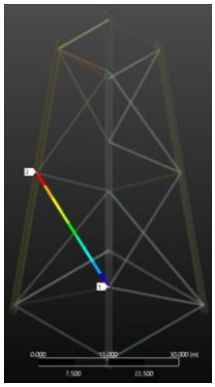

Figure 40 ASAS, member 20BBT+25BBT

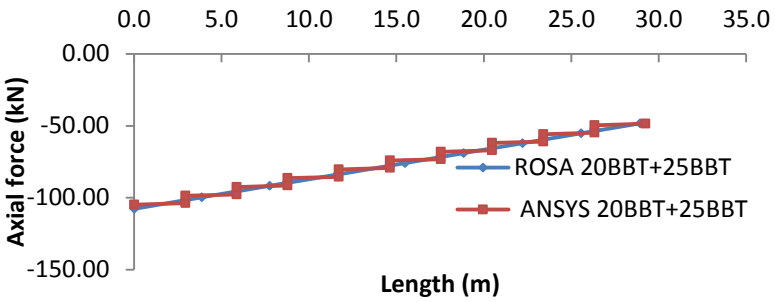

ROSAP presents a difference of 0.74% above ASAS in the most loaded member length.

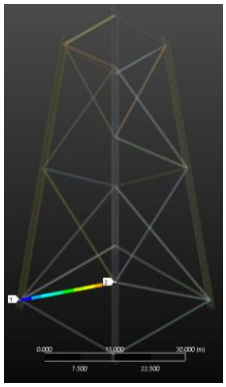

Figure 41 ASAS, member 13BBV+15BBV

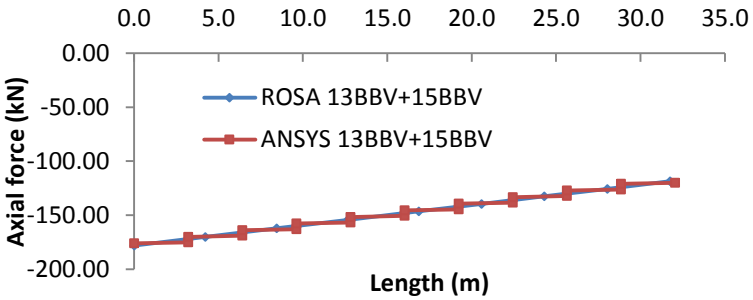

ROSAP presents a difference of 1.17% above ASAS.

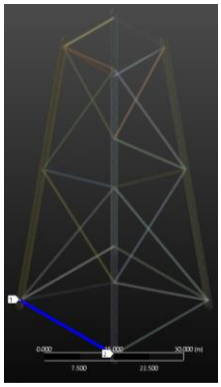

Figure 42 ASAS, member 13BBH

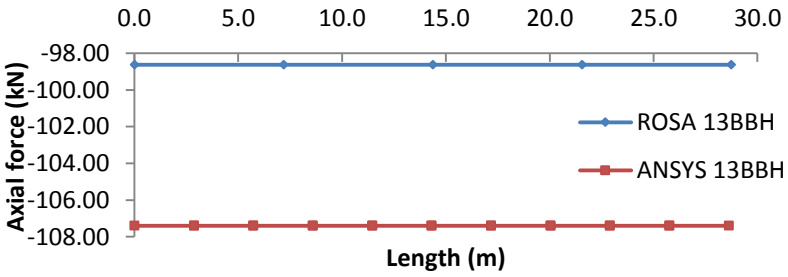

ROSAP shows a uniform loading in compression which is shows the larger difference with a 8.90 % below ASAS.

Overall the results present a good agreement, regarding the order of magnitude of the axial showing a reasonable behaviour for tension and compression of the cross braces in study.

3.4 WAVE LOADING CASE

This analysis consist of running the 50-year wave, by using Stream function theory (no. order 25). The wave loading direction is aligned with x-axis, direction 0º, with H=19 m and T=12.82 s.

3.4.1 NODAL DISPLACEMENTS

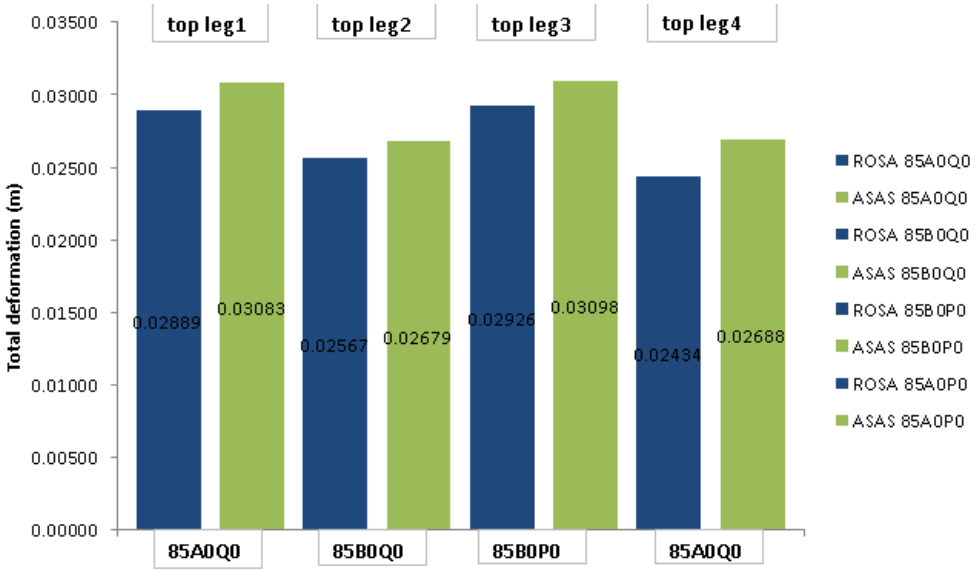

Figure 43 Nodal displacements, wave loading

ASAS displays larger nodal displacements at interface level, Figure 32, for wave loading. The total deformation difference percentage is a 6.33%.

3.4.2 REACTIONS IN THE SUPPORTS

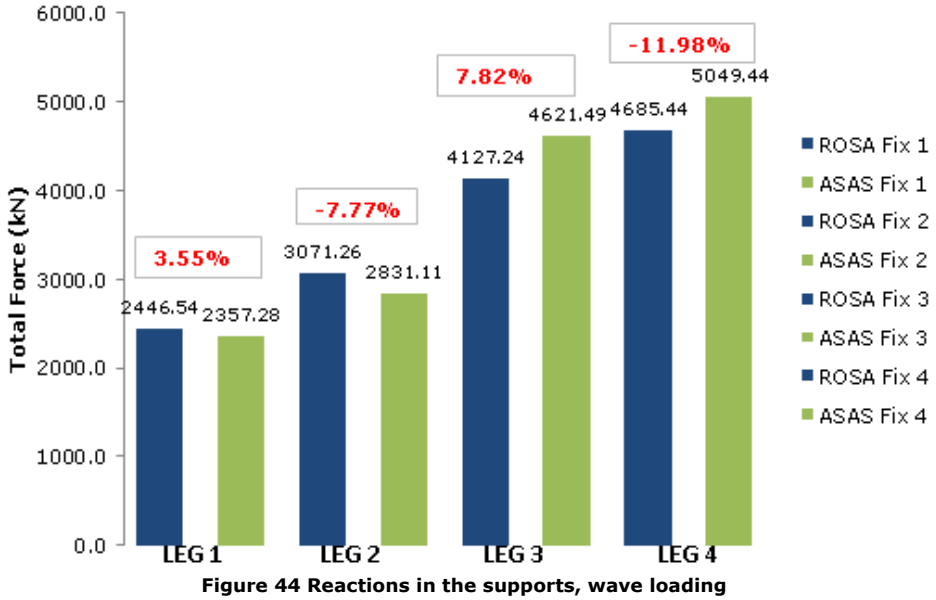

Figure 44 Reactions in the supports, wave loading

ASAS fixed support			ROSAP fixed support		
10A0Q0	**result**	**units**	**10A0Q0**	**result**	**units**
Fx	-534.80	kN	Fx	571.70	kN
Fy	205.45	kN	Fy	-277.96	kN
Fz	-2286.60	kN	Fz	2362.51	kN
Total	**2357.28**	**kN**	**Total**	**2446.54**	**kN**
10A0P0	**result**	**units**	**10A0P0**	**result**	**units**
Fx	-1988.80	kN	Fx	2071.18	kN
Fy	-462.28	kN	Fy	353.90	kN
Fz	4618.20	kN	Fz	-4187.88	kN
Total	**5049.44**	**kN**	**Total**	**4685.44**	**kN**
10B0Q0	**result**	**units**	**10B0Q0**	**result**	**units**
Fx	-1727.10	kN	Fx	1895.29	kN
Fy	-200.55	kN	Fy	280.64	kN
Fz	-2234.30	kN	Fz	2400.36	kN
Total	**2831.11**	**kN**	**Total**	**3071.26**	**kN**
10B0P0	**result**	**units**	**10B0P0**	**result**	**units**
Fx	-786.04	kN	Fx	652.48	kN
Fy	456.69	kN	Fy	-347.08	kN
Fz	4531.20	kN	Fz	-4060.53	kN
Total	**4621.49**	**kN**	**Total**	**4127.24**	**kN**
TOTAL ASAS	**14859.32**	**kN**	**TOTAL ROSAP**	**14330.48**	**kN**

Table 4 Component and total reaction in the supports, wave loading

Overall, the total reaction in the supports compared between both models differs a 3.56%, with ASAS above ROSAP total reaction, Table 3.

3.4.3 MEMBER AXIAL FORCES

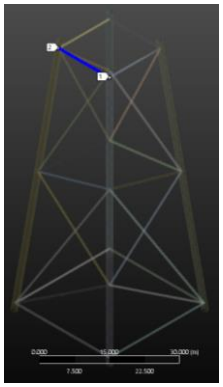

Figure 45 ASAS, member 50BBH

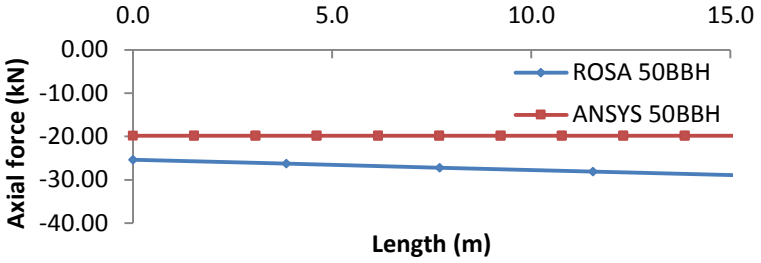

Difference 0.49% of ASAS above ROSAP.

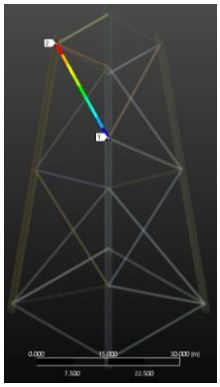

Figure 46 ASAS, member 40BBT+45BBT

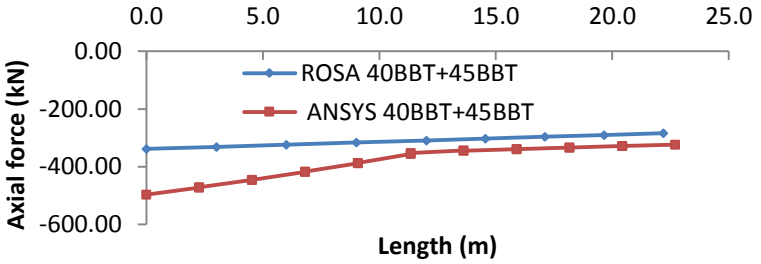

The compression axial force seems to converge closer to the interface level around -300 kN. The deviation in the lowest joint of the member goes up to almost a 50%.

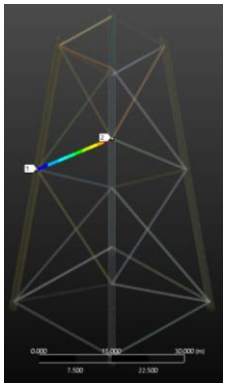

Figure 47 ASAS, member 30BBV+35BBV

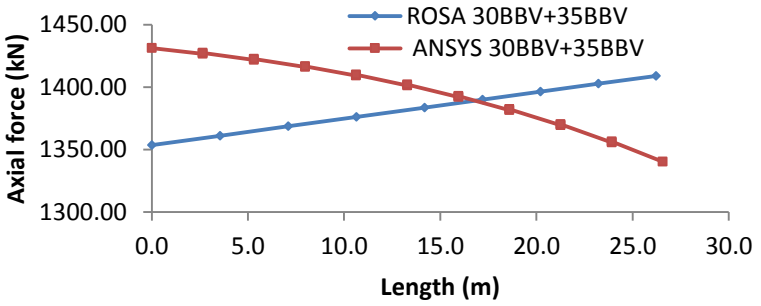

Despite both members are in tension. This is the only member for which the axial force shows a different trend in both programs. The deviation reaches a 5.74% of ASAS above ROSAP.

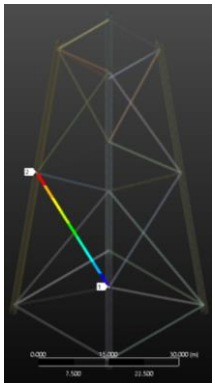

Figure 48 ASAS, member 20BBT+25BBT

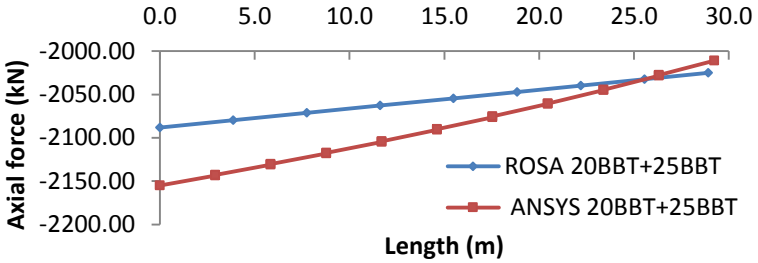

The larger difference occurs in the lowest joint, with a deviation of ROSAP 3.20% above ASAS.

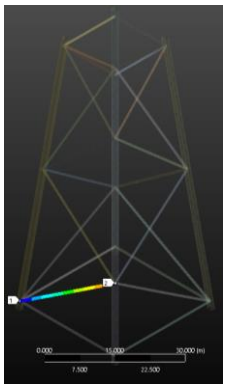

Figure 49 ASAS, member 13BBV+15BBV

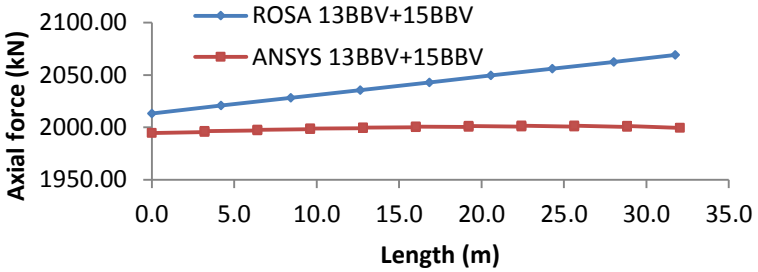

While both programs have a trend of increased loading, ROSAP accounts for an axial force a 3.36% higher than ASAS in the largest point.

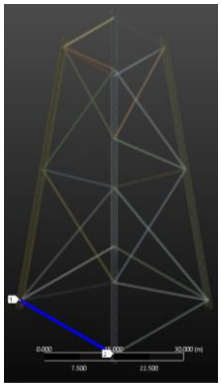

Figure 50 ASAS, member 13BBH

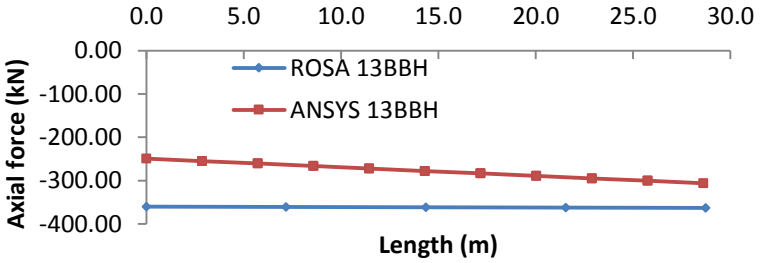

ROSAP presents a uniform loading in compression, while ASAS shows a lower of axial compression which increases towards the opposite face loaded.

3.5 CONCLUSIONS

The results included in sections 3.2 and 3.3, indicate a reliable setup of the models in ROSAP and ASAS. The major difference found in the NFA is 1.2% for the 5th mode shape, while the rest of natural frequencies obtained in the modal analysis match with a deviation under a 1%. The static load case, concludes with more notable differences. Mainly these can be noticed when the axial member forces are compared. Overall, the maximum difference is shown for the cross brace 13BBH, at the supports level, where ASAS exceeds the ROSAP axial compression by an 8.90%. The nodal displacements at interface level, and reactions in the supports deviates under 1% as presented in sections 3.3.1 and 0 respectively.

Turning now to the wave loading case, there are notable differences between ASAS and ROSAP. The larger deviations are found comparing one by one the cross braces axial forces. As an explanation, it could be pointed out that ASAS calculates the forces on Morison elements using Morison relative equation (1), while ROSAP applies Morison equation (2). The former, accounts for the structure motion (velocity and acceleration) [12], while the latter does not include these terms.

$$\{F/L\} = \rho \cdot A \cdot \{\ddot{v}\} + C_a \cdot \rho \cdot A\{\ddot{v} - \ddot{u}\} + \frac{1}{2}\rho \cdot C_D \cdot D|\{\dot{v} - \dot{u}\}|\{\dot{v} - \dot{u}\} \quad \textbf{(1)}$$

$$\{F/L\} = \rho \cdot C_m \cdot \{\ddot{v}\} + \frac{1}{2}\rho \cdot C_D \cdot A \cdot \dot{v}|\dot{v}| \quad \textbf{(2)}$$

$\{F/L\}$	Vector of loads per unit length
ρ	Fluid density
A	Cross sectional area perpendicular to fluid direction
D	External diameter of the tube element
Ca	Added mass coefficient
Cm	Inertia coefficient $Cm = Ca + 1$
Cd	Drag coefficient
$\dot{v}, \ddot{v}$	Fluid velocity and acceleration
$\dot{u}, \ddot{u}$	Structure velocity and acceleration

Based on the results, it is concluded that ASAS is validated to assist in further analysis, and carry out the semi-submersible load transfer from AQWA.

4. SEMI-SUBMERSIBLE HYDRODYNAMIC MODEL

The hydrodynamic modelling of the semi-submersible has a relevant role on the overall performance of the structure. The scope in this chapter, is to design and test a semi-submersible suitable for the reduced water depth in Moray Firth.

The job carried out here, is mainly based on findings presented in [6]. The design flowchart is followed as shown in Figure 15. The assessment of the semi-submersible starts by defining basic geometry such as main column diameter, heave plates, and ballast levels. After checking that the condition of hydrostatic stability ensures the buoyancy, the platform is studied with regarding natural frequencies and RAOs. The latter step is critical, since the results are an indicator of the floating foundation behavior in irregular sea-states.

It is assumed that the mooring lines implemented in [6] will need redesign, in order to suit the environmental conditions of the selected location.

4.1 SEMI-SUBMERSIBLE DESCRIPTION

A semi-submersible, is a floating platform supported by columns. These columns provide the buoyancy on the platform, and serve as support for the structures installed on the topside. Ballasting adds weight and stability to the floater by increasing the mass of the overall system, foundation and wind turbine.

Other elements shown in Figure 7, such as the heave and/or pontoons are installed for improvement of the floater behavior in the sea. The effect of these elements regards a decrease of heave and rotational motions (roll and pitch), due to the water entrapped which counteracts the response of the semi-submersible.

From oil and gas literature [3], it could be pointed out a reference for natural frequency values in semi-submersibles.

Semi-Submersible	Eigenperiods (sec)
Surge	>100
Sway	>100
Heave	19-35
Roll	50-90
Pitch	50-90
Yaw	>100

Table 5 Oil&Gas Semi-submersibles, reference eigenperiods

Although the eigenperiods in Table 5 serve for large semi-submersibles, these are a useful to determine the validity of the results when addressing this floating foundation in offshore wind. It can be observed that the natural periods presented, are relatively large, which indicates the platform eigenperiods should be above the most common sea-states peak periods.

4.1.1 HYDRODYNAMIC BEHAVIOR

The hydrodynamic behavior is principally referred to the platform motions, which are the 6 rigid-body DOF: surge, sway, heave, roll, pitch, and yaw. Due to these motions, tension is introduced in the mooring system, and most importantly, the platform response is transferred to the wind turbine. The six DOFs aforementioned must account for mild motions to lessen the effects on the structural elements that form a FOWT.

The semi-submersible must account for buoyancy, to ensure the integrity of the wind turbine installed on the topside. The buoyant elements in the platform are the main columns.

A remarkable characteristic in a semi-submersible regards its natural frequencies and RAOs. While another floating concepts, such as a TLP is constrained for certain DOFs i.e. heave, semi-submersible are compliant in all DOFs. Due to the mooring system, catenary lines, the restoring forces acting on the platform are small since these account for the suspended weight of the mooring lines in the sea.

The semi-submersible has a soft behavior on the horizontal plane, these refers to surge and sway motions. The semi-submersible subjected to wave and wind loading, drifts until the tension induced by the mooring lines rises to keep the platform in station.

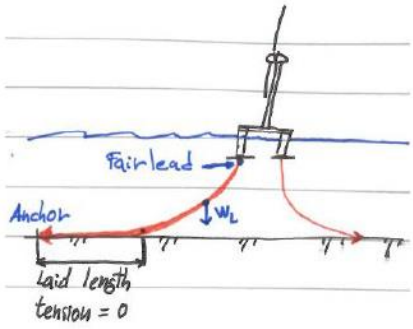

Figure 51 Mooring lines restoring concept

This tension depends on the mooring line submerged weight, W_L in Figure 51. The suspended length of the catenary accounts for the restoring force in stationkeeping, and it varies together with the laid length on the seabed.
This also implies that rotational motions, pitch and roll occur during displacements.

Therefore, the key to minimize motions relies on the natural frequencies of the structure, and the location where the semi-submersible is installed conditions the design process. In order to achieve mild motions, the platform natural frequencies must be tuned out of the wave spectrum, which is covered in section 4.4.2.

4.1.2 BALLAST

The ballast provides stability to the floating foundation, and it is installed inside the main columns. The ballasting material for a semi-submersible is normally water $\rho = 1025\ kg/m^3$, although concrete or combination of both might be used. The use of ballast is also beneficial from the structural point of view, the water column height inside the main columns exert a hydrostatic pressure that balances the same height of external hydrostatic pressure on the submerged column.

Due to the geometry and dimensions of the main columns, the platform would be normally buoyant. However the steel weight of the hull is insufficient for station keeping reasons, and additional stability is provided by ballasting. The ballast material must be constrained inside the main columns to avoid motions induced by external loading, and be confined in chambers.
There are three options to ballast a floater:

- Passive ballast, with fixed properties.
- Active ballast, varying the levels of ballast according to platform response.
- Combination of both, one passive always present and set properties accordingly to environmental loading conditions.

For a floating structure in open sea, a combined system would be the most appropriated to respond effectively against extreme seas and varying water levels. Due to limitation in AQWA, this study only applies a passive ballast level which is fixed to the platform dimensions.

4.1.3 MOORING SYSTEM

Different mooring systems are suitable for floating foundations. These are mainly three: tethers, taut-legs and catenary.

The difference between them relies on the pretension of the lines. Whereas tethers, taut legs are cables in pretension, the catenary line is freely suspended in the sea between the fairlead position and the anchor. The characteristic that distinguishes tethers and taut-legs is that the latter is not perpendicular with the seabed.

Conceptually the design of a semi-submersible is done by the use of catenary lines. The fairlead is installed in the semi-submersible and the anchor hold into the seabed. Each catenary is divided in four parts: anchor, length of the catenary laying on the bottom soil, suspended part and fairlead.

Considering anchor and fairlead as fixed positions on the seabed, and semi-submersible respectively. The restoring forces are based on the mooring line weight. The submerged length suspended in water contributes to the station keeping. Besides, the laid length varies as the platform moves by increasing or decreasing the weight contribution for on each catenary.

The water depth is an important factor to consider in the design mooring lines:

- Deep waters imply the use of large catenaries. While the weight contribution benefits station keeping, the tension induced on the fairlead could increase considerably. This is due to a large suspended length compared to laid length. A solution to reduce fairlead tension could be the installation of subsea buoys.

- Oppositely, when the water depth range is within shallow-intermediate, the problem regards the lack of enough suspended length. As a result the restoring mooring forces become small. The fix proposed for this situation consist of mounting clump weights on the catenary line.

The catenary system is spread from the fairlead position as multiple lines. This produces a notable footprint along with the floating foundation. As recommended practice, it can be found in [3] that the footprint should be from 5-20 times the water clearance, distance between fairlead and sea-bottom, Figure 52.

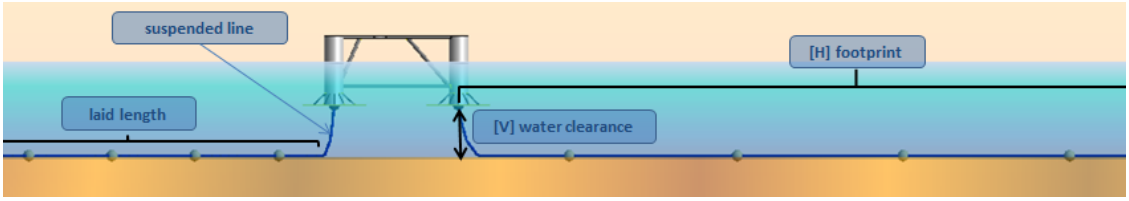

Figure 52 Catenary footprint [H] and water clearance [V]

4.1.4 ANCHOR SYSTEM

The seabed soil conditions the design of anchor systems. Some relevant parameters are the density and shear strength of the bottom soil, as these contribute as resistant mechanisms.

The anchor system must provide with enough strength to resist effectively the uplifting tension induced by mooring lines motions consequence of the platform response.

Various anchors could show to be suitable for a given soil. The following list mention some of the alternatives:

- Gravity anchors
- Suction piles
- Driven piles
- Plate anchors

An study of the soil is not included in this document, and the anchors are considered fully clamped on the seabed. Anchor and mooring system, require a special focus to determine the right setup to be implemented.

4.1.5 HEAVE PLATES

A heave plate could be classified as a shell structure. The element is wide in the horizontal plane and has a reduced height.

The main purpose of heave plates is to provide additional drag and mass in the direction perpendicular to the water surface, z-axis, to the main columns. The addition of mass, benefits the response of the platform against the most critical motions, roll/pitch and heave. The former two rotational motions, are critical as the response is translate to the nacelle level on the wind turbine.

In the interest of providing with more stability the semi-submersible, heave plates are a installed. The modelling is detailed in section 4.2.5.

The review of diverse literature in the topic [13] [9], and further testing conducted in [6], indicates that heave plates with hexagon-shaped yield better performance reducing motions than circular-shaped ones. This is mainly due to a larger drag coefficient in the former compared to a circular. Therefore the heave plate model implemented for the semi-submersible is hexagon-shaped.

4.1.6 CROSS BRACES AND STIFFENERS

These elements are included to reinforce the semi-submersible hull.

Cross bracing could be disposed joining main columns and topside. All cross braces must be flooded to avoid problems related with hydrostatic pressure.

Stiffeners fall under the same category serving as reinforcement of structural elements. For this case, the stiffeners are placed as a joint between each main column and the heave plate.

4.2 SEMI-SUBMERSIBLE DESIGN

The modelling stage is carried out in ANSYS AQWA. A preliminary design involves to setup the geometry based on supporting the offshore wind turbine, which properties are included in Table 10.

The semi-submersible model in this document, is compound by two distinctive elements: pressure panels and Morison elements. To identify properly which type of element should be used to model the semi-submersible, section 4.2.2 shows a view of the problem based on the Keulegan-Carpenter number and the sea-states in Moray Firth.

The major interest on the hydrodynamic analysis is to determine wave loading and motions on the semi-submersible. To produce accurate results, the structural elements need to be identified for modelling purposes so that the wave exciting forces and resulting motions are calculated with the most suitable theory: potential flow or flow separation. The criteria for modelling is defined in section 4.2.2, where the main columns and cross braces are classified with reference to Keulegan-Carpenter number.

4.2.1 SEA-STATES

The sea-states are given by the metocean data in Moray Firth. These are shown below in Table 6.

SEA	Hs (m)	Tp (s)	wp (rad/s)	Wind speed (m/s)
1	1.25	7.04	0.893	4.40
2	2.25	7.73	0.813	8.10
3	3.25	8.53	0.736	11.50
4	4.25	9.17	0.685	15.00
5	5.25	9.75	0.644	18.60
6	6.25	9.78	0.642	22.40
7	7.25	10.50	0.598	25.00
8	9.00	13.40	0.469	25.00

Table 6 Sea-states in Moray Firth

The sea-states are described by JONSWAP Spectrum. A sea-state for this spectrum is defined by three parameters: significant wave height (Hs), peak period (Tp), and the peak enhancement factor (γ).

In order to produce a plot of JONSWAP spectrum, it is required to define the range of frequencies:

ω_{min}	Lower frequency bound
$\Delta\omega$	Frequency steepness
ω_{max}	Upper frequency bound

Table 7 Frequency range and steepness

The formulation for JONSWAP Spectrum is as follows:

$$S_J(\omega) = A_\gamma \cdot S_{PM}(\omega) \cdot \gamma^{exp\left(-0.5\cdot\left(\frac{\omega-\omega_p}{\sigma\cdot\omega_p}\right)^2\right)} \quad \textbf{(3)}$$

Where $S_{PM}(\omega)$ is the Pierson-Moskowitz spectrum:

$$S_{PM}(\omega) = \frac{5}{16}\cdot H_S^2 \cdot \omega_p^2 \cdot \omega^{-5} \cdot exp\left(-\frac{5}{4}\cdot\left(\frac{\omega}{\omega_p}\right)^{-4}\right) \quad \textbf{(4)}$$

The peak enhancement factor is fixed to 3.3, for the North Sea. By using (3) for the given sea-states the energy spectrum is shown in Figure 53.

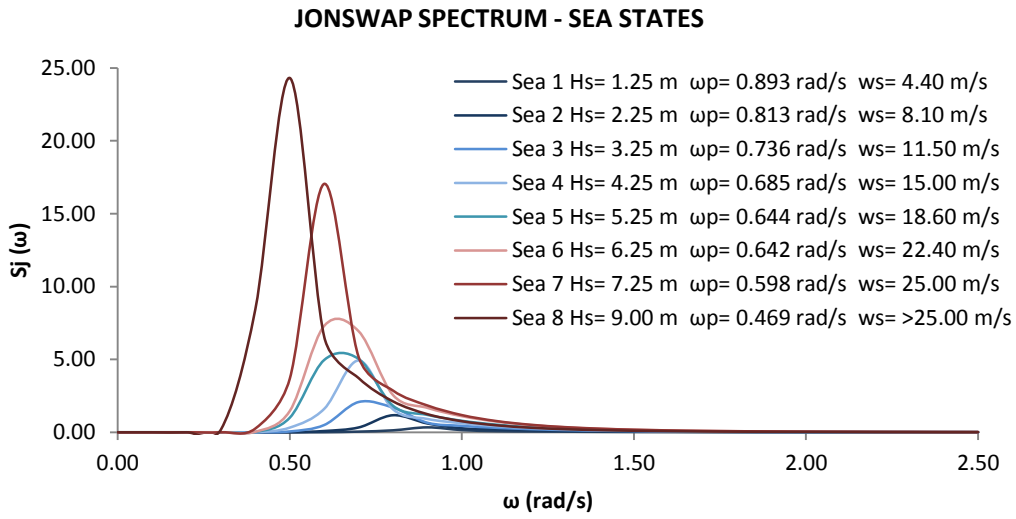

Figure 53 Sea-states JONSWAP Spectrum

4.2.2 WAVE LOADING

The semi-submersible is mainly subjected to wave loading. The reference to determine the validity of the theory applied taken in this document is the Keulegan-Carpenter number (5). When KC > 2, flow separation occurs and the body subjected to wave loading is better modelled by Morison elements. On the other hand, for KC < 2 potential flow theory applies, which is a diffraction / radiation problem.

$$KC = \frac{uT}{D} \quad \textbf{(5)}$$

In order to obtain the KC number, u horizontal fluid velocity needs to be calculated. Depending of the water depth classification: shallow, intermediate, deep. In linear wave theory, the velocity is calculated with a different set of formulas for each of the water depths aforementioned.

Firstly, the sea-states in Table 6 is classified as shallow, intermediate or deep water. For this the wave length (λ) is calculated according to the formulas given in [14]. The classification depends on the wave length (λ) and water depth 40.2 m, with the following criteria:

Shallow waters	Intermediate waters	Deep waters
$d/\lambda < 1/20$	$1/20 < d/\lambda < 1/2$	$d/\lambda > 1/2$

Table 8 Water depth criteria for classification

SEA	Hs (m)	Tp (s)	λ (m)	d/λ	Classification
1	1.25	7.04	77.25	0.52	Deep Waters
2	2.25	7.73	92.47	0.43	Intermediate Waters
3	3.25	8.53	111.17	0.36	Intermediate Waters
4	4.25	9.17	126.49	0.32	Intermediate Waters
5	5.25	9.75	140.45	0.29	Intermediate Waters
6	6.25	9.78	141.18	0.28	Intermediate Waters
7	7.25	10.50	158.44	0.25	Intermediate Waters
8	9.00	13.40	226.06	0.18	Intermediate Waters

Table 9 Sea-states classification

In view of the results in
Table 9, the fluid horizontal velocity is calculated as follows for deep (6) and intermediate waters (7).

$$u = \omega a e^{kz} sin(\omega t - kx) \quad \textbf{(6)}$$

$$u = \omega a \frac{\cosh k(z+d)}{\sinh kd} sin(\omega t - kx) \quad \textbf{(7)}$$

Where ω is the peak frequency in rad/s, a is the wave amplitude $Hs/2$, $k = 2\pi/\lambda$ is the wave number, z stands for the depth on which the velocity is calculated, and d corresponds to the water depth.

To account for the maximum velocity the term $sin(\omega t - kx)$ is considered equal to 1 in both (6) and (7).

The velocities obtained, yield the following KC Numbers which are plotted for the main column Figure 54, and braces Figure 55, to justify the modelling choice as diffraction/radiation elements or Morison elements.

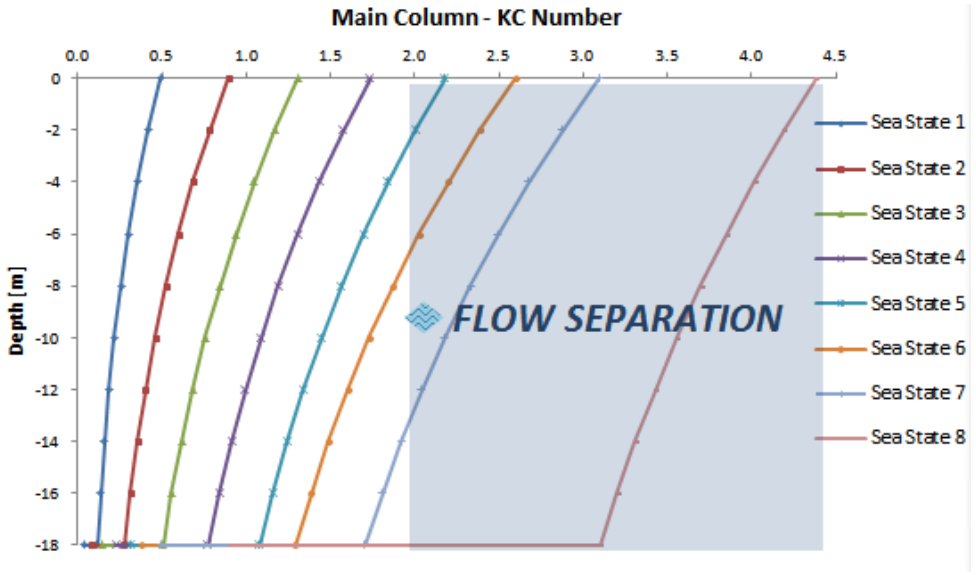

Figure 54 KC Number for main columns, diameter 8 m, varying with water depth

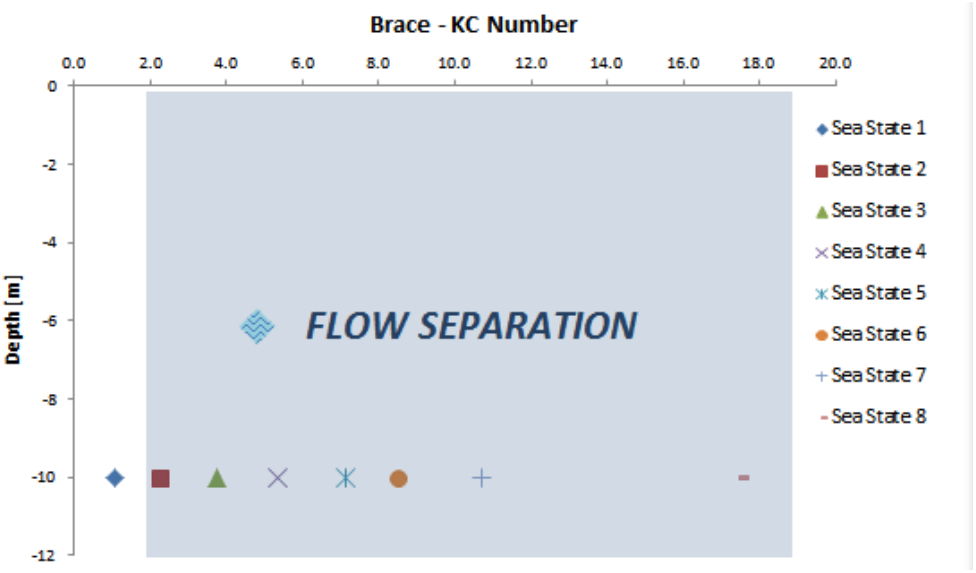

Figure 55 KC Number for brace members. Diameter 1.626 m

It can be seen that the main columns fall mostly on the potential flow area, while the cross braces could be considered exclusively in the flow separation. Therefore, the modelling of the semi-submersible is carried out with a combination of diffraction/rad. For the hull structure, and Morison elements for cross-braces.

4.2.3 WIND TURBINE

The wind turbine used for this project is the NREL 5MW offshore wind turbine [13]. To implement it, different point masses are included in the hydrodynamic model. A point mass is defined by position w.r.t. the semi-submersible, mass and moments of inertia. The point masses included are: tower, nacelle and hub, while the rotor mass is include as a lumped mass, due to software limitation for including properly the moments of inertia of the later.

The properties of the wind turbine can be seen in Table 10, from the literature [13]:

Parameter	Wind turbine	Units
Rating	5	MW
Control	Pitch-to-feather	-
Cut-it, Rate, Cut-out wind speed	3, 11.4, 25	m/s
Cut-in, Rated Rotor Speed	6.9, 12.1	rpm
Rotor Mass	110,000	kg
Nacelle Mass	240,000	kg
Nacelle Inertia about Yaw Axis	2,607,890	kg m^2
Tower Mass	247,160	kg
Tower Inertia about Roll/Pitch Axis	122,090,000	kg m^2
Tower Inertia about Yaw axis	1,756,800	kg m^2
Hub Mass	56,780	kg
Hub Inertia about Low-Speed Shaft	115,926	kg m^2

Table 10 NREL 5MW Wind Turbine properties

4.2.4 PLATFORM MASS

The platform mass is estimated on regards of the main column diameter and submerged volume. The mass of the hull determines the ballast levels and should enable the condition of buoyancy.

For input in ANSYS AQWA. The platform mass is calculated by an empirical formula, considered as good engineering practice [6]:

$$M = 0.225 \times V \times \rho \quad \textbf{(8)}$$

Where M is the platform primary steel, V is the submerged volume, and ρ the water density. Despite cross braces, stiffeners and heave plates are fully submerged. The volume in (8) is exclusively referred to the displaced volume of water by the main columns.

The platform mass is input in ANSYS AQWA as a point mass, which also accounts for the moments of inertia. To obtain the moments of inertia, the model is transferred to ANSYS Mechanical.

The semi-submersible parameters are determine by iteration, and the final properties are summarized in Table 16

4.2.5 HEAVE PLATES

The modelling of heave plates in ANSYS AQWA presents some difficulties. Due to the thin geometry of this structural element, the use of pressure panels do not capture the effects of heave and roll/pitch as the heave plate is collinear with the horizontal fluid velocity. There is no direct path to implement a heave plate without modelling it independently.

ANSYS recommends to model heave plates by Morison disc elements. A disc element is defined by diameter, z-axis drag coefficient Cdz, and z-axis added mass Caz which are normal to the disc. The difficulty relates to the geometry input of a hexagonal-shaped heave by using a Morison disc.
Moreover, a disc element lacks of mass and thickness. Mass and moments of inertia need to be calculated, along with the buoyancy that accounts for the submerged volume.

To solve this problem the following steps are suggested:

- Define heave plate circular diameter, at least twice column diameter [6]
- Determine the side length for a hexagon that produces the same area as the circle
- AQWA:
  - Input Morison disc element with the diameter of the circle
  - Input doubled drag and added mass coefficients of the hexagon
  - Input Point mass for the disc: mass and moments of inertia
  - Input Buoy point for the disc: buoyancy of submerged volume

To determine the mass and moments of inertia of the heave plate, a FEM is setup in ANSYS Mechanical. In order to validate the heave plate FEM by shell element elements for plates, and beam elements for the stiffeners. The model is tested for hydrostatic pressure conditions based on the position of the heave plate for still water.

As a limit is set that the maximum principal tension should remain below 300 Mpa. The test for a heave plate 18 meters below LAT results in a Maximum principal stress of 260 Mpa. The FEM is shown in Figure 56 ,and the properties of the heave plate designed in Table 11.

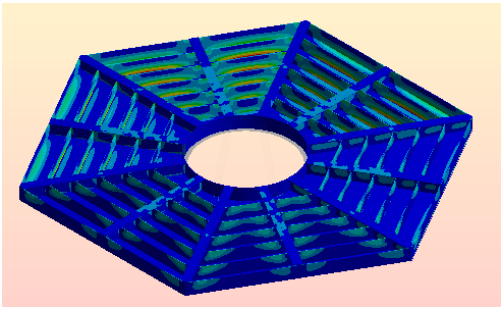

Figure 56 Heave plate model in ANSYS Mechanical for main column 8 m. diameter

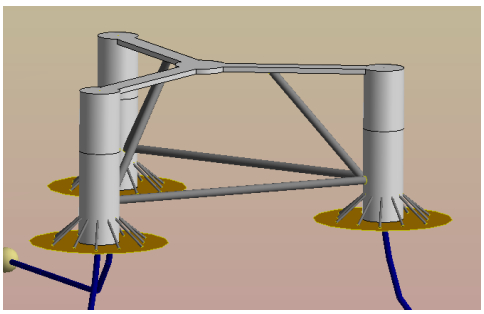

Figure 57 Morison Disc Elements in ANSYS AQWA

HEAVE PLATE		UNITS
Mass	4.619E+05	kg
Volume	58.83	m3
Ixx = Iyy	2.413E+07	kg m2
Izz	4.814E+07	kg m2

Table 11 Heave plate properties

As a note, it is important to consider that disc are considered single-sided in ANSYS AQWA. The heave plate modelled in the semi-submersible is subjected to loading on both sides, and as a consequence drag and added mass coefficients must be doubled.

The average drag coefficient for an hexagonal-shaped heave plate is taken as $Cdz = 7.5$, with added mass $Caz = 1$. These must be twice for analysis purposes as mentioned in [12].

4.2.6 CROSS BRACES AND STIFFENERS

The modelling of cross bracing members and stiffeners is done by use of Morison tube elements. As shown in 4.2.2, accordingly to KC-number, a the dimensions of the tubular sections fall under the category of flow separation.

The drag and added coefficients applied are based upon documentation [13], which relates to the diameter of the tube. The cross brace diameter is 1.626 m and the coefficients are $Cd = 0.63$ $Ca = 0.63$. All Morison tube elements are set as flooded.

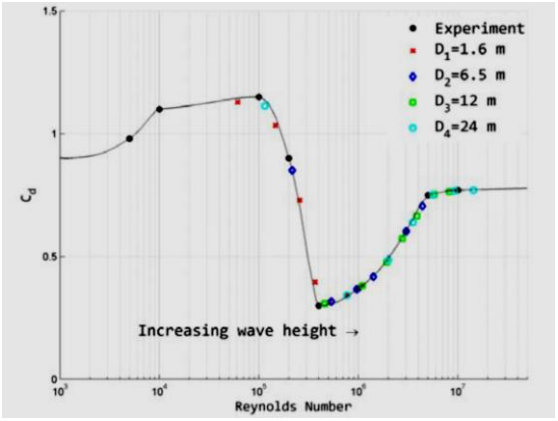

Figure 58 Cd as a function Re number [13]

Diameter (m)	Averaged Cd (-)
1.6	0.63
6.5	0.56
12	0.61
24	0.68

Table 12 Averaged Cd values for diameters [13]

4.2.7 CATENARY SYSTEM

The catenary system is input as non-linear catenary in ANSYS AQWA. Due to the water depth in Moray Firth, the catenary line is supplied with four clump equidistant along the length. The mooring system is spread with one catenary attached to each of the columns with an angle of 120 degrees. The properties for mooring lines are shown in Table 13, and clump weights in .

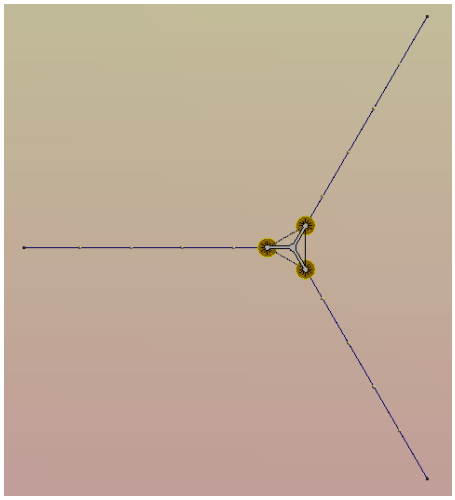

Figure 59 Mooring lines setup

MOORING LINES		UNITS
No. Catenary	3.00	-
Angle between lines	120.00	º
Depth to anchors w.r.t LAT	-40.20	m
Depth to fairleads w.r.t. LAT	-18.00	m
Mooring line diameter	0.08	m
Mass per unit length	250.00	kg/m
Extensional stiffness	8.000E+08	N
Maximum admissible tension	7.500E+06	N
Drag coefficient	1.10	-
Added mass coefficient	1.00	-
Unstretched length	380.00	m

Table 13 Mooring lines properties

Figure 60 Clump weight [15]

CLUMP WEIGHT		UNITS
No. Clump weight per line	4.00	-
Diameter	450.00	mm
Height	630.00	mm
Weight	180.00	kg

Table 14 Clump weight properties [15]

4.3 NREL FAST AND TURBSIM

The study of the platform behavior in irregular sea-states, includes wave and wind loading. Whereas the sea-states are input as JONSWAP spectrum, and wind as ISO spectrum in AQWA. In order to account for the wind loading on the wind turbine, the rotor thrust force is computed.

TurbSim, is used to generate a full turbulent wind field according to a defined wind speed. The output from TurbSim, is then input onto FAST to compute a aeroelastic simulation of the wind turbine for that wind loading.

The rotor thrust force is extracted as a result of the simulation. These results are given as a time-series, for a duration 600 seconds. The mean value is then taken, and increased by a safety factor of 1.35, given for environmental loading in [16]. The rotor thrust force computed for the different sea-states can be seen below in Figure 61, for each of the wind speeds associated with the sea-states as displayed in Table 6.

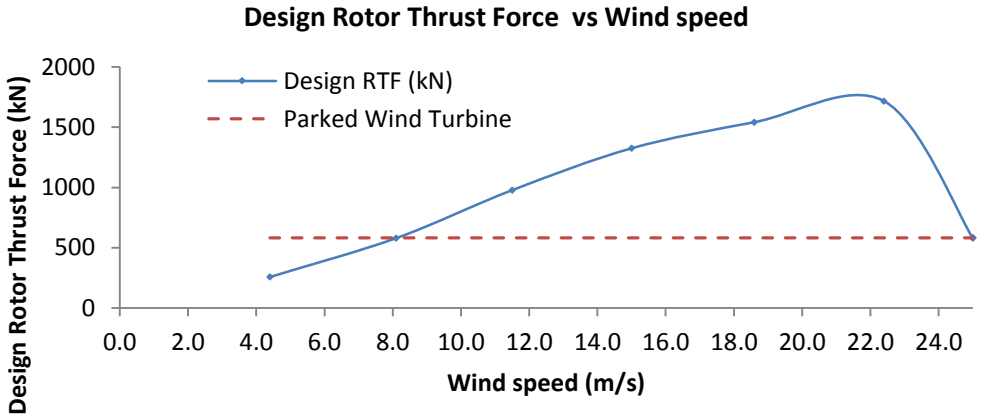

Figure 61 Design Rotor Thrust Force (kN) computed in FAST for the wind speeds range (m/s)

4.3.1 WIND LOADING

For further analysis in the mechanical model, chapter 5, wind loading accounts for the forces and moments as a result of the wind acting on the wind turbine. An aeroelastic simulation is run with a flexible model of the wind turbine, applying a wind speed of 11.5 m/s, Figure 62. The simulation is carried out in FAST 7, for a land-based wind turbine. The resulting sectional forces at the base of the tower are input later on at the interface level (TP) of the semi-submersible.

The simulation has a duration of 600 seconds. The forces and moments are extracted and averaged from the time-series. The components (Fx and My) are increased by a safety factor of 1.35 for being variable environmental loads, as recommended in [16]. The component Fz, corresponds to the wind turbine weight, and it is considered as a permanent load. A summary table of the tower base forces and moments can be seen in Table 15:

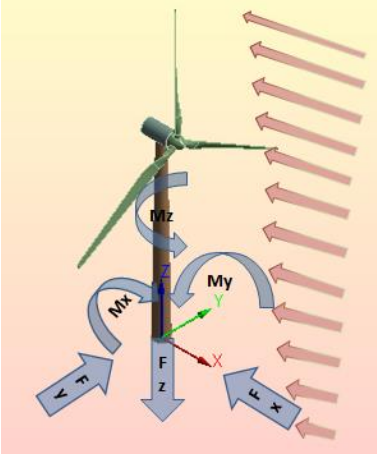

Figure 62 Wind turbine base sectional forces

Fx (shear force)	-838.04	kN
Fy (side-to-side force)	±10.05	kN
Fz (wind turbine)	-6874.17	kN
Mx (side-to-side moment)	±6768.67	kNm
My (overturning moment)	76496.35	kNm
Mz (yaw moment)	±297.51	kNm

Table 15 Wind turbine base sectional forces

4.4 SEMI-SUBMERSIBLE ANALYSIS: TMORAY

The semi-submersible is named as TMoray, after its geometry T-Trifloater ,and location the Moray Firth. Accordingly to the design basis established in 4.2 the characteristics of the hydrodynamic model are shown in Table 16 below.

SEMI-SUBMERSIBLE T Moray		UNITS
Platform		
Platform Primary Steel	6.344E+05	kg
Platform CM w.r.t. SWL	2.16	m
Platform Roll/Pitch Moment of Inertia	4.105E+08	kg m2
Platform Yaw Moment of Inertia	6.646E+08	kg m2
Platform Draft	18.00	m
Columns		
No. Columns	3	-
Column Diameter	8.00	m
Column Height	32.00	m
Column Offset w.r.t. centreline	36.00	m
Heave Plates		
No. Heave plates	3	-
Heave Plate Diameter	27.40	m
Heave Plate Height	1.00	m
Tube Elements		
No. Braces	6	-
Brace Diameter	1.626	m
No. Stiffeners per Column	12	-
Stiffener Diameter	0.508	m

Ballast		
Water Ballast Height in each Column	4.00	m

Table 16 TMoray properties

FOWT Mass summary	MASS	UNITS
Platform Primary Steel	6.344E+05	kg
Heave Plates inc. Stiffeners	1.277E+06	kg
Braces	9.554E+05	kg
Ballast	6.029E+05	kg
Mooring lines inc. Clump weight (no anchors)	1.042E+05	kg
Wind Turbine (rotor/hub/nacelle/tower)	6.539E+05	kg
Full-System Total Mass	**4228.3**	**Tn**

Table 17 TMoray mass summary

4.4.1 Response Amplitude Operators

The RAOs (9), correspond to normalised motions of the six-rigid body DOF in the frequency-domain. To compute the RAOs a regular unit wave amplitude is run through the structure for one direction, 180 degrees. The range of frequencies to compute the RAOs goes from 0.1 to 1 rad/s. Extra points are included to represent the peak of response for Heave and Pitch natural frequencies included section 4.4.2.

$$RAO = \frac{floating\ body\ response}{wave\ amplitude} \quad (9)$$

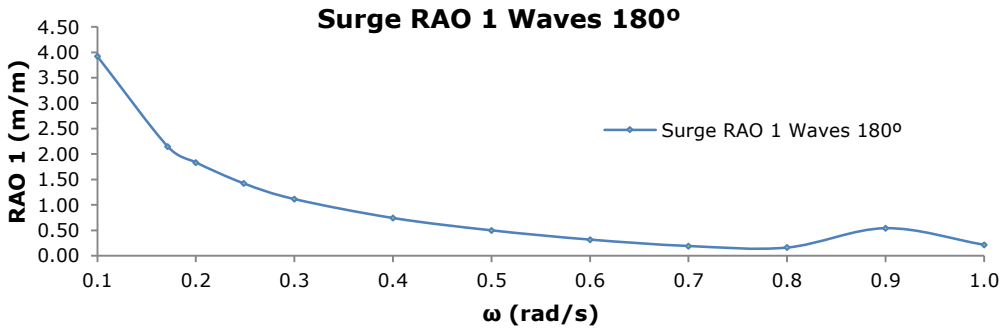

Figure 63 RAO 1 Surge, waves 180º

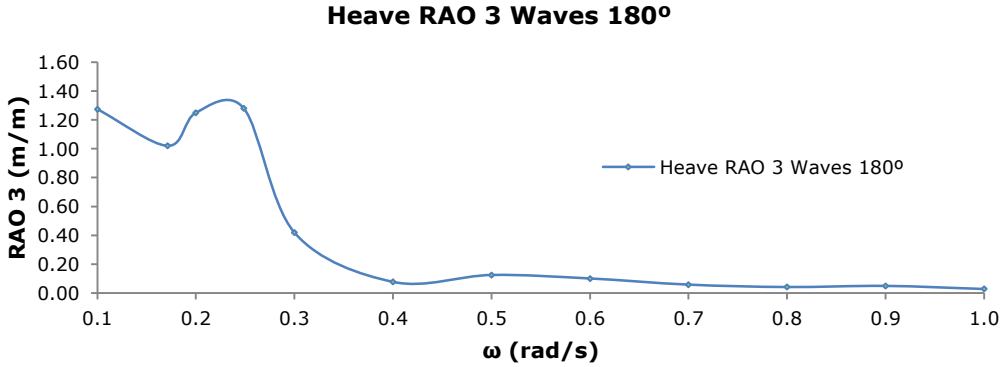

Figure 64 RAO 3 Heave, waves 180º

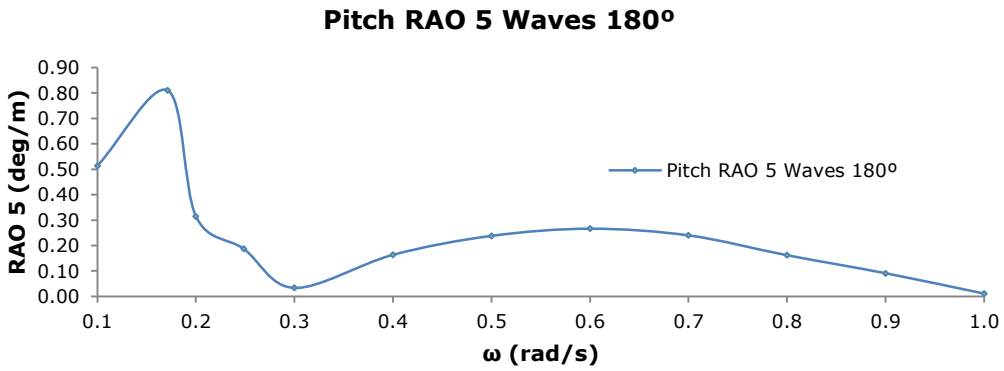

Figure 65 RAO 5 Pitch, waves 180º

The results in this section validate the design for further steps. The response in surge lies within predicted responses, where the maximum response maximum occurs in the low frequency range < 0.2 rad/s. Heave RAO remains within an acceptable limit below 2 m/m, as stated in literature [3] and [17]. On the other hand, Pitch RAO approaches to 1 deg/m which is a relatively high response.
Despite this, the latter is considered valid as the Roll/Pitch natural frequency is below the peak frequency of the sea-states in Moray Firth. This is shown in the next section 4.4.2.

4.4.2 NATURAL FREQUENCIES

The natural frequencies are determine within AQWA-LIBRIUM, these correspond to the 6 DOF shown in **Figure 8.**

DOF	f (Hz)	ω (rad/s)	T (s)
Surge	0.0025	0.0159	395.17
Sway	0.0025	0.0159	395.17
Heave	0.0396	0.2486	25.27
Roll	0.0273	0.1714	36.66
Pitch	0.0273	0.1714	36.66
Yaw	0.0010	0.0063	997.33

Table 18 Eigenfrequencies / Eigenperiods

To justify the correctness of the design, in conjunction with the RAOs obtained in 4.4.1 the following plot in includes the natural frequencies obtained over the sea-states JONSWAP Spectrum. Figure 66, clearly shows how the designed semi-submersible eigenfrequencies are out of the energy spectrum. As a result the design is validated according to design basis.

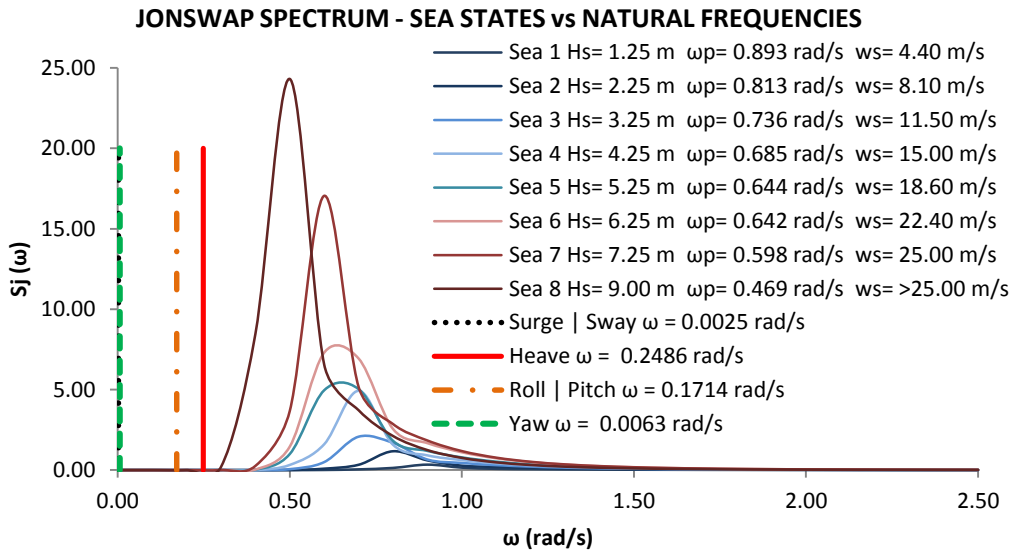

Figure 66 JONSWAP Spectrum – Sea States vs Natural frequencies

4.4.3 IRREGULAR SEA-STATES BEHAVIOUR

This step aims to represent the irregular sea-states behaviour of the semi-submersible on the given location.

The data to extract from this section are the maximum and minimum significant motions. The charts generated below could be considered as the RAOs for irregular seas. The significant values describe the platform response in irregular seas.

The motions of the platform, nacelle acceleration, and airgap, are the values evaluated during the analysis. The process consist of running the irregular sea-states as omnidirectional in ANSYS AQWA, in order to obtain the response in a range of wave heading directions for the eight sea-states. Additionally, the rotor thrust force shown in Figure 61 is included at the nacelle level accordingly to each sea-state.

After the analysis, the 3 hour time-series of each sea-state is computed to extract 1/3 of the maximum response for: surge, sway, heave, roll, pitch, yaw, and nacelle acceleration. However, 1/3 of the minimum air-gap values are taken since it is a limiting factor to avoid wave loading on the topside, which must always be positive.

As a reminder, the air-gap is referred to the distance between the free surface elevation of the sea and the bottom of the topside, Figure 9. To register this parameter a control node is input in the hydrodynamic model.

Due to symmetry, only half of the structure is analysed regarding wave and wind loading directions. The directions are 0, 60, 90, 120 and 180 degrees, Figure 67. In every case, wind and waves are considered as collinear.

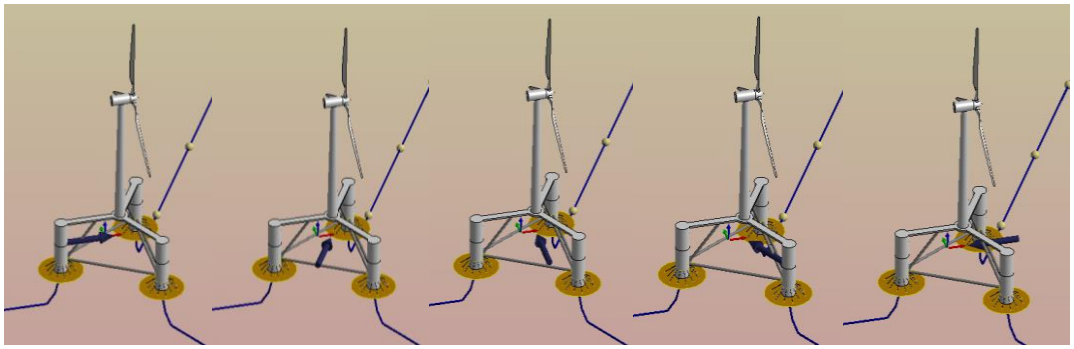

Figure 67 Irregular sea-states Wave loading direction (blue arrow)

The overview of the resulting plots, allow to identify the less favourable directions for wind and wave loading.

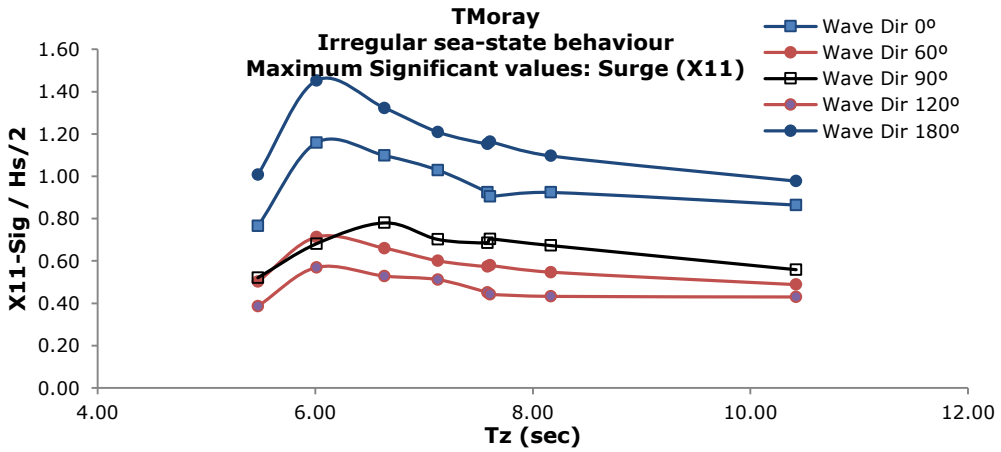

Figure 68 TMoray Maximum significant Surge

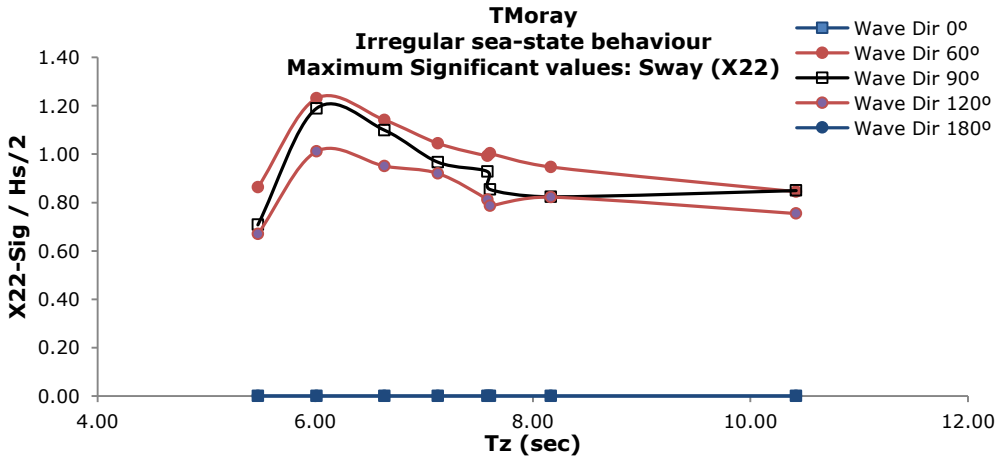

Figure 69 TMoray Maximum significant Sway

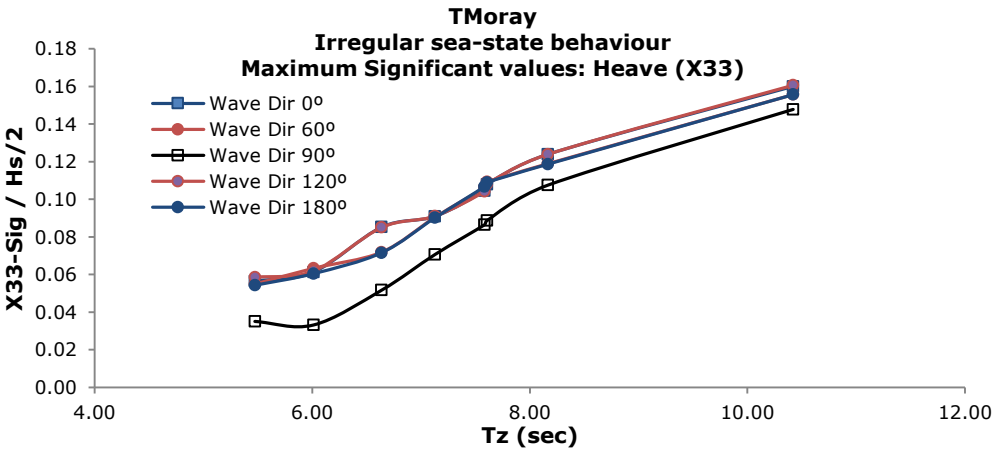

Figure 70 TMoray Maximum significant Heave

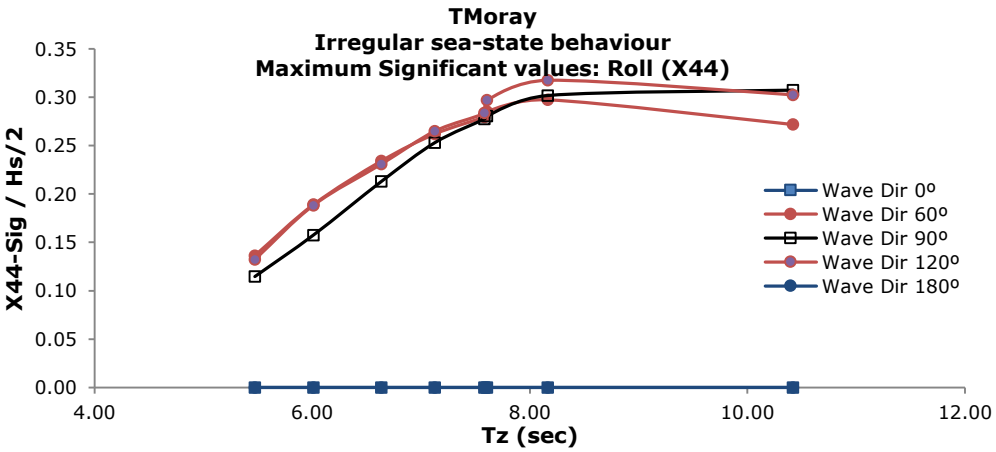

Figure 71 TMoray Maximum significant Roll

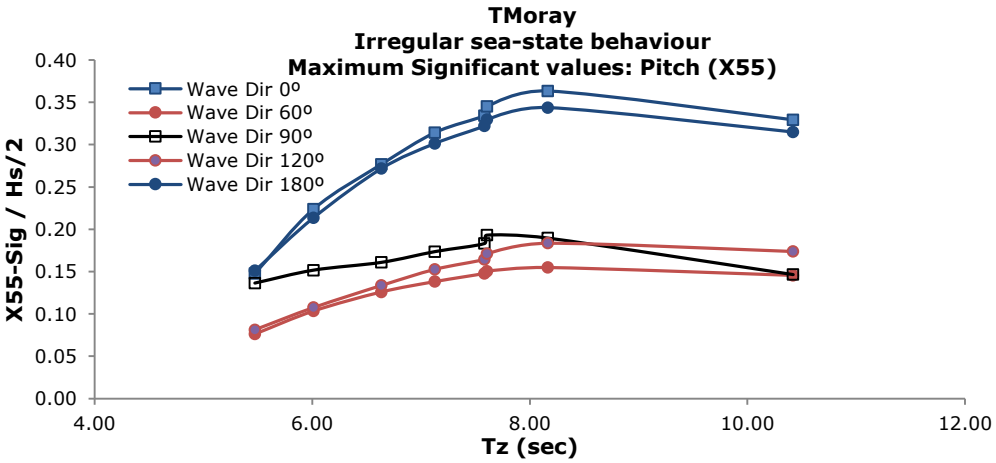

Figure 72 TMoray Maximum significant Pitch

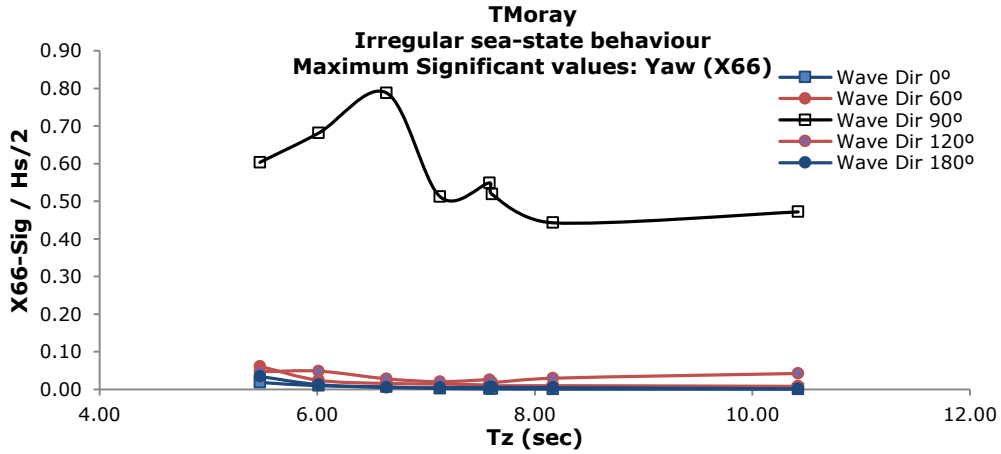

Figure 73 TMoray Maximum significant Yaw

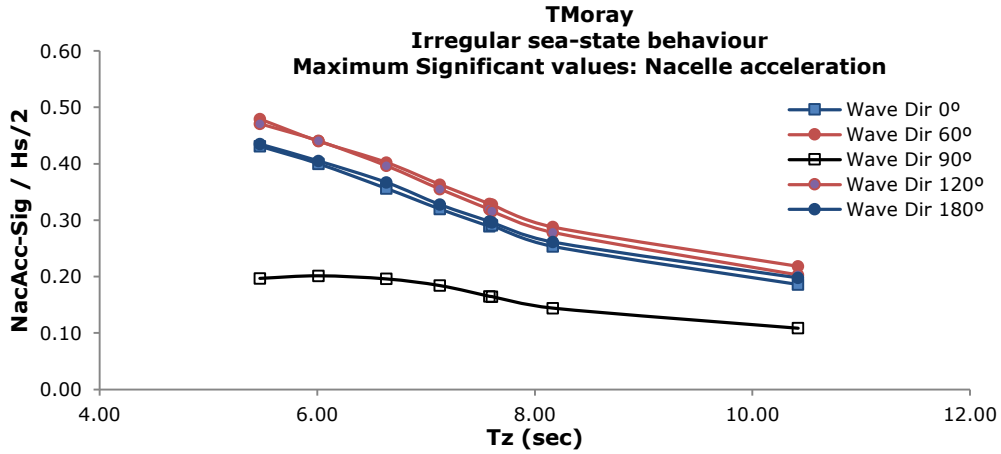

Figure 74 TMoray Maximum significant Nacelle acceleration

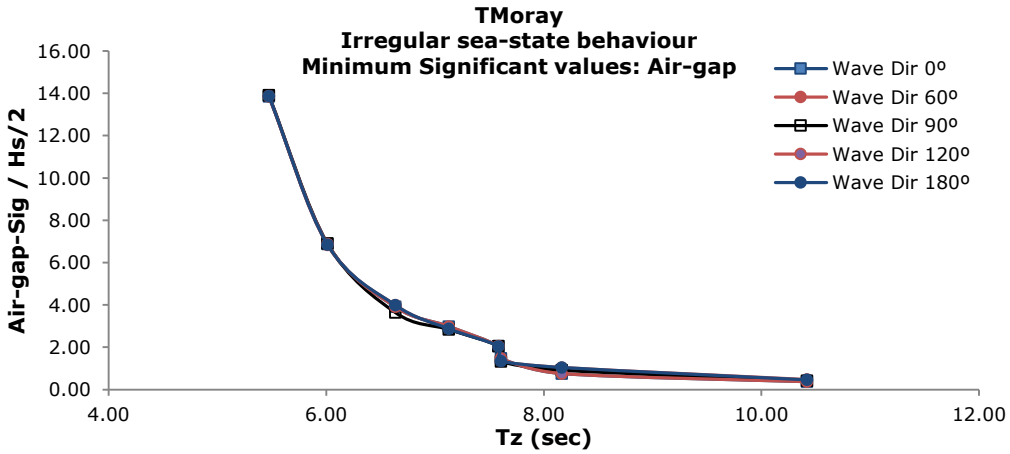

Figure 75 TMoray Minimum significant Air-gap

4.4.4 EXTREME SEA EVALUATION

As a final step to validate the hydrodynamic model, the semi-submersible is subject to the 50-year wave loading with Hs=9.2 m, and Tp=13.4 s.
The parameters of control in this case are maximum nacelle acceleration, minimum air gap, and maximum tension in the mooring lines. In order to account for uncertainty, different random seeds are used to generate the irregular-sea. The random seeds are combined with an increasing peak enhancement factor γ in JONSWAP Spectrum. As a result a total of 18 irregular sea-states are analysed, to extract the extreme values. A summary of the analysis is shown in Table 19.

Case	Environ. Load Direction	γ	Seed
1	0º	3.3	368001
2			935232
3			515047
4		5.5	38150
5			140249
6			443313
7		7.0	555189
8			426992
9			613377
10	180º	3.3	539313
11			672694
12			60693
13		5.5	239291
14			564866
15			439376
16		7.0	921090
17			372529
18			148620

Table 19 Extreme sea, load cases

The procedure is based extracting the maximum and minimum values from the time-series during the irregular sea generated with the 50-year wave, and the rotor thrust force when the wind turbine is parked, Figure 61.

4.4.4.1 MINIMUM AIR-GAP

The extreme sea is run for the mentioned cases in Table 19. The minimum air-gap values are extracted and presented in Figure 76 below.

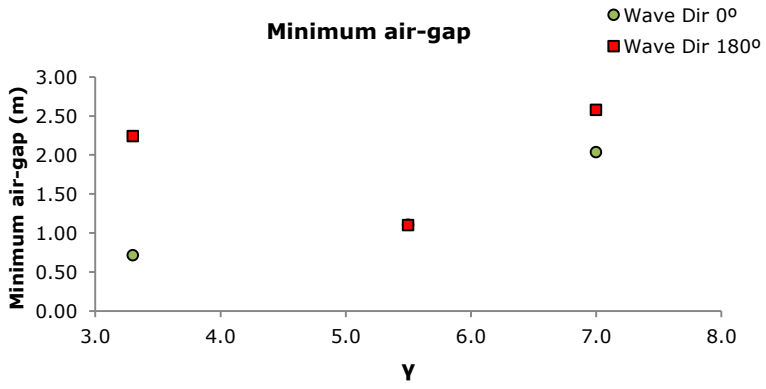

Figure 76 Minimum air-gap for extreme sea. Environmental loading directions 0º and 180º

It can be observed that when the platform is subjected to environmental loading heading from 0 degrees the air-gap values are less favourable.

4.4.4.2 MAXIMUM MOORING LINES TENSION

The maximum tension is the peak value registered during the analysis of the extreme sea, for each of the mooring lines. The results are presented in Figure 77 and Figure 78.

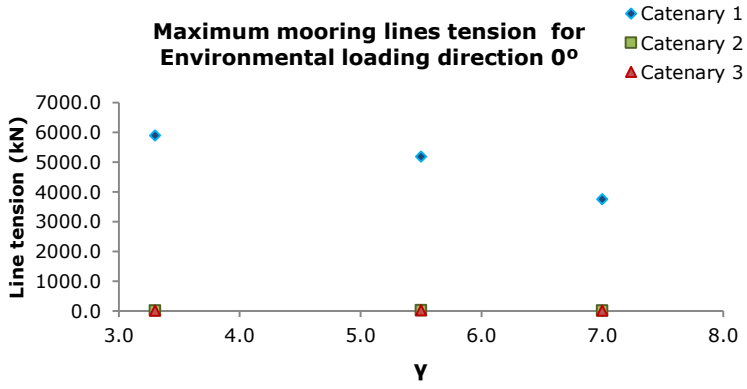

Figure 77 Maximum mooring lines tension. Environmental loading direction 0 degrees

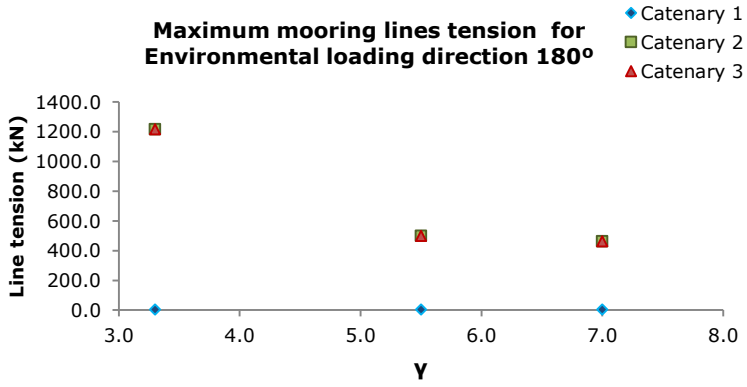

Figure 78 Maximum mooring lines tension. Environmental loading direction 180 degrees

It is clear that one of the consequences of including the clump weights along the catenary has influenced the mooring lines loading. This is reflected also in the previous section 4.4.4.1, where environmental loading with a direction of 0 degrees presents the less favourable air-gap values.

For 0 degrees, the mooring line 1 takes almost the full loading induced on the platform. On the other hand, for 180 degrees, the tension on the lines is split evenly between lines 2 and 3. However, due to the clump weights implement the catenary 1 remains unloaded.

4.5 CONCLUSIONS

The design of a semi-submersible has proven to be a complex task for reduced water depth conditions, such as Moray Firth. One of the main issues in the design regards the mooring lines. It is observed that a conventional catenary system is not suitable for reduced water depth conditions. Initial testing of semi-submersible models with a conventional catenary system yielded high responses in RAOs, invalidating further analysis.

As only working alternative and presented in the results, clump weights are implemented to constrain the platform motions by adding mass on the catenary. As a result, the RAOs analysis in section 4.4.1 present satisfactory values comparing these with previous studies [6].

The main concern about mooring lines, regards the event of extreme sea. Whereas, the line maximum tension appears to be highly uneven between catenary lines, depending of the environmental loading direction.

Despite the air-gap values and nacelle acceleration in extreme sea remain reasonable, for the feasibility of semi-submersibles in reduced water depth conditions it is recommended a strong focus for the design of alternative mooring systems in future works.

The design process described in Figure 15, which is followed in the present document, has proved to be a proper flowchart to validate the hydrodynamic design.

5. SEMI-SUBMERSIBLE MECHANICAL MODEL

In this thesis, the design of the semi-submersible is divided in two finite element models: hydrodynamic and mechanical. The hydrodynamic model is characterised by a simple geometry, which is used to solve the diffraction/radiation problem. As a result, the wave excitation forces and moments are computed for the wetted surfaces of semi-submersible hull, which subsequently yields the pressures and motions on the centroid of the mesh panels.

In the mechanical model of the semi-submersible, the main interest refers to stresses and deformations. Initially, the foundation is subjected to wind loading computed in FAST 7 by applying the wind turbine tower base sectional forces. This step, enables to identify the high stress regions on the TP. Besides, the stress level is evaluated for different configurations of the semi-submersible topside.

Identified the high stress regions, the hotspot stress is used later on in chapter 7, to determine the fatigue life of the TP.

The platform needs to be re-modelled to conduct the FEA of the mechanical model with the internals, which are not present in the hydrodynamic model. Furthermore, since the pressures and motions in hydrodynamic model are calculated based over a rigid body, the shell elements in the mechanical model of the semi-submersible are to be reinforced by design of the internals. The author suggest the following flowchart as work procedure to achieve the evaluation of the TP fatigue life:

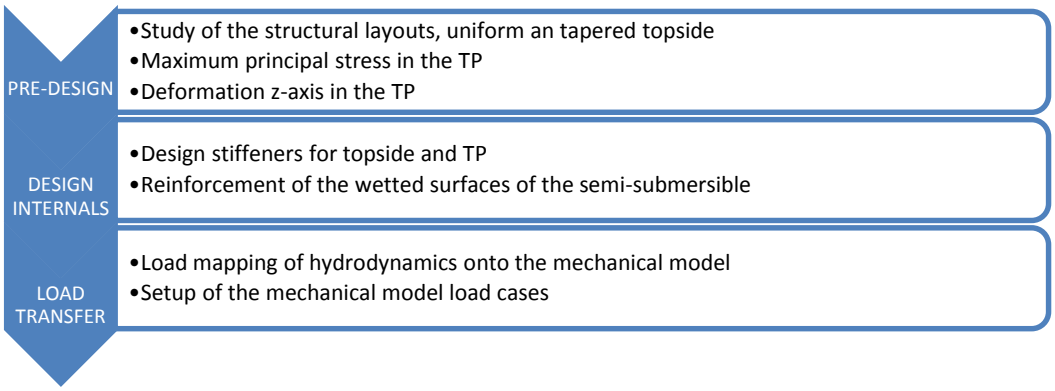

Figure 79 Mechanical model flowchart

The structural steel used in the plated structures and tubular member in this design is classified as S355, which is regarded as high strength steel (HS) in DNV-OS-C101 [18].

5.1 PRELIMINARY DESIGN

The mechanical modelling is an intensive iterative process. Before designing the internals, initial evaluation of different semi-submersible layouts is carried out. These layouts regard the topside geometry. The starting point is to verify which structural configuration amongst the four shown in Figure 17 and Figure 18, yields lower stress level and deflection in the TP. For this purpose, control nodes are defined on the mechanical model as shown in Figure 80.

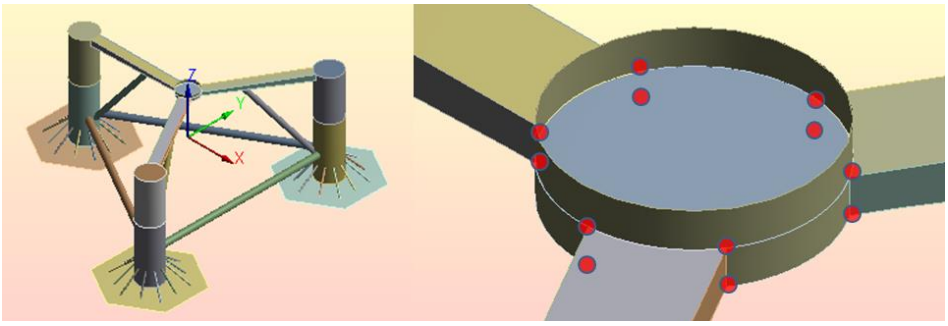

Figure 80 Control nodes around the TP

5.1.1 PRELIMINARY STUDY OF THE MODELS

Four models are considered. These are divided in two groups, uniform box girder topside and tapered box girder topside, both tested with and without reinforcement braces as shown in Figure 17 and Figure 18.

In order to select one of the models, both groups are subjected to standard Earth gravity and the wind turbine weight applied on the TP, Figure 81. The structure is fixed on the heave plates, and read out values are directional deformation in z-axis and maximum principal stress on the TP.

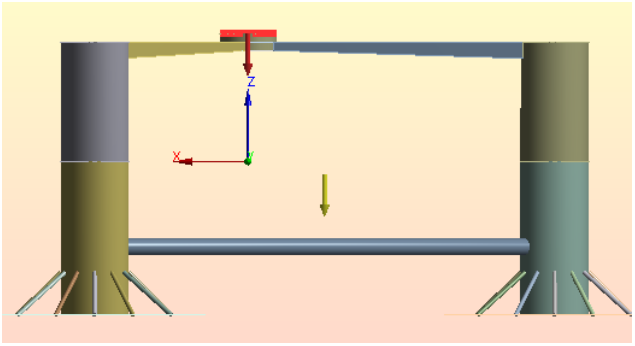

Figure 81 Preliminary design setup

For all the models, mesh control is inserted in ANSYS to use quadrilateral shell elements, and ensure an element size of 0.25 m with Mapped Face Meshing and Sizing respectively. A summary of the results shown in Table 20, and plots of the maximum principal stress presented in Figure 82.

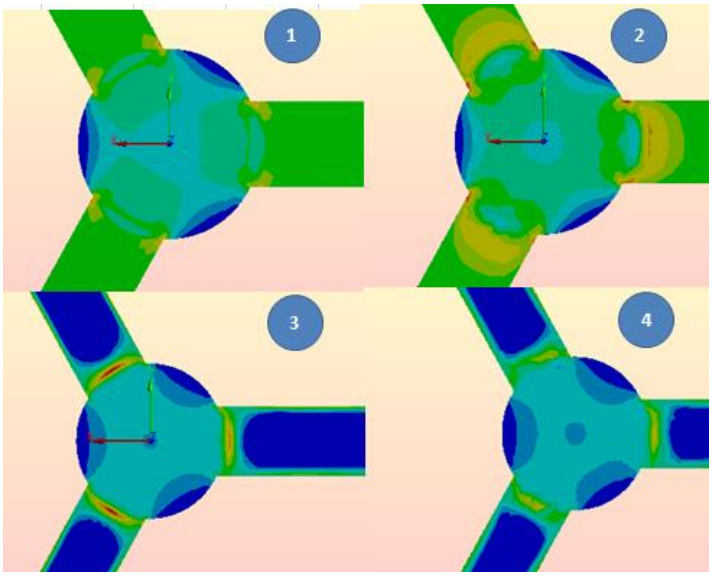

Figure 82 Bottom view of the TP in the four models. Maximum principal stress

MODEL	uz (m)	σ max principal (Mpa)
1. Uniform box girder topside	-0.9626	689.64
2. Tapered box girder topside	-0.6579	502.03
3. Uniform box girder topside + reinforcements	-0.0211	146.76
4. Tapered box girder topside + reinforcements	-0.0202	114.49

Table 20 Results summary from preliminary design

The models 1 and 2 are discarded due to large maximum stress level and deflections on the TP.

Regarding models 3 and 4. While the deflection on the TP is a 4.3% for the uniform box-girder above the tapered topside, the stress level in the uniform box-girder is a 22% higher w.r.t. tapered. In view of the results, the tapered box-girder topside is chosen for the design of the internals.

5.2 DESIGN OF THE INTERNALS

With the purpose of reinforcing the semi-submersible hull, and the whole topside-TP, the design of the internals focus on determining the optimal number of the plate stiffeners.

The three configurations shown in Figure 83 are evaluated in a transient analysis with the structure subjected to wind loading. The wind loading consist of applying the shear force and overturning time-series on the TP, along with Earth's gravity and the wind turbine mass.

Additionally, it is included the design of the main column internals, Figure 84. The semi-submersible column is subjected to hydrostatic and hydrodynamic pressure due to the ocean environment. Moreover, internal hydrostatic pressure is present inside of the main columns due ballasting. To simplify the analysis, the columns are analysed individually applying internal and external hydrostatic pressure to study the stress level. A stress criteria is defined in 5.2.1 for the hydrostatic load case, allowing a margin for further analyses including hydrostatic and hydrodynamic pressure in the full model.

The wind loading applied in the simulations for the design of the internals is presented in section 4.3.1.

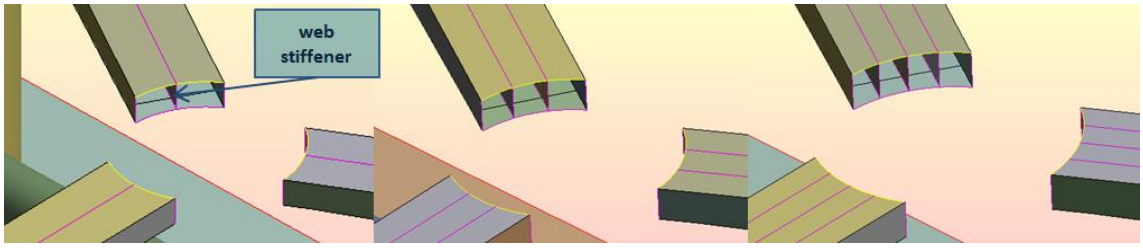

Figure 83 Increasing number of web stiffeners in the topside

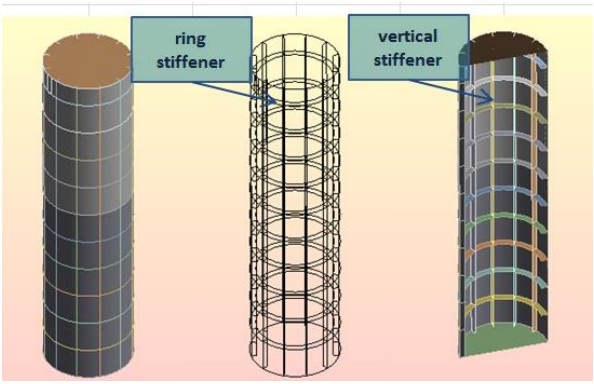

Figure 84 Rings and vertical stiffeners in the main columns

5.2.1 MAIN COLUMNS

This section covers the design of the stiffeners in the main columns. This structural part is subjected to the hydrodynamic loading. For this study, the main column is considered individually. The main column is subjected to hydrostatic pressure on the hull structure. For this conditions, the author considers as a good practise that the maximum principal stress should be $\leq 100\ MPa$, for the an optimum design of the main column internal stiffeners.

Earth gravity, and hydrostatic loading are applied with a fluid density of $\rho = 1025 \frac{Kg}{m^3}$ on the external face and the interior of the column. The column is fixed at the bottom.

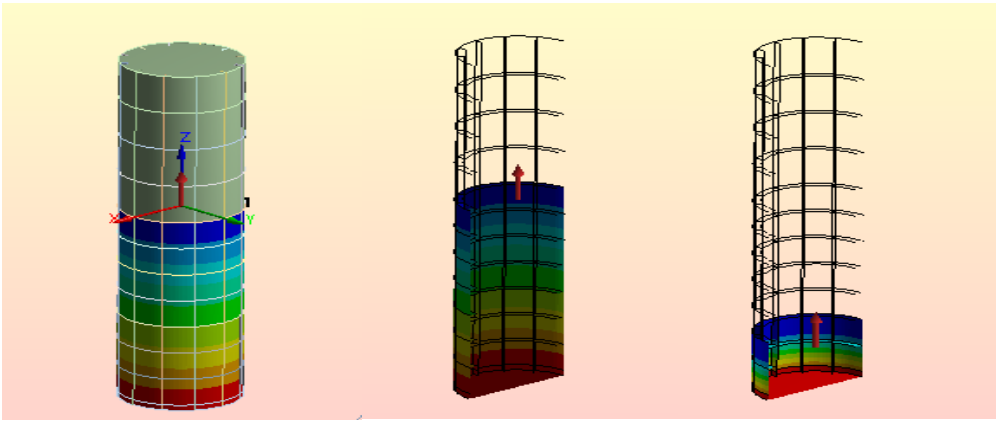

Figure 85 From left to right: Main column, Hydrostatic loading (ocean on external face) , hydrostatic loading (ballast on internal face)

There are 12 vertical stiffeners are placed symmetrically w.r.t. z-axis of the main column, from bottom to the top. These are chosen as 12 to coincide in number and position with the heave plate stiffeners. Besides, ring stiffeners are distributed along the main column length. The number of ring stiffeners is larger below LAT, as it is the part of the column subjected to the hydrostatic and hydrodynamic pressure.

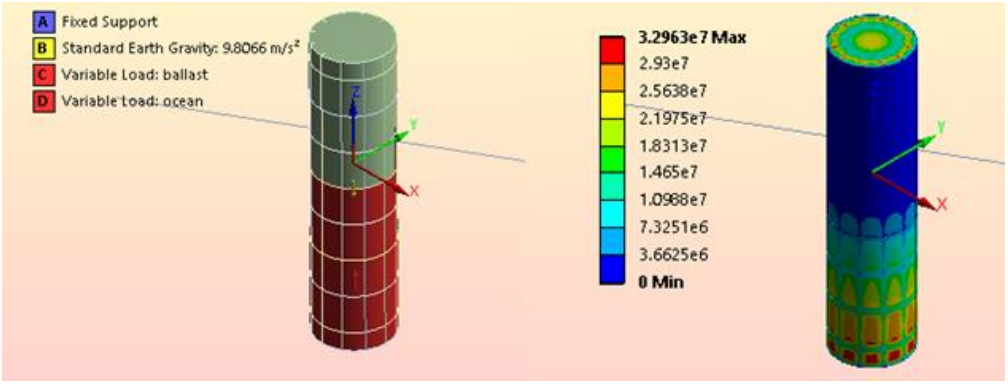

Figure 86 Main column analysis and results for Model 1

COLUMN	UNITS	MODEL 1	MODEL 2
No Ring stiffeners	-	8	8
No Vertical stiffeners	-	12	12
Main column wall thickness (tmc)	mm	20	20
Ring stiffener thickness (trc)	mm	25	20
Vertical stiffener thickness (tvc)	mm	15	20
Total steel mass per column	Tn	183.99	187.62
Max. Equivalent Von-Misses stress	Mpa	32.96	33.14
Max. Principal stress	Mpa	37.05	37.30

Table 21 Main column stiffeners analysis

The result obtained for the first model are within the criteria defined at the beginning of this section. Thus, the stiffeners from model 1 are chosen to be implemented in the full semi-submersible model.

5.2.2 TOPSIDE AND TRANSITION PIECE DESIGN

The three topside variants, and TP are analysed in the three transient analysis. Longitudinal stiffeners are included to strength the topside arms against the bending induced by wind loading. The three models shown in Figure 83, are tested for an increasing number of web stiffeners resulting in: two, three and four box-girder cells.

A simple static analysis of full model indicates a high bending stress induced by wind loading on the topside For this reason, despite box-girder sections generally present a good behaviour against torsion, on the conservative side, transversal stiffeners are added in the topside on the length between the TP and the joint with the inclined cross braces, as shown in Figure 88 for the three models.

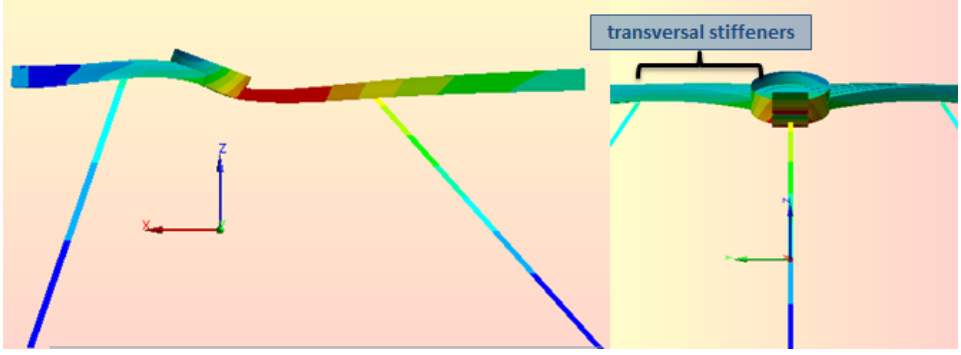

Figure 87 Side and front view of the topside 4 cells model with transversal stiffeners. Deformations x60

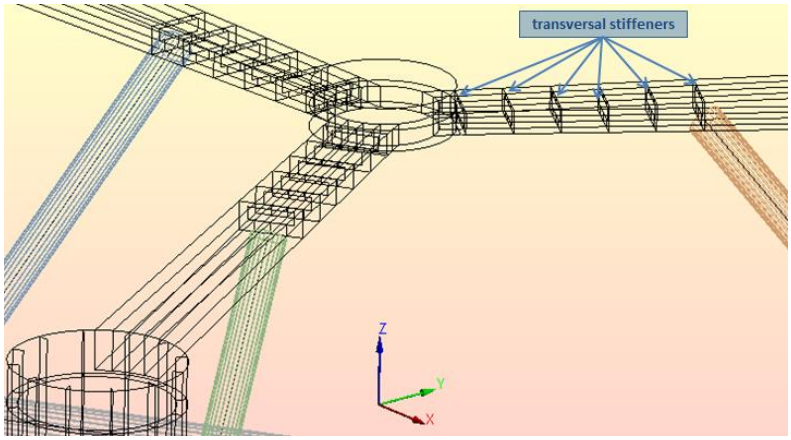

Figure 88 4 cells model with transversal stiffeners added

The transient analysis of the structure is setup subjecting the semi-submersible to: self-weight, wind turbine weight, plus the overturning moment and shear force shown in section 4.3.1. The setup for the transient analysis presented in Figure 91. Hence a time-step (dt) of 0.05s is used to compute the wind loading on the flexible tower model in FAST 7, the same dt is set for the transient analysis.

5.2.2.1 DESCRIPTION OF THE TOPSIDE

The topside consist of tapered box-girder section which has 2 meters height on the side of the column and 1 meter height on the joint with the transition piece. Shell elements are used to model the semi-submersible topside. Since a conceptual design is intended, the thicknesses of the topside elements for the models of study stated in 5.2.2, are fixed as shown below in Table 23.

Element	Thickness (m)
Top/Bottom Flange	0.060
Web/Stiffener	0.035
Torsion Stiffeners	0.035

Table 22 Topside elements thickness

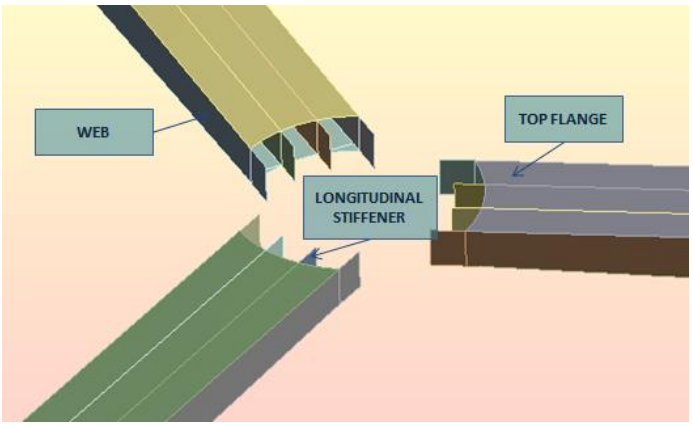

Figure 89 Topside elements view

5.2.2.2 DESCRIPTION OF THE TRANSITION PIECE

The TP is a can-shaped shell model, and considered welded to the topside arms. The can section is divided in two cylindrical shells with a diameter of 6.50 meters, separated by a round plate in the middle which serves as continuation of the topside flanges. Topside web stiffeners enter in the TP, and connect to an internal stiffener ring.

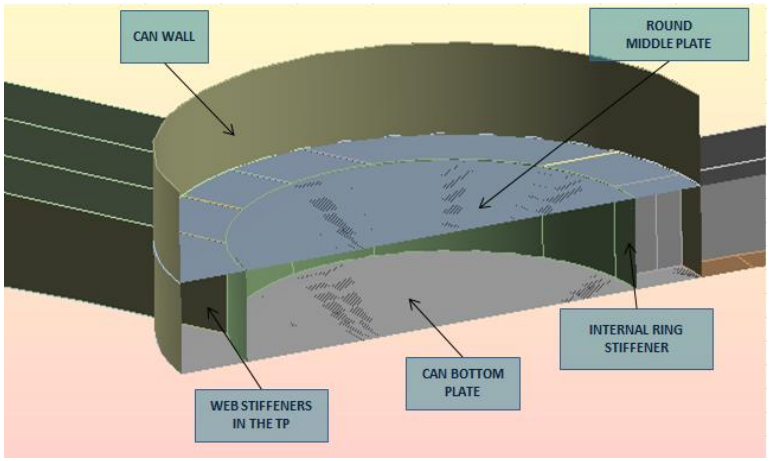

Figure 90 Section of the TP

The design of the transition piece has fixed plate thicknesses as follows:

Element	Thickness (m)
Can wall	0.090
Internal ring stiffener	0.060
Middle plate	0.060
Bottom plate	0.060

Table 23 TP elements thickness

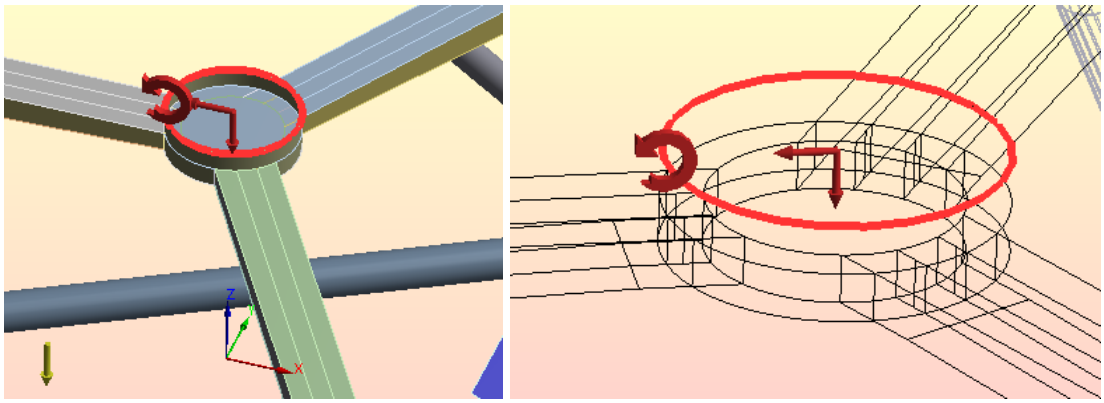

Figure 91 TP overturning moment, shear force, and wind turbine weight

5.2.3 TRANSIENT ANALYSIS RESULTS

The transient analysis is used to select the mechanical model. The time-series of the wind loading at the base tower from FAST are input for a running time of 150 seconds. The stress is read-out along on the TP corners where the stress level is higher, according to the environmental loading direction shown in Figure 91, as maximum principal stress. The time-series of the resulting maximum principal stress on the TP are shown below in Figure 92.

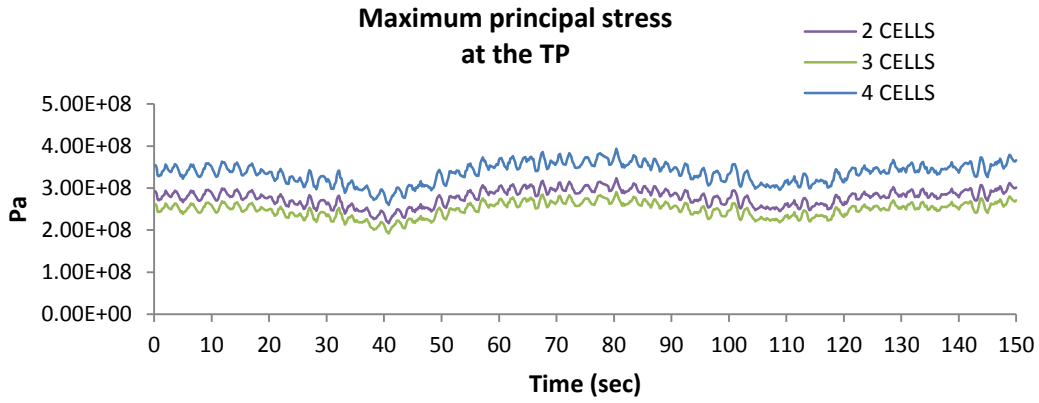

Figure 92 Transient analysis time-series for the three semisub mechanical models

Accordingly to the results obtained, the box-girder with three cells is chosen as the mechanical model to study the fatigue life.

5.3 CONCLUSIONS

The preliminary design in section 5.1, is a useful guide to determine the most suitable topside configuration. The simplicity of the load case, represents an good overview of the topside and TP points of interest.

In section 5.2.2, the addition of wind loading allows to identify the high stress regions on the TP, and the influence of wind loading for a three-arm topside. The high stress areas are located in the connection of the can section with the topside. Accordingly, these joints are the focus area for the fatigue life study conducted in chapter 7.

The wind turbine loads, shear force and overturning moment, have a significant influence of the TP stress levels. For further analyses, it is important to remark that the stress level in the TP is strongly dependent of the wind loading direction. Hence higher load levels are observed in the arm which is on the leeward direction of the wind.
Large structural self-weight may result in large deflections and stresses subjecting the semisub to the same loading as shown in section 5.2.3.

For a more detailed study, the topside section can be improved by modifying the stiffeners design. As a recommendation for further work, typical box-girder designs in bridges could be implemented on the semi-submersible.

Additionally, a summary of the structural steel mass is presented in for comparison with the approach taken to determine the mass in the hydrodynamic model.

FOWT Mass summary	Hydrodynamic (Tn)	Mechanical (Tn)
Platform Primary Steel	634.4	
Heave Plates inc. Stiffeners	1446.2	2871.2
Braces	953.8	
Ballast	602.9	602.9
Mooring lines inc. Clump weight (no anchors)	227.2	227.2
Wind Turbine (rotor/hub/nacelle/tower)	653.9	653.9
Full-System Total Mass	**4518.4**	**4355.2**

Table 24 Structural steel mass for the hydrodynamic and mechanical model

As shown in Table 24, the full-system mass in the hydrodynamic model is a 3.6% over the mechanical. In chapter Semi-submersible hydrodynamic model4, the equation (8) is used to estimate the primary steel weight for the hydrodynamic design. In view of the results obtained, after designing the internals in the mechanical model it could be remarked the small deviation between models, and thus validate the design procedure for a semi-submersible design.

6. LOAD TRANSFER: FROM HYDRODYNAMIC TO MECHANICAL MODEL

6.1 INTRODUCTION

At present, the load transfer between a hydrodynamic and mechanical model is not a straightforward process. The so-called hydrodynamic loading, or load mapping, consist of allocating the centroid panel pressures from AQWA-LINE analysis (diffraction/radiation), to the mesh panels of the mechanical model in ASAS.

The pressure on the panel centroid corresponds to the sum of the incident, diffracted and radiated wave at a given phase as defined in AQWA-WAVE manual [19]. The facet pressure is stored in the hydrodynamic database generated by AQWA-LINE.

$$P_\theta = \frac{H}{2}(P_r \cos\theta + P_i \cos\theta) \quad \textbf{(10)}$$

P_θ	Pressure on the facet at wave phase θ
H	Wave height
P_r, P_i	Real and imaginary components of the pressure from AQWA-LINE

Additionally, the static pressure needs included in the mechanical model by inputting Hydrostatic pressure in the wetted surface areas. The load transfer mechanism refers to the forces and moments for a unit amplitude wave, period, phase and direction.

However, there is an distinct limitation for the present software capabilities. This issue refers to the semi-submersible behaviour in irregular sea-states, and the lack of tools to implement the mooring lines in a mechanical model.

The current version of ANSYS is able to map the hydrodynamic loads for a given wave height, period, phase and direction. The software uses the mesh from the hydrodynamic model to assign the pressures in the mechanical model mesh, by the position of the panels in the model. This is done for one wave, frequency, phase, and direction.

As shown in equation (10), the pressure scales linearly with the wave height. Therefore, in order to recreate a load mapping for an irregular sea-state, the objective is to compute the load transfer functions. In section 6.3, the flowchart presented in Figure 21 is described to obtain the load transfer functions.

6.2 LOAD TRANSFER REQUIREMENTS AND RECOMMENDATIONS

Previous to the load transfer, here is presented a list with some requirements and recommendations to consider:

- In order to allocate the hydrodynamic pressure. The global coordinate system of hydrodynamic and mechanical model must be the same.
- The models must be equivalent. The wetted surfaces, subjected to wave exciting forces and moments, in the mechanical model must share the same positions as the hydrodynamic. On the other hand, internals can be freely designed to strength the former.

- The hydrodynamic data base, needs to be in *neutral format*. This is done by the application *AQWA2NEUT*, which converts the *hyd* file from the AQWA-LINE analysis. This file is read in ASAS with the command OCREAD.

- The wetted surfaces of the mechanical model, must be set to element type SURF154 to apply the hydrodynamic loading.

- Morison elements must be included in the hydrodynamic model.

- For Morison elements, flooded/non-flooded, drag and added mass coefficients need to be input again in the mechanical model. It is recommended to set the element type to PIPE288.

6.3 TIME-DOMAIN: FROM IRREGULAR SEA-STATE TO STRESS LEVELS

The irregular sea-state is described by JONSWAP spectrum as stated in section 4.2.1. The water surface elevation of an irregular sea propagating, Figure 93, is represented by sum of the individual wavelets with a distributed random phase constant for time t as:

$$\eta = \sum_{i=1}^{n} a_i \cdot \cos(-\omega_i t + k_i x + \theta_i) \quad \textbf{(11)}$$

a_i Wave amplitude
ω_i Angular frequency
k_i Wave number $k = 2\pi/\lambda$
θ_i Random phase from 0 to 2π

The wave amplitude is obtained from JONSWAP spectrum as:

$$a_i = \sqrt{2 \cdot \Delta\omega \cdot S(\omega_i)} \quad \textbf{(12)}$$

$\Delta\omega$ Frequency steepness
$S(\omega_i)$ Wave spectrum from equation (3)

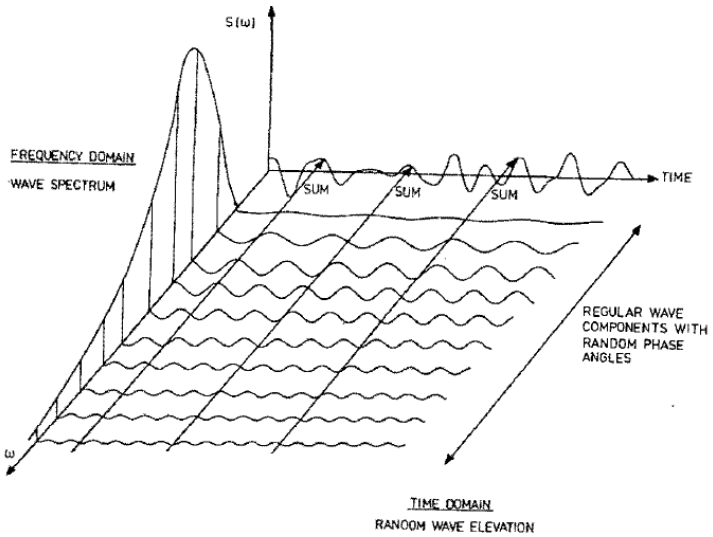

Figure 93 Irregular sea in the time-domain [17]

Based on equations (10) and (11), the stress time-series on a point of interest of the structure can be determine by the assumption that the stress varies linearly with the wave height. Therefore by steeping, or phasing, the wave through the structure it is possible to represent stress in function of the phase, angular frequency and direction w.r.t. the local axes of the structure.

Initially, the frequency steepness is defined to determine the range of wave frequencies to analyse in the structure.

Secondly, phase steepness is chosen to discretise the stress level between 0 and 2π is chosen. The phase steepness is constant range for all the wave frequencies.

Thirdly, and based on the linearity assumption aforementioned, a series of wavelets with unit amplitude are steeped through the structure for the range of wave frequencies defined. Thereby, the read-out of the stress values from each analysis, enables to compute the effective hot spot stress, and thus the stress transfer functions as shown in Figure 94.

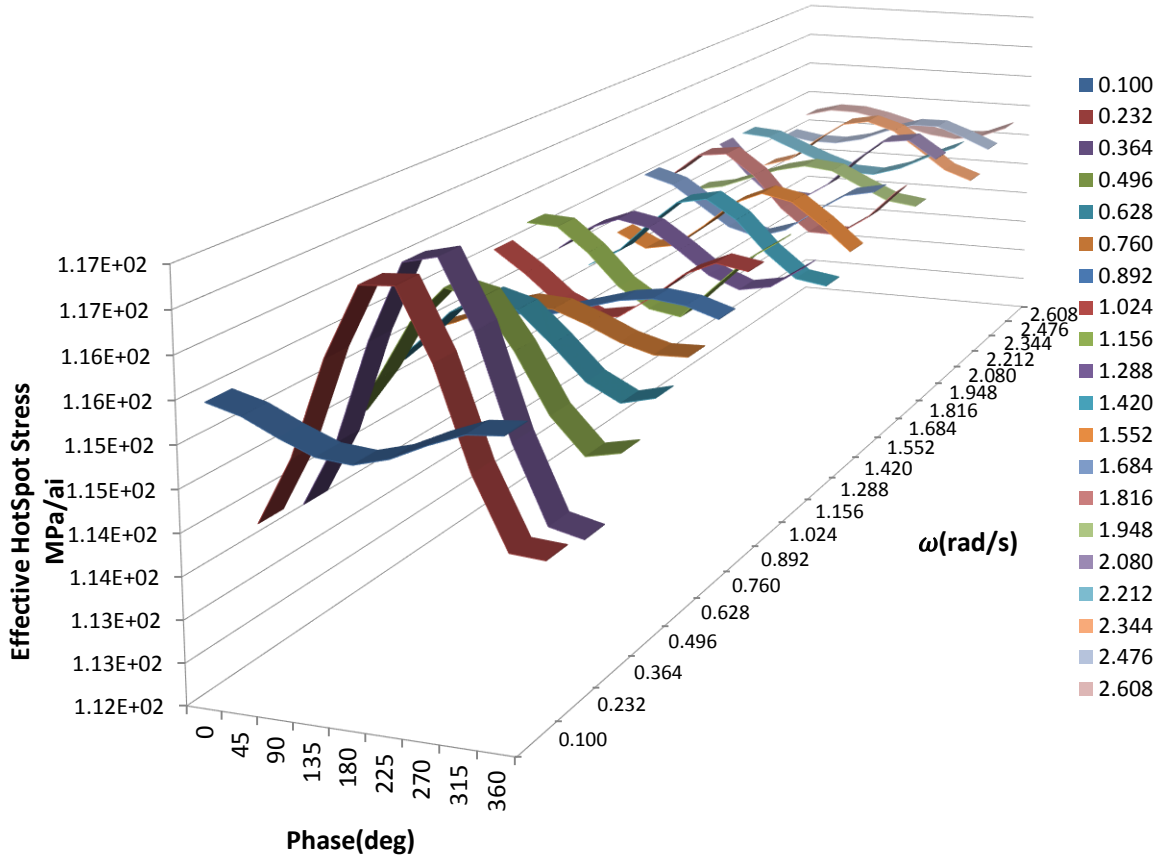

Figure 94 Example. Effective hotspot stress functions

The stress functions (ω, θ, α), on a point of interest are stored in a matrix $\{\sigma_{\omega,\alpha}\}$ to obtain the stress time-series, Figure 96, in combination with equation (11) follows:

$$\sigma_{t,\alpha} = \eta \times \{\sigma_{\omega,\alpha}\} \quad \textbf{(13)}$$

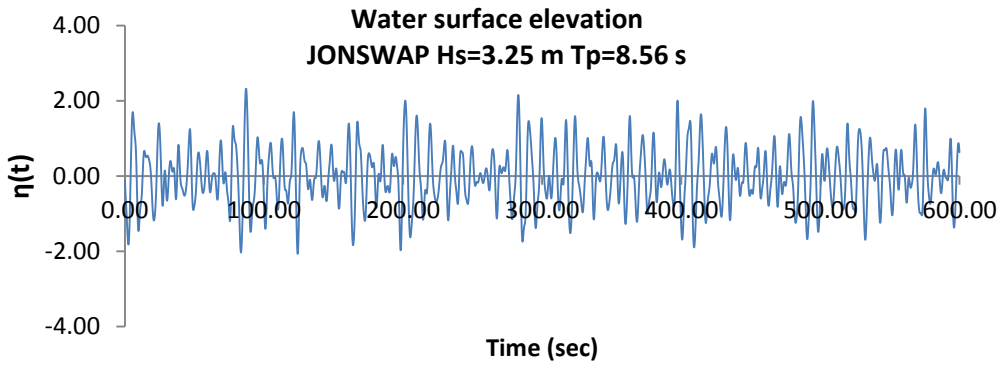

Figure 95 Example: 600s Irregular sea-state, wave surface elevation

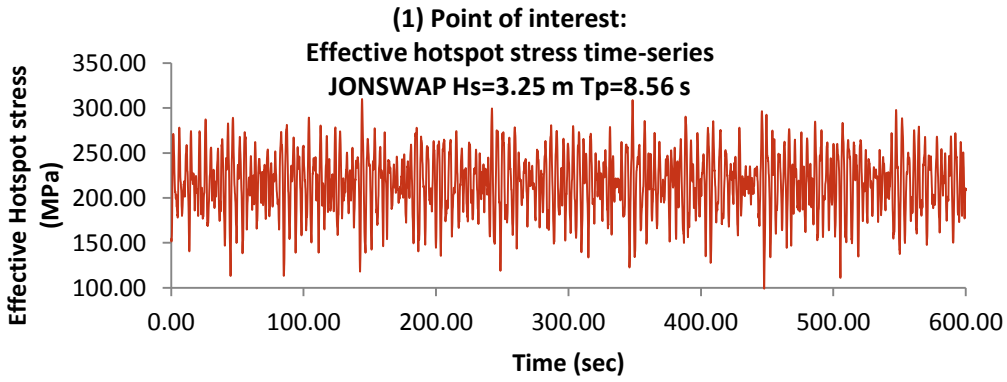

Figure 96 Example: 600s Effective hot spot stress computed from stress transfer functions

6.4 SEMI-SUBMERSIBLE LOAD CASES

Each point of interest in the semi-submersible has as many stress transfer functions as the defined range of wave frequencies and directions. The mechanical model of the semi-submersible from chapter 5 is setup for wave loading.

The hydrodynamic database generated by AQWA-LINE in chapter 4 is imported via AQWA2NEUT. Due to computational resources, the mechanical analysis with wave loading to obtain the stress transfer functions is set according to the following points:

- Wave frequencies are uniformly distributed for twenty steps for sea-state of analysis, Figure 97.

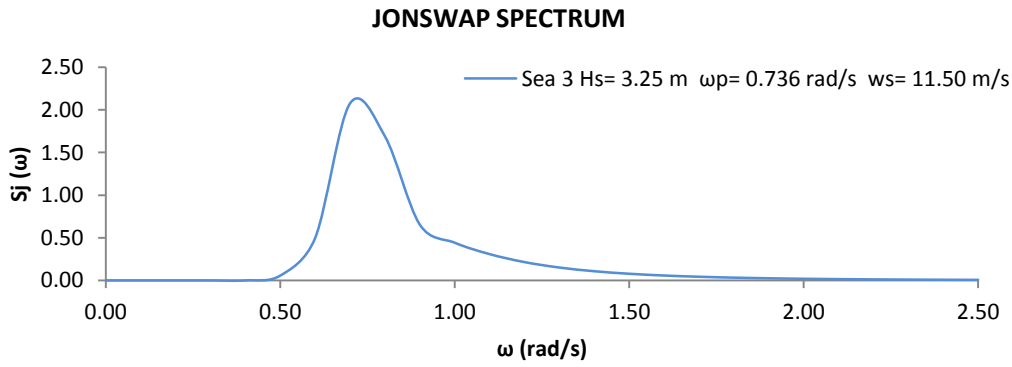

Figure 97 JONSWAP Spectrum. Sea-state associated with rated wind speed

- For each frequency, the wave steepness from 0 to 2π consist of nine steps.

- Due to 2-fold symmetry on the semi-submersible. The environmental loading directions of analysis are four 0/60/120/180 degrees w.r.t. semisub local axes. As shown in Figure 98.

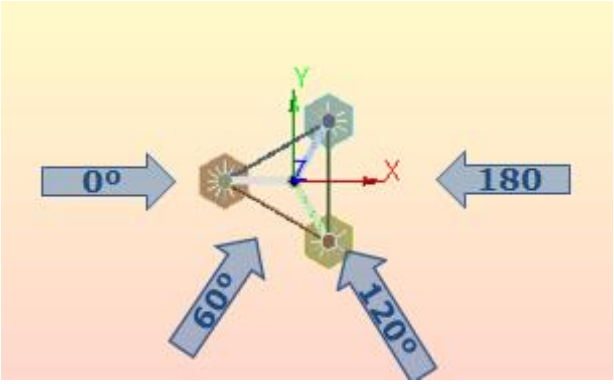

Figure 98 Environmental loading directions to compute the load transfer functions

- The points of interest are 12, as presented in the mechanical model chapter 5, Figure 102. These correspond to the joints between the topside and TP in the bottom and top positions.

- In order to compute the effective hot spot stress, the read-out values are the membrane and bending stress of the aforementioned points. This is done accordingly to DNV-C203-RP in section 4.3.6 and used together with equation (14).

From the effective hot spot stress data obtained, the transfer functions are computed in Matlab to produce the stress-time series. A summary of the total number of analyses conducted is shown below in Table 25:

MECHANICAL MODEL ANALYSES SUMMARY	
(1) Points of interest	12
(2) No frequencies to discretize JONSWAP Spectrum	20
(3) No directions (halved due to symmetry)	4
Wave Steps (phase) for each (2) (3)	9
Read out points membrane and bending stress for each (1)(2)(3)	2
Total Mechanical Model Analysis	**720**
Total Transfer Function Equations one per (1) (2) (3)	**960**
Total read-out values	**17280**

Table 25 Summary of load transfer chapter

6.5 CONCLUSIONS

As shown in this chapter, the load transfer is not a direct procedure from setup to output, which demands considerable amount of post processing of the results. The knowledge needed for the task accounts for APDL snippets, Matlab scripting, and a careful setup of the numerous simulations to carry out in order to generate the load transfer functions.

The procedure developed in this section account for a considerable amount of steps, from the preliminary design to the final stages of the mechanical model.

In order to satisfy the requirements specified in DNV-RP-C203, the 8-node shell elements are must be used, and the mesh size in the detail of study for plated structures shall be within $t \times t \leq element\ size \leq 2t \times 2t$.

Taking into account that the plate thickness (t) is 35 mm, this results into a large number of elements. Therefore, in chapter 7, the submodeling technique is used to obtain the stress transfer functions, by creating a submodel of the transition piece. The number of analysis conducted just for the mechanical model goes up to 720, for a range of: 20 frequencies, 9 wave steps and 4 loading directions. Together with a refined mesh size, the computational resources for a finer discretisation of the frequencies than 20 results prohibitive for a single workstation.

7. TRANSITION PIECE FATIGUE LIFE

7.1 EFFECTIVE HOTSPOT STRESS

The fatigue life of the TP is evaluated with the hotspot stress method

Due to the significant bending observed in the TP, Figure 92, the read-out values are the membrane stress and bending stress, on the paths shown in Figure 102. These are used to calculate the effective hot spot stress according to section 4.3.6 in DNV-RP-C203 [11].

$$\Delta\sigma_{e,hot\ spot} = \Delta\sigma_{a,hot\ spot} + 0.6\Delta\sigma_{b,hot\ spot} \quad \textbf{(14)}$$

$\Delta\sigma_{a,hot\ spot}$ Membrane stress
$\Delta\sigma_{b,hot\ spot}$ Bending stress

The recommended practice, justifies the reduction factor due to load redistribution to other areas with reduced stress than during the crack growth.

In chapter 6, the effective hot spot stress is computed for the points of interest in the TP including wind and wave loading. The effective hot spot stress is used together with the S-N Curve in this chapter to assess the fatigue life of the transition piece.

7.1.1 SUBMODELING

The large dimensions of the semisubmersible compel the use of submodeling to refine the mesh size on the TP, and reduce the analysis time. For a detail the modelling of the TP, the mesh element size is refined down to 35 mm in the high stress regions.

The submodeling technique consist of solving the full model with a coarse mesh, and cut-off the area of interest to solve this with a refined mesh size. The field of displacements from the coarse mesh in the full model is transferred to the submodel on the cut-boundaries.

However, the submodel needs to be validated. This is done by checking that stress path along the cut-boundaries in the submodel are comparable to the same stress path in the full model. To benchmark the submodel, a simple setup with wind loading, and self-weight is setup as shown in Figure 99 and Figure 100.

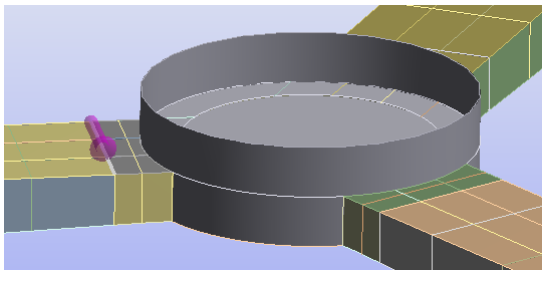

Figure 99 Full model cut-boundary path

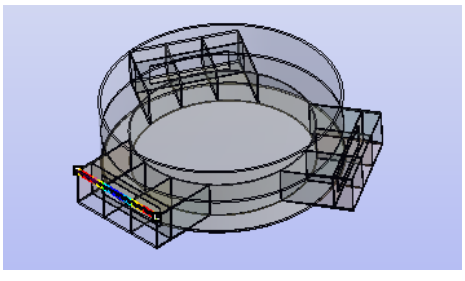

Figure 100 Submodel cut-boundary path

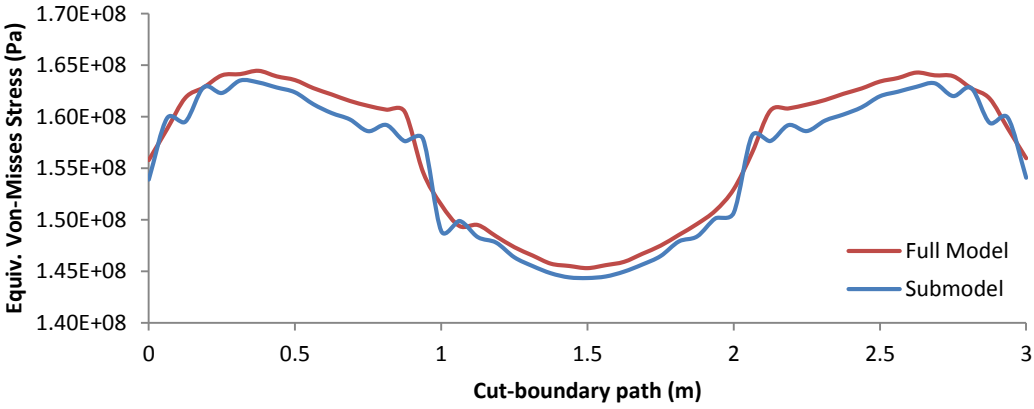

Figure 101 Eqv. Von-Mises Stress along the cut-boundary path

The results from the static analysis present a good agreement between the full model and submodel at the cut-boundary. Therefore, the submodel of the transition piece is validated to compute the effective hotspot stress including wave loading from the hydrodynamic load transfer.

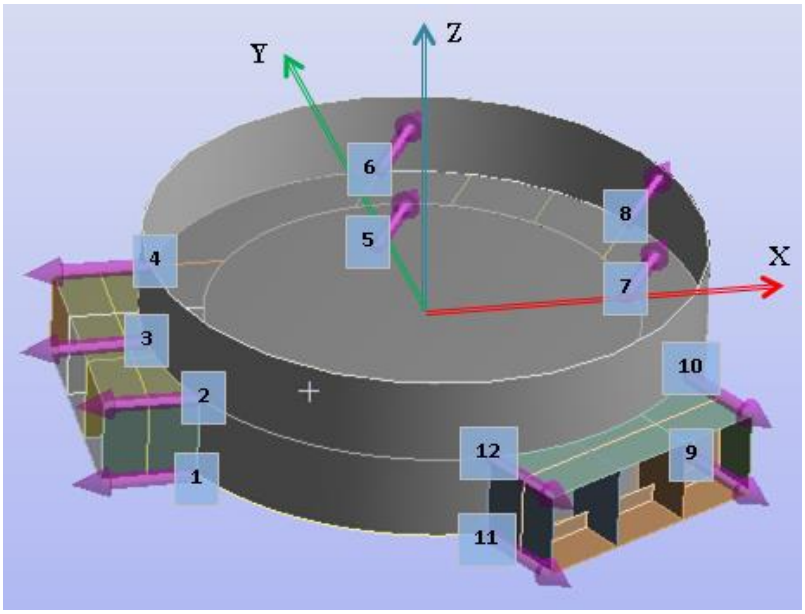

Figure 102 Transition piece. Numbered paths to evaluate the stress level

7.2 FATIGUE DAMAGE CALCULATION

The fatigue life estimation is based upon linear cumulative damage, Palmgreen-Miner rule. This approach consist of using the S-N curves together with the effective hot spot stress time-series computed in chapter 6. The S-N curves for air environment included in DNV-RP-C203 are shown in Figure 103, to assess the fatigue life of the transition piece.

The stress time-series, or histogram, is divided by a blocks of stress ranges and number of repetitions [11]. To calculate the accumulated damage on the structural detail, the formula included in the recommended practice is stated as:

$$D = \sum_{i=1}^{k} \frac{n_i}{N_i} = \frac{1}{\bar{a}} \sum_{i=1}^{k} n_i (\Delta\sigma_i)^m \leq \eta \quad \textbf{(15)}$$

D	Accumulated fatigue damage
n_i	Number of cycles for stress range i
N_i	Number of cycles to failure for constant stress range $\Delta\sigma_i$
k	Number of stress blocks
$\bar{a}$	Intercept of the design S-N curve with the $\log N$ axis
$\Delta\sigma_i$	Stress block i
m	Negative slope of the S-N curve
η	Usage factor = 1, Design Fatigue Factor from DNV-OS-C101 Fatigue Limit States

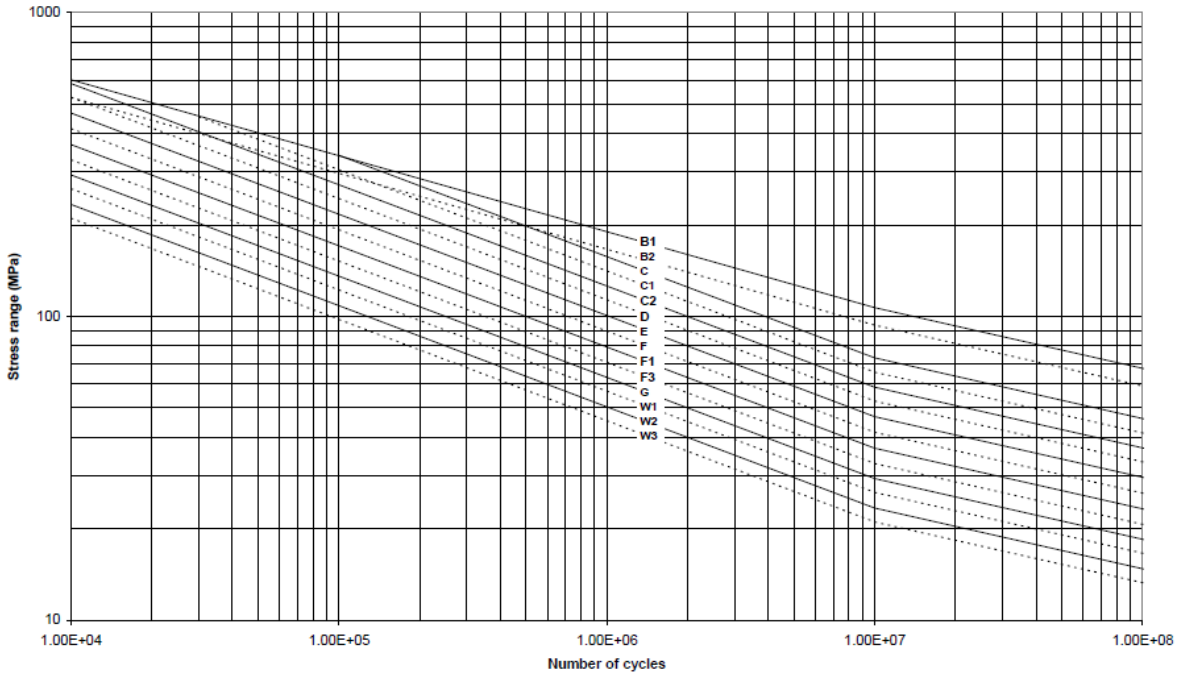

Figure 103 DNV-RP-C203 S-N Curves in air

The D-curve is recommended for plate structures and stress calculated from FE analysis.

7.3 RAINFLOW COUNTING

The rainflow counting method is used to identify the stress blocks and number of cycles in a stress time-series. This step is followed by Palmgreen-Miner's to obtain the accumulated damage in section 7.2.

The effective hotspot time-series (EHT) of each point of interest on the TP is analysed for the environmental loading directions defined in section 7.4. Consequently, each point has 4* EHT where the cycles and half-cycles are counted and assigned the stress range between tension peaks and compression toughs. This stress range defines a block.

For this task the script written by A. Nieslony is used [20] on the time-series.

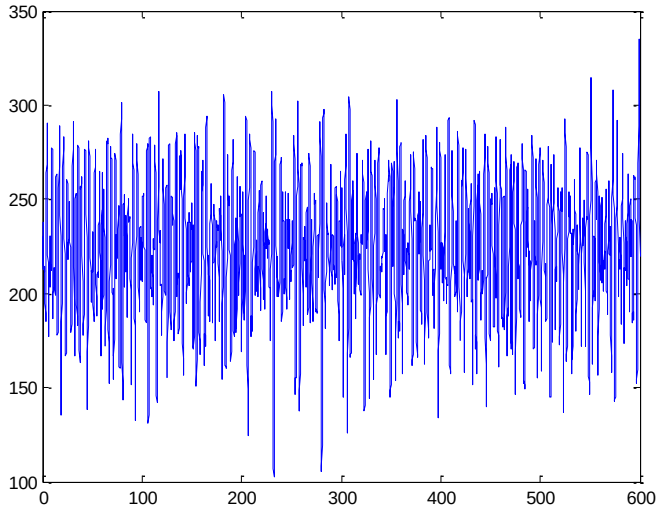

Figure 104 Example EHT time-series

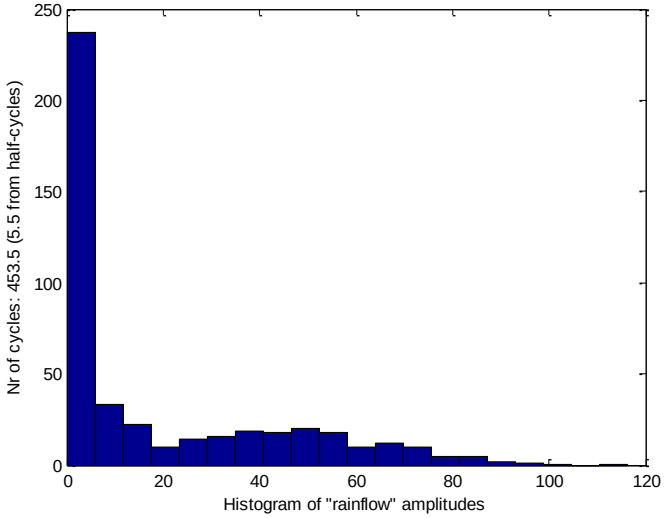

Figure 105 Example Number of cycles per stress amplitude blocks

**Note that 60º = 300º and 120º = 240º yield the same stress levels due to 2-fold symmetry.*

7.4 LOAD CASES

The load cases are divided by the environmental loading directions of study. As stated in 2.3, the wave loading is limited to one irregular sea-state. The sea-state corresponds to the one for which the wind speed is closest to the rated wind speed for the wind turbine reference NREL 5MW.

The wave spectrum is considered omni-directional, and as a consequence so is the wind loading, for wind and waves are considered collinear during the analyses. For the loading cases, it is assumed that waves and wind are collinear. To calculate the fatigue life, the wind rose in Moray Firth shown in Figure 106, is taken into account for the environmental loading direction distribution.

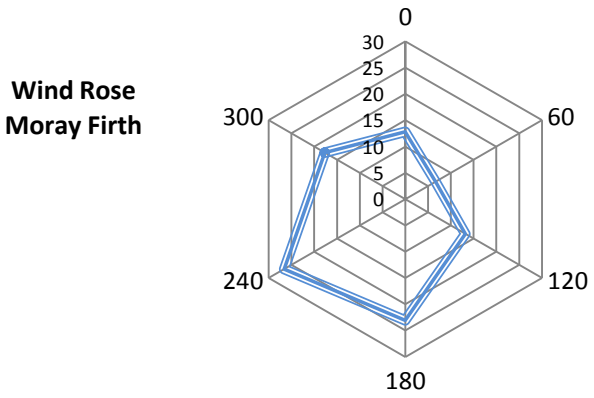

Figure 106 Moray Firth Wind Rose for 60 degrees sectors

The environmental loading directions are divided in sectors of 60 degrees. Whereas, the probability of the loading direction is taken from Figure 106.

Load case	Direction (deg)		Duration (%)	Wind speed (m/s)	Wave Spectrum	Hs (m)	Tp (s)	Γ
1	0	N	12.78	11.5	JONSWAP	3.25	8.56	3.3
2	60	NE	6.65	11.5	JONSWAP	3.25	8.56	3.3
3	120	SE	13.20	11.5	JONSWAP	3.25	8.56	3.3
4	180	S	23.05	11.5	JONSWAP	3.25	8.56	3.3
5	240	SW	26.63	11.5	JONSWAP	3.25	8.56	3.3
6	300	NW	17.70	11.5	JONSWAP	3.25	8.56	3.3

Table 26 Environmental loading cases

The sea-state is run for 3 hours duration, for each of the directions via Matlab script. During each analysis for 0/60/120/180 degrees, the stress level is output in each of the 12 points of interest. This results in 12 effective hotspot stress time-series per each direction

All the load cases defined, include the effects of: hydrostatic pressure from directional wave loading, ballast hydrostatic pressure inside the main columns, and wind turbine sectional forces at the TP as a result of directional wind loading.

Since the semi-submersible designed has 2-fold symmetry, it is considered that the positioning of the floating foundation could benefit the extension of the fatigue life in the TP. The main idea behind this consist of calculating the damage for each point, and direction with a probability of occurrence of a 100%. Afterwards, the semi-submersible is rotated on the location applying the duration of this sea-state for a given direction in agreement with the percentages in Table 26.

To illustrate the positioning concept, a series of figures in presented below. Additionally, an example to calculate the fatigue life on one point is presented in the form of an equation. The combinations of positioning and environmental loading duration are shown in Figure 107, Figure 108, Figure 109, Figure 110, Figure 111, and Figure 112.

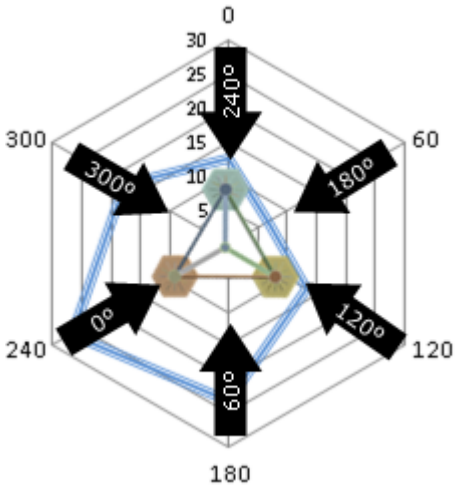

Figure 107 Position 1

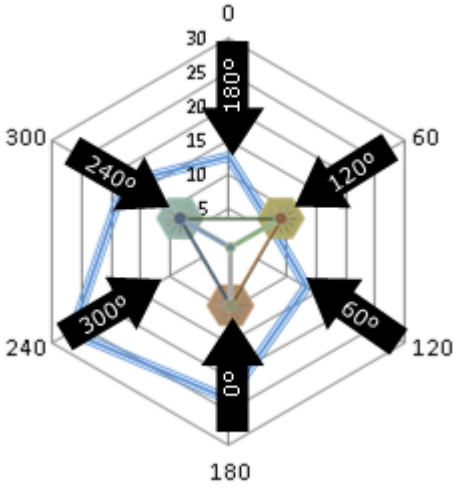

Figure 108 Position 2

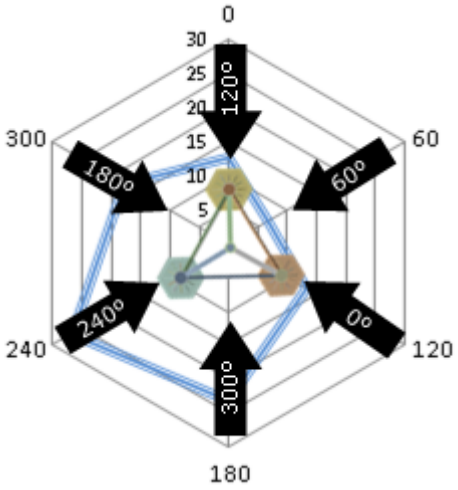

Figure 109 Position 3

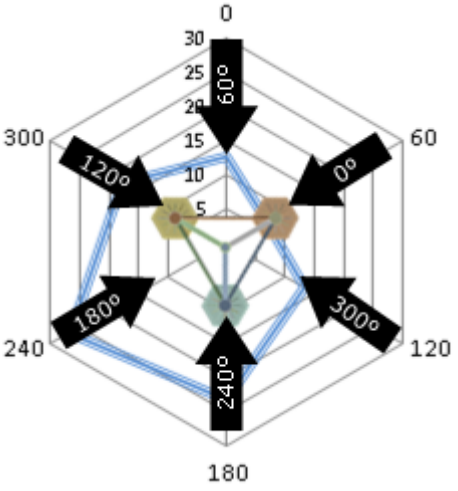

Figure 110 Position 4

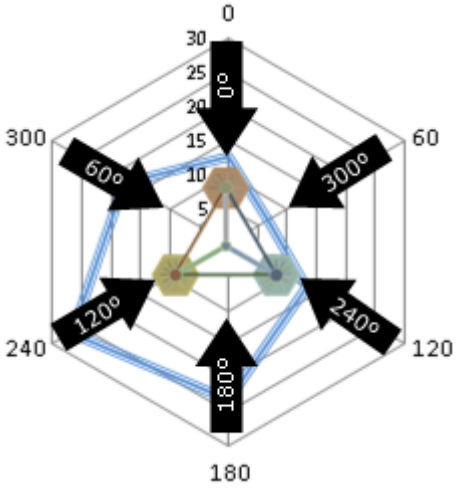

Figure 111 Position 5

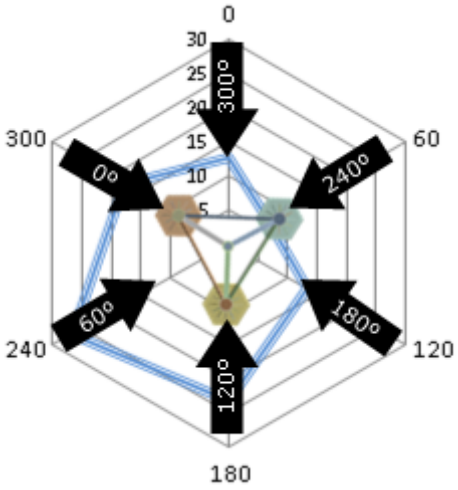

Figure 112 Position 6

The black arrows in the positioning figures above, represent the local coordinates axis for which the stress transfer functions are calculated. Overlapping the semisubmersible figure over the wind rose, allows to identify clearly the year-duration the environmental loading direction for of each point of interest. Hereunder is presented in equation (16), an example of the life-time for the point of interest [1] from Figure 102, given the position 1 shown in Figure 107.

$$Life[1] = \frac{\frac{10800}{D_{1(0)}\cdot\%_{240}+D_{1(60)}\cdot\%_{180}+D_{1(120)}\cdot\%_{120}+D_{1(180)}\cdot\%_{60}+D_{1(240)}\cdot\%_{0}+D_{1(300)}\cdot\%_{300}}}{3600\cdot24\cdot365} \quad \textbf{(16)}$$

Once applied rainflow counting to the stress time-series of each point, the stress blocks are identified for input in the D-curve. For each direction in the local coordinate axes of the semi-submersible shown in Figure 98, the accumulated damage is obtained.

Thus, as a general formula for each of the points of interest in combination with the different positions, the directional duration of the sea-state is taken in account as shown in equation (17)

$$Life(i,j) = \frac{t}{\frac{\sum_{i=1}^{n} D_{i,j}\cdot P_{j(i)}}{T}} \quad \textbf{(17)}$$

Where:

t Total time of stress time-series in seconds
T 1-year time in seconds
$D_{i,j}$ Accumulated damage of point i for the position j
$P_{j(i)}$ Duration of the sea-state in percentage for position j on point i

To conclude, the six combinations according to the positioning are summarised below. This results in 6 fatigue-life values for each of the 12 points of interest.

SemiSub Local (deg)	Wind Rose (deg)	% over Di
0	240	26.63
60	180	23.05
120	120	13.20
180	60	6.65
240	0	12.78
300	300	17.70

Table 27 Position 1 combination

SemiSub Local (deg)	Wind Rose (deg)	% over Di
0	180	23.05
60	120	13.20
120	60	6.65
180	0	12.78
240	300	17.70
300	240	26.63

Table 28 Position 2 combination

SemiSub Local (deg)	Wind Rose (deg)	% over Di
0	120	13.20
60	60	6.65
120	0	12.78
180	300	17.70
240	240	26.63
300	180	23.05

Table 29 Position 3 combination

SemiSub Local (deg)	Wind Rose (deg)	% over Di
0	60	6.65
60	0	12.78
120	300	17.70
180	240	26.63
240	180	23.05
300	120	13.20

Table 30 Position 4 combination

SemiSub Local (deg)	Wind Rose (deg)	% over Di
0	0	12.78
60	300	17.70
120	240	26.63
180	180	23.05
240	120	13.20
300	60	6.65

Table 31 Position 5 combination

SemiSub Local (deg)	Wind Rose (deg)	% over Di
0	300	17.70
60	240	26.63
120	180	23.05
180	120	13.20
240	60	6.65
300	0	12.78

Table 32 Position 6 combination

7.5 TRANSITION PIECE FATIGUE LIFE RESULTS

To obtain the accumulated damage, equation (15), the number of cycles per stress block from rainflow counting, section 7.3, is used as input on the S-N Curve D.

Table 2-1 S-N curves in air

S-N curve	*$N \leq 10^7$ cycles*		*$N > 10^7$ cycles* $\log \bar{a}_2$ $m_2 = 5.0$	*Fatigue limit at 10^7 cycles *)*	*Thickness exponent k*	*Structural stress concentration embedded in the detail (S-N class), ref. also equation (2.3.2)*
	m_1	$\log \bar{a}_1$				
B1	4.0	15.117	17.146	106.97	0	
B2	4.0	14.885	16.856	93.59	0	
C	3.0	12.592	16.320	73.10	0.15	
C1	3.0	12.449	16.081	65.50	0.15	
C2	3.0	12.301	15.835	58.48	0.15	
D	3.0	12.164	15.606	52.63	0.20	1.00
E	3.0	12.010	15.350	46.78	0.20	1.13
F	3.0	11.855	15.091	41.52	0.25	1.27
F1	3.0	11.699	14.832	36.84	0.25	1.43
F3	3.0	11.546	14.576	32.75	0.25	1.61
G	3.0	11.398	14.330	29.24	0.25	1.80
W1	3.0	11.261	14.101	26.32	0.25	2.00
W2	3.0	11.107	13.845	23.39	0.25	2.25
W3	3.0	10.970	13.617	21.05	0.25	2.50
T	3.0	12.164	15.606	52.63	0.25 for SCF ≤ 10.0 0.30 for SCF >10.0	1.00

*) see also section 2.11

Table 33 S-N Curves parameters [11]

For the S-N Curve D the parameters are:

m_1 3.0
$\log \bar{a}_1$ 12.164
$\log \bar{a}_2$ 15.606 with $m_2 = 5.0$
$\Delta\sigma_{limit}$ 52.63 at $N = 10^7$ cycles, reference in Figure 103
k 0.20

Thus, the stress cycles for each stress range is calculated as:

$$\log N = \log \bar{a}_i - m_i \log\left(\Delta\sigma \left(\frac{t}{t_{ref}}\right)^k\right) \quad (18)$$

Where:

$$i = \begin{cases} 1, & \Delta\sigma > \Delta\sigma_{limit} \\ 2, & \Delta\sigma \leq \Delta\sigma_{limit} \end{cases}$$

t_{ref} 25 mm, reference plate thickness
t Plate thickness in mm
$\Delta\sigma$ Stress range
N Number of cycles to failure for constant stress range $\Delta\sigma$

Once calculated the N for each point and direction, D is obtained from equation (15). The possible combinations due to environmental loading direction, and positioning of the semi-submersible, yield a matrix of 12 rows (points of interest) and 6 columns (combinations) with the fatigue life of the TP, based on equation (17).

	Position1	Position2	Position3	Position4	Position5	Position6
P1	7.06	7.20	9.19	6.36	6.98	9.31
P2	7.77	7.79	9.51	6.70	7.46	9.70
P3	7.06	7.28	9.10	6.38	7.07	9.22
P4	7.49	7.34	9.30	6.40	7.00	9.49
P5	2.94	3.25	4.21	7.19	4.56	3.48
P6	2.91	2.99	4.08	7.05	4.27	3.37
P7	2.89	3.04	4.11	7.12	4.35	3.39
P8	2.98	3.37	4.30	7.30	4.71	3.56
P9	8.60	9.48	12.51	12.83	10.79	11.79
P10	8.79	9.94	12.81	13.11	11.28	12.08
P11	8.46	9.39	12.47	12.71	10.70	11.75
P12	9.15	10.18	12.97	13.29	11.46	12.26

Matrix 1 Transition Piece points of interest fatigue-life

The red-shaded areas remark the least fatigue-life points in the TP. To illustrate fatigue-life matrix, the following figures label the calculated fatigue-life years next to the point of interest.

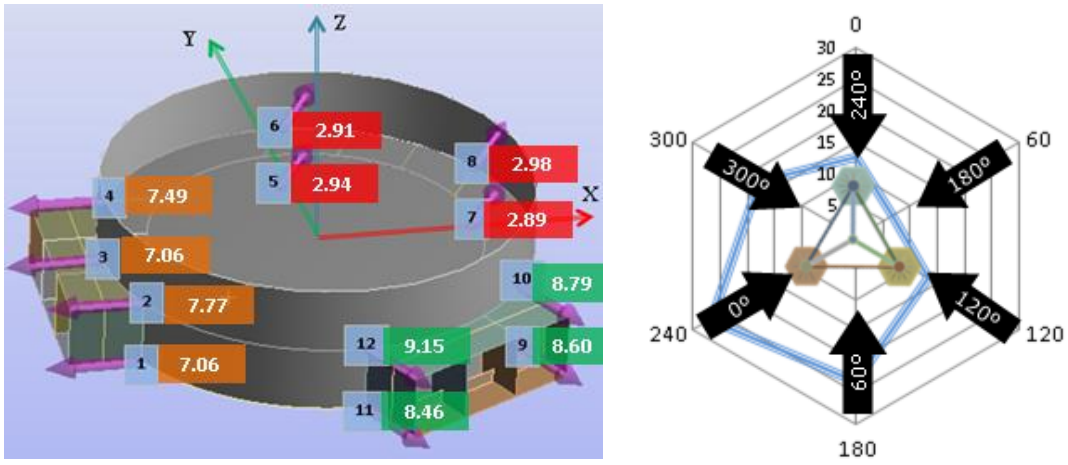

Figure 113 Fatigue life for position 1

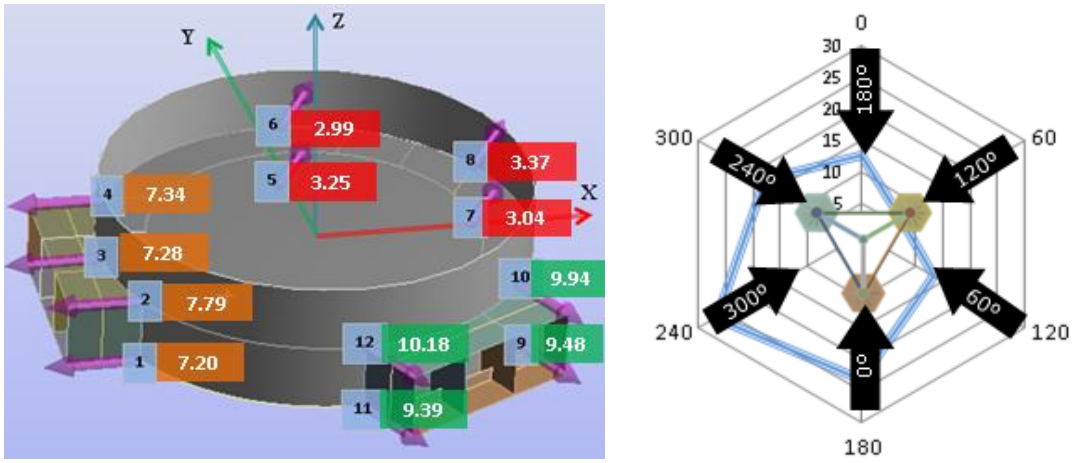

Figure 114 Fatigue life for position 2

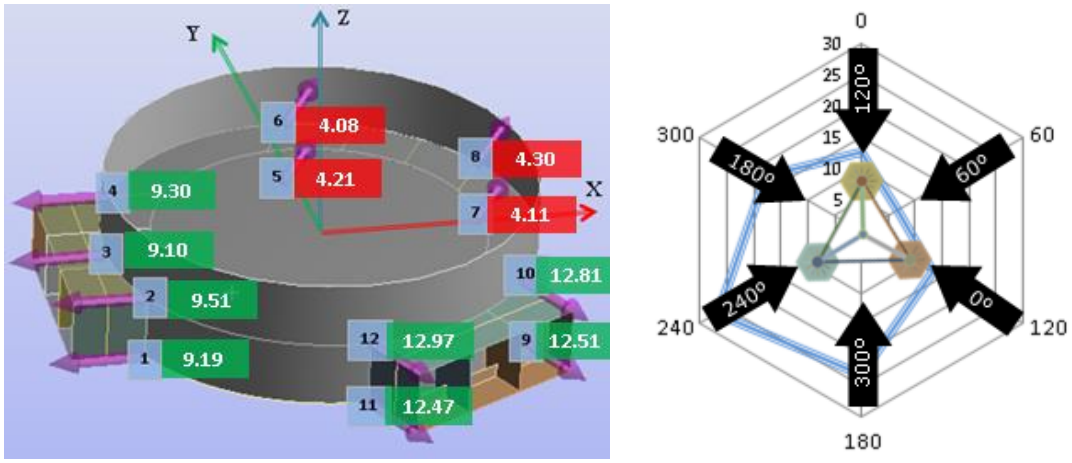

Figure 115 Fatigue life for position 3

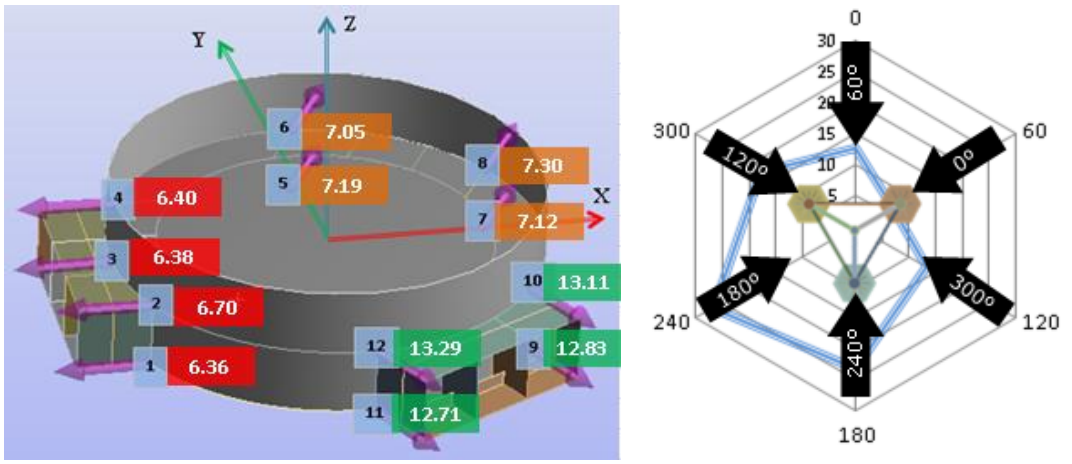

Figure 116 Fatigue life for position 4

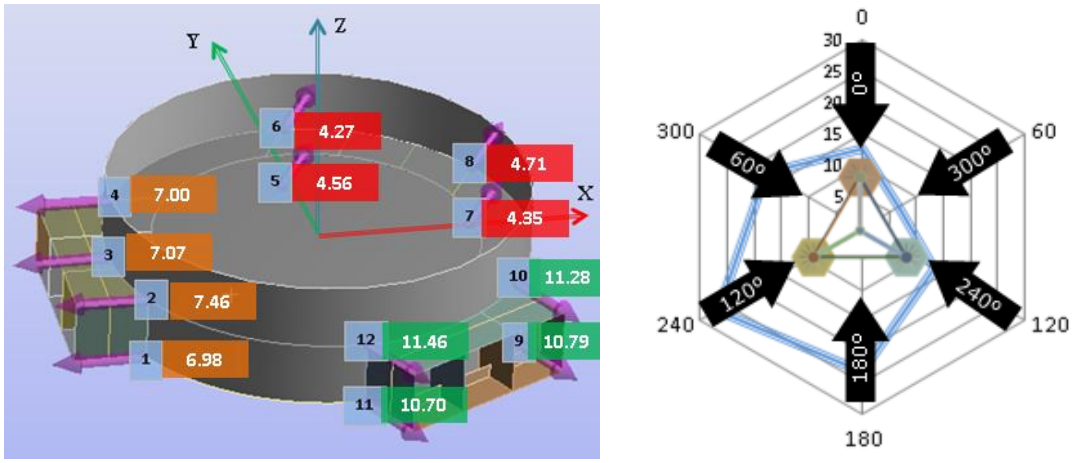

Figure 117 Fatigue life for position 5

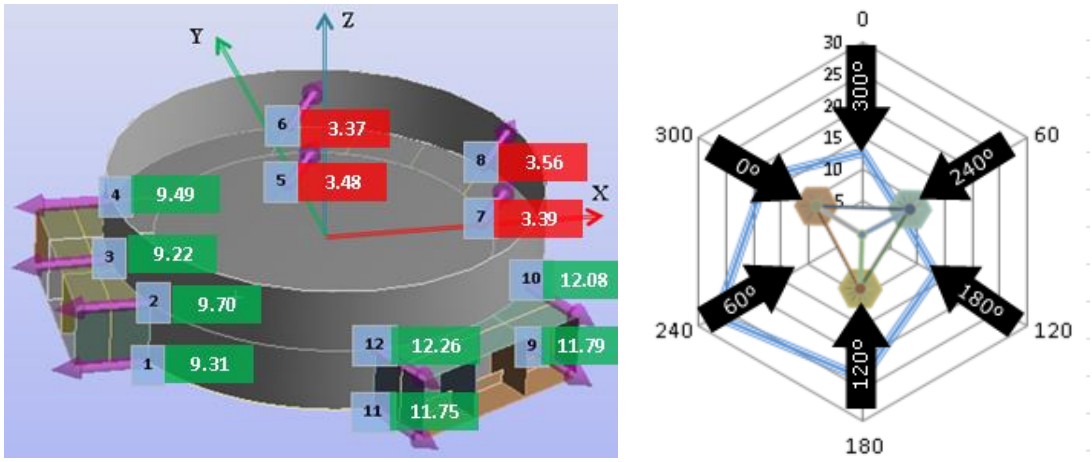

Figure 118 Fatigue life for position 6

7.6 CONCLUSIONS

Based on the results presented in Matrix 1, the minimum fatigue-life of the 6 positions of study is 2.89 years on position 1. Whereas, the scope of 25-years fatigue life is not achieved in any of the possible combinations. The most favorable position for the semi-submersible on this design corresponds to position 4, as shown in Figure 118. Where the minimum value is a maxima of 6.36 years compared with the rest of positions. Thus, the crack is assumed to be initiated on the point of interest 1, almost simultaneously with point 3, which are located on the bottom flange joints of the TP. Despite this, it is observed that position 4 would present fatigue problems within 6-7 years on 8 out of 12 joints.

Analyzing the overall fatigue life with respect the different positions, the fatigue life of the semi-submersible design carried out in this MSc thesis is about 7.8 years.

	Position 1	Position 2	Position 3	Position 4	Position 5	Position 6
Average Fatigue Life	6.34	6.77	8.71	8.87	7.55	8.28

In general, the TP joints on the bottom flange present the least fatigue-life. These joints are subjected to high bending stress in tension due to the overturning moment induced by wind loading.

8. FINAL REMARKS

Whilst the hydrodynamic behaviour of floating offshore wind foundations is a frequent topic published during the last years, this MSc thesis presents a workflow of hydrodynamics and mechanical design.

The main motivation that started this project aimed to provide an overview of semi-submersible design for offshore wind. Since no other works have been publishing regarding the design of internals, and hydrodynamic load transfer in a similar manner before, this conceptual design enables future authors to retake part of the concepts exposed. The approach presented in this document is subjected to further improvement, especially on the mechanical model and internals design.

Despite the fatigue life achieved in this study, remains under an optimal between 20-25 years, the methodology developed has proved to present satisfactory results in hydrodynamics, and linearized hydrodynamic load transfer. Rather than limiting the hydrodynamic study to time-series of the platform response, a complete assessment is included with RAOs, irregular sea-state behaviour, and extreme sea-state evaluation. The latter taking into account critical aspects such as air-gap and nacelle acceleration for an FOWT.

The transition piece is a critical element in the offshore foundation since it acts as link between the foundation and the wind turbine. Although wind loading has a significant contribution to the stress levels on the TP, transmitted from the wind turbine base into the foundation, wave loading induces notable stress ranges on the TP joints in function of the wave phase, Figure 94. Whereas these stress ranges have a direct influence in fatigue-life.

The linearization assumption taken to compute the stress time-series for an irregular sea-state in chapter 6, might be the key factor resulting in large stress ranges which consequently reduce the fatigue-life.

Nowadays, hydrodynamic load transfer on diffraction elements is a demanding and highly time-consuming task. The lack of FEA tools with a full implementation of hydrodynamic-mechanical, and published procedures to analyse an irregular sea-state with hydrodynamic load transfer to study the fatigue life on diffraction elements, is a notable challenge for future works on the topic. Although wind loading is included in this project and increased by a safety factor, it is far from a fully coupled simulation of wind and waves which would account for the aerodynamic damping of the wind turbine.

In this thesis, there is a large amount of post-processing data, ranging from hydrodynamic-mechanical design to the TP fatigue-life, including the disciplines and techniques as presented.

9. FURTHER WORK

Whereas this conceptual design is focused on the fatigue-life of the semi-submersible transition piece, and developing a hydrodynamic load transfer methodology, hereunder more detailed studies are proposed.

The state-of-the-art tools, i.e. AQWA and ASAS, are subjected to continuous development since ANSYS will bring this two modules functionalities closer in future releases. Presumably, an effective hydrodynamic load transfer would allow to compute transient analyses of irregular sea-states within the software. On top of that, the mooring lines, neglected in this analysis are yet to be implemented in the mechanical module.

However, the author has a suggestion for other people with interest on this topic. The proposed process is outlined below:

- [Hydrodynamic model] Compute the RAOs for the representative range of wave frequencies, i.e. 0.1 to 1.0 rad/s
- [Mechanical model] Include 3 springs per mooring line in the mechanical model. Since buoyancy on diffraction elements is not functional in ASAS/Mechanical, one of the three springs per mooring line must be placed above to balance self-weight.
- [Mechanical model] Run a transient analysis via OCREAD to compute the hydrodynamic forces for each one frequency at the time until the platform response is uniform and similar to the one obtained in the corresponding RAO.
- Tune the stiffness of the springs in consequent parametric analyses until the platform response in the mechanical model matches that in the hydrodynamic model. For each frequency and direction running unit amplitude waves.
- [Mechanical model] In order to compute the stress transfer functions, as presented in chapter 6, the spring stiffness should be modified accordingly to wave frequency.

As explained above, this task requires a large amount of time and computational resources to complete the fine tuning of the springs. The author has tested himself the proposed approach but neglected the implementation due to its difficulty and time. Currently, ANSYS does not support modal and transient analysis coupled when wave loading is applied, this condition obliges to conduct a full transient analysis, and thus large computational times. However, it is expected that the springs system properly tuned would result in comparable results between the hydrodynamic model platform response, and the total reaction forces in the mooring lines/springs.

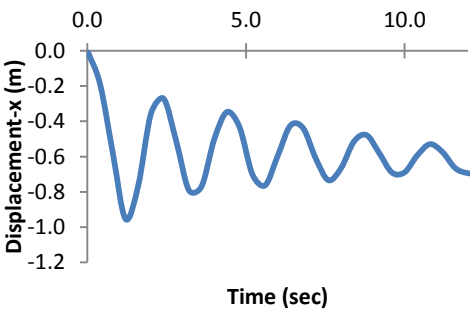

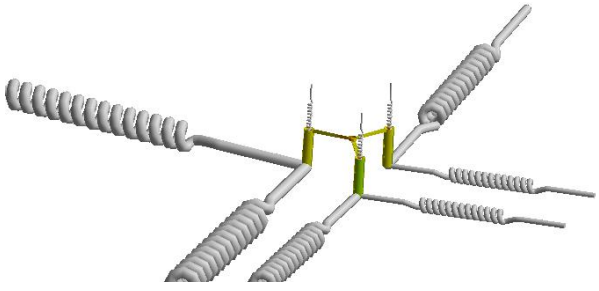

Furthermore, other structural elements than the TP on the semi-submersible require of a detail assessment in braces, heave plates, columns, and topside joint with the semisub column. Since the former are directly subjected to wave loading, and determine the dynamic response, and the topside joints act as transmission element of the wind loading into the floating foundation.

Alternatively, to the modelling and submodeling conducted in this master thesis, yet the author suggest another approach to reduce the overall analysis time. This would consist of dividing the structure in Craig-Bampton superelements to condense the semi-submersible in a reduced system. The initial assumption is that these would be located on interface level and cross-bracing joints. It is assumed that the recent release of FAST 8 would allow to benchmark semi-submersible natural frequencies with ANSYS (CMS fix method), and full-system eigenfrequencies, in order to validate the use of the condensate system.

10. BIBLIOGRAPHY

[1] ANSYS, [Online]. Available: http://www.ansys.com/Products/Other+Products/ANSYS+ASAS.

[2] DNV website, [Online]. Available: http://www.dnv.com/press_area/press_releases/2013/dnv_kema_releases_floating_offshore_wind_turbine_structures_standard.asp.

[3] S. Chakrabarti, Handbook of Offshore Engineering, ELSEVIER, 2005.

[4] Friede & Goldman, LTD, [Online].

[5] wikipedia, [Online]. Available: http://en.wikipedia.org/wiki/Semi-submersible.

[6] F. V. Puche, "Semi-Submersible Platform Design," Esbjerg, 2014.

[7] S. Chakrabarti, Numerical Models in Fluid Structure Interaction, WIT Press, 2005.

[8] E. Gaba, "wikipedia," March 2008. [Online]. Available: http://en.wikipedia.org/wiki/Moray_Firth.

[9] E. E. B. T. M. Marit I. Kvittem, "Effects of hydrodynamic modelling in fully coupled simulations fo a semi-submersible wind turbine," ELSEVIER, 2012.

[10] wikipedia, "rainflow counting," [Online]. Available: http://en.wikipedia.org/wiki/Rainflow-counting_algorithm.

[11] Det Norske Veritas A/S, "Fatigue Design of Offshore Steel Structures," DNV, 2012.

[12] ANSYS, Inc., "AQWA Reference Manual," Century Dynamics Ltd., 2011.

[13] J. J. M. M. H. S. A. G. A. C. a. C. L. A. Robertson, "Definition of the Semisubmersible Floating System for Phase II of OC4," 2012.

[14] G. Moe, "Linear Wave Theory," Trondheim, NTNU, pp. 235-259.

[15] IKM Gruppen.

[16] Det Norske Veritas, "DNV-RP-C205 Environmental Conditions and Environmental Loads," Det, 2010.

[17] O. M. Faltinsen, Sea loads on Ships and Offshore Structures, Cambridge University Press, 1990.

[18] Det Norske Veritas, "DNV-OS-C101," 2011.

[19] ANSYS, "AQWA WAVE 15.0," 2013.

[20] A. Nieslony, "Rainflow counting," 2010.

[21] Y. Bai, Marine Structural Design, ELSEVIER, 2003.

[22] G. Fulton, D. Malcolm, H. Elwany, W. Stewart, E. Moroz and H. Dempster, Semi-Submersible Platform and Anchor Foundation system for Wind Turbine Support, NREL National Renewable Energy Laboratoy, 2007.

[23] M. L. B. J. Jason M. Jonkman, "FAST User's Guide," NREL National Renewable Energy Laboratory, 2005.

[24] J. Jonkman, "Dynamics Modeling and Loads Analysis of an Offshore Floating Wind Turbine," NREL National Renewable Energy Laboratory, 2007.

[25] D. M. H. E. W. S. E. M. a. H. D. G.R. Fulton, "Semi-Submersible Platform and Anchor Foundation Systems for Wind Turbine Support," NREL National Renewable Energy Laboratory, 2007.

[26] S. B. a. A. B. W. Musial, "Feasibility of Floating Platform Systems for Wind Turbines," NREL National Renewable Energy Laboratory, 2003.

[27] T. Sarpkaya, Wave Forces on Offshore Structures, Cambridge, 2010.

[28] L. Z. a. H. W. Jing Zhao, "Motion Performance and Mooring System of a floating Offshore Wind Turbine," Institute of Ocean Renewable Energy system, Harbin, China, 2012.

[29] Det Norske Veritas A/S, "Design of Floating Wind Turbine Structures," DNV, 2013.

[30] Neptune Offshore Engineering Developement Co., Ltd., noed.com.cn.

[31] Norwegian University of Science and Technology, ipt.ntnu.no.

[32] Offshore Moorings, offshoremoorings.org.

[33] DELMAR, delmarus.com.

[34] World Oil, worldoil.com.

[35] "the engineer," [Online]. Available: http://www.theengineer.co.uk/.

[36] PADT, "Submodeling," [Online]. Available: http://www.padtinc.com/blog/the-focus/submodeling_ansys_mechanical.